# Design of Multi–Scroll Chaotic Oscillators

by

**M. C. Rodolfo Trejo Guerra**

In partial fulfillment of the requirements for the degree of

**DOCTOR IN SCIENCES WITH SPECIALLITY IN ELECTRONICS**

in the

**National Institute of Astrophysics, Optics and Electronics**

January 2012

Tonantzintla, Puebla

Supervised by:

**Dr. Esteban Tlelo Cuautle, INAOE**
**Dr. César Cruz Hernández, CICESE–UABC**

# Abstract

Chaotic oscillators have been intensively studied since a few decades and constitute a field for some potential applications in electronics, which are still in development. For instance, the efforts in designing continuous time chaotic oscillators and their design using integrated circuit technology have been considered only in a very few works. In this manner, this Thesis pretends to stretch the gap between theoretical chaotic dynamical systems, particularly the multi-scroll oscillators and their integrated realizations in order to establish the basis for future chaos-based applications.

Moreover, multi-scroll chaotic attractors are a particularly intriguing topology of chaotic continuous dynamical systems, which are seen in many piecewise-linear (PWL) based nonlinear function cases of chaotic oscillators. The main advantages in the use of these PWL functions are the obtention of partial analytical solutions and the relatively simple design as well as the modularity required for the change of attractors, i.e. by growing the number of scrolls.

In this manner, this Thesis starts by describing the theoretic concepts related to the generation of chaotic behavior by homoclinic and heteroclinic orbits. Then, the diverse architectures of continuous chaotic motion in the literature are briefly reviewed and compared. An analysis in the complexity based on the global Lyapunov exponents is surveyed and a particular dynamical system is selected. A new multi-scroll attractor is obtained by applying saw-tooth-like nonlinear functions.

The system design requirements are obtained and then the need of a new nonlinear cell becomes evident. At this point, this voltage-to-current cell is being proposed by using comparators implemented with floating gate MOS (FGMOS) transistors, which

are analyzed in depth and adapted to a whole third order dynamical system to generate multi-scroll chaotic behavior.

Design simulations are presented before and after the layout, and the results are confirmed by the experimental observations made over the fabricated multi-scroll chaotic oscillator prototype. Additionally, a process-voltage-temperature (PVT) analysis is performed to show the robustness of the integrated chaotic oscillator with respect to variations in temperature and process corners.

Some of the most original contributions of this work are the analysis of the Lyapunov exponents for multi-scroll PWL-based chaotic systems, the system description of a new multi-scroll oscillator, the design requirements for this type of nonlinear circuits, the proposed V-I FGMOS based nonlinear comparator with capacitive internal references and the integrated circuit design of the first 5-scroll chaotic oscillator.

# Resumen

Los osciladores caóticos han sido estudiados desde hace unas pocas décadas y se han encontrado aplicaciones potenciales que aun estan en desarrollo. A pesar de esto, la realización integrada de osciladores caóticos en tiempo continuo ha sido considerada escasamente. La investigación reportada en esta Tesis espera estrechar la distancia entre los sistemas dinámicos caóticos, particularmente los osciladores caóticos de múltiples enrollamientos y las realizaciones a nivel de circuito integrado en tecnologías CMOS.

Entre los sistemas caóticos continuos, los atractores caóticos de multiples enrollamientos (*multi-scroll attractors*) describen comportamientos particularmente interesantes generados en muchos de los casos de osciladores basados en funciones lineales a tramos ($PWL$ por sus siglas en inglés). Entre las principales ventajas de la aplicación de estas funciones, se encuentra la obtención de soluciones analíticas parciales, la relativa simplificación del diseño y la modularidad obtenida, que permite hacer cambios al tipo de atractor; por ejemplo al acrecentar el número de enrollamientos.

De esta forma, esta Tesis comienza describiendo algunos conceptos teóricos relacionados con la generación de comportamiento caótico basado en órbitas homoclínicas y heteroclínicas. Se realiza una breve revisión y comparación de los diversos diseños propuestos para la realización de osciladores caóticos de múltiples enrollamientos. Se analiza la complejidad en términos de los exponentes globales de Lyapunov. Se selecciona un sistema dinámico particular y se propone la generación de un nuevo attractor de múltiples enrollamientos por medio de funciones no lineales tipo diente de sierra.

Posteriormente los requerimientos de diseño son analizados, con lo que se evidencía la necesidad de una celda no lineal. Dicha celda es propuesta utilizando comparadores basados en transistores MOS de compuerta flotante ($FGMOS$). Se realiza un análisis a fondo y se describe la aplicación del comparador para generar múltiples enrollamientos en sistemas dinámicos de tercer orden.

Posteriormente, se realizan simulaciones sobre el diseño antes y después de layout. Los resultados son confirmados por las observaciones experimentales realizadas sobre el prototipo fabricado. Además, se presentan análisis en simulación sobre las variaciones en proceso, voltaje y temperatura ($PVT$) para mostrar la robustez del diseño integrado al respecto.

Algunas de las contribuciones originales de este trabajo de investigación son el análisis de los sistemas caóticos basados en funciones PWL en términos de los exponentes de Lyapunov, la descripción a nivel sistema de un nuevo oscilador generador de múltiples enrollamientos, el análisis de los requerimientos de diseño para este tipo de circuitos, el comparador FGMOS que utiliza referencias internas y el diseño y obtención del primer oscilador caótico implementado con tecnología de circuitos integrados de 5 enrollamientos.

# Acknowledgements

*This work is specially dedicated to my family, my loved wife Judith Onchi V., who always showed her patient support in all senses, and my soon Héctor Rodolfo, who has been by himself, the greatest product I have ever being in. I extend a dedication to my parents Ada Adela Guerra A.† and Rodolfo Trejo V., whose have been a living example in life; to all my family and close friends.*

*My most sincere gratitude for the guidance, support and encouragement of my advisors, Dr. E. Tlelo Cuautle in INAOE and Dr. César Cruz Hernández in CICESE, thanks for opening new horizons in my mind, for all their advices, for the people I could meet trough, and for their interesting talks.*

*I also want to thank Dr. Jesús Manuel Muñoz Pacheco, who gave me good advise and the opportunity to grow, to Dr. Mariano Jiménez Fuentes in CITEDI-IPN for his amazing lectures and his advice, and to all my teachers as well as Dr. Murphy Arteaga, Martha Olmos, Cornelio Posadas and also to all the INAOE staff.*

*I extend my gratitude to all my partners and friends, specially to Ismael Cosme, Francisco Sánchez, Edgar López and Victor Carbajal.*

*I want to specially recognize José Antonio Fraga Valle, Roberto Javier Romero y Viloria and Jorge Varona Salazar, for their support, transparency, and the amazing stories I have lived trough.*

*Not less important is my appreciation to the CONACyT (Consejo Nacional de Ciencia y Tecnología) for its essential support through the scholarship 204229, and the projects 48396–Y and 131839–Y.*

# Contents

# Chapter 1

# Introduction

Chaotic motion is characterized by random like, high spectra behavior which exhibits high dependence on initial conditions. In the generation of chaotic oscillators, some proposed approaches uses polynomial forms [1], sinusoidal functions [2], delay based functions [3], hysteretic functions [4–8] or piece-wise linear (PWL) functions [9]. This last approach offers the advantages of been relatively simpler to analyze and produce. Some of the PWL-based systems exhibit multi-scroll attractors, a characteristic observed in the state space which is possible due to the creation of several equilibrium points.

In the application side, most of the potential applications in engineering, exploit the deterministic nature of chaotic signals [10, 11], while others are related to the random behavior. For example, the synchronization and transmission of encrypted information [12–18], the use of chaotic radars [19–21], the signal reconstruction [22]; and the noise and random bit generators [23, 24].

While the majority of the proposed implementations are done by using traditional Opamps, the use of the operational transconductance amplifier (OTA) [25], the tanh() function based transconductor [26], the current mirror [27], the multiplier cells [28], the floating gate CMOS (FGMOS) [29], the unitary gain cell (UGC) [32, 33], or the current feedback operational amplifier (CFOA) has also been proposed [34–37]. In particular, there has been little concern in the realization of such continuous chaotic oscillators using integrated circuit technology.

In this Thesis, the integrated realization of such systems using a conventional CMOS technology and taking into consideration the circuit non-idealities, is explored. Some relevant issues are the number of scrolls, the central operation frequency, the use of internal references, the CMOS design criteria and the experimental results.

## 1.1 Introduction to chaos

Chaotic oscillators have their origin in nonlinear dynamical systems, its main characteristic is the apparently random behavior while bounded. The chaotic system signals (which are also called states, solutions or trajectories) does not settle in any particular value, nor show periodicity. This produces a wide spectra in most of the cases. However, since the solutions are provided from differential (or differences) equations, the system is deterministic, this means that ideally, every point in the trajectory may be predicted by an initial state (initial condition).

A consequence of the diversity on spectra and the deterministic nature, is the fact that chaotic behavior is well characterized by its sensitivity to initial conditions. This means that a couple of near points in the solution space will evolve in a very different manner. This was discovered by the meteorologist Edward Lorenz, a pioneer in chaos theory because of his research on weather prediction [38]. Back in the sixties, he developed a mathematical model of the air convection which took him to a simplified nonlinear dynamical system that showed to be highly sensitive to initial conditions. The conclusion of that work was the long term unpredictability of the weather, which is also a characteristic of chaotic phenomena, since any state can only be represented by a finite precision value.

It was since nineties, that many research is been done on this field, due to the growing capacities of computing. A remarkable design of a continuous chaotic oscillator is the case of the two-scroll Chua's circuit [39, 40], which has shown to generate a rich variety of chaotic dynamics in a relatively simple implementation. The long term trajectories of such systems are observed by a geometric perspective in the state space which is known as strange attractor or chaotic attractor. In some cases such as the Chua's circuit, the attractor is composed by scrolls.

Recently, many new chaotic oscillatory systems have been proposed. In all cases a nonlinear part is required to obtain more equilibriums than the origin and eventually obtain attraction regions. Some approaches uses polynomial forms [1], sinusoidal functions [2], delay based functions [3], hysteretic based functions [4–8] or piece-wise linear (PWL) functions [9]. This last case has been specially chosen by numerous research works because of the capacity to obtain at least partial analytical solutions [41] (for the linear segments), while the obtention of such solutions for other nonlinearities are very hard to reach [42]. This motivates the development of new PWL-based generalizations for the Chua's dynamical system, some of them showing more amount of scrolls (multi-scroll attractors).

In this way, another realization of multi-scroll chaotic oscillators has been obtained with the use of a canonical third order form which has proved to produce scrolls in reticular fashion in the three directions of the phase plane [34] by the use of different nonlinearities.

By introducing experimental realizations, the sustained chaotic behavior proved to be much more than an artificial effect in the limited arithmetics of computer programs. In fact, many of the proposed chaotic systems are accompanied by experimental results and circuit realizations that also probe the functionality of the required nonlinear functions. Thus, sometimes the reference has been made informally to the circuit instead of the system, in minor cases, the point of discussion is the circuit implementation. Regardless the circuit realizations have additional considerations to be made such as the bias conditioned signal excursion, the tolerances and variations of the discrete used components, frequency and other limitations of the active devices (mainly Opamps).

A first multi-scroll generalization of the Chua's circuit [43] proves some of these limitations because of the increasing reduction of the linear function segments and the consequently loos of scrolls. In order to preserve the attractor, the use of more uniform PWL functions is observed in later literature [44–46]. However, there are many drawbacks to survey in the design of continuous chaotic oscillators. The generated attractors of the electronic realizations will be always limited by the biasing, the circuit parasitics and the number of scrolls. Thus, new proposals are exploring the frequency spectrum and the amount of sensitivity that these systems can show, with the aim of growing the system complexity without changing the attractor shape (i. e. the number of scrolls).

Other open field is centered in the frequency limitations of the generated spectra. Since most of the proposed designs are based in Opamps, the use of other active cells may be advantageous. Such is the case of the operational transconductance amplifier (OTA) based design [25], the *tanh()* function based transconductor [26], the current mirror based design [27], the multiplier cells [28], the floating gate CMOS (FGMOS) design [29], or the unitary gain cell (UGC) [32, 33]. Another remarkable active cell is the current feedback operational amplifier (CFOA) [34–37], because of its higher frequency performance than conventional Opamps and its mixed mode operation which gives it the capacity to operate signals both in voltage and current mode, this can even lead to a reduction on the oscillator topology.

Integrated realizations are scarce in literature (see [25, 29, 47–49]), most of the works focuses on mathematical descriptions. In general, one can conclude the need of analog design applied to these realizations. These reasons have motivated this investigation towards the achievement of multi-scroll behavior in an integrated CMOS compatible design.

The Thesis is organized as follows: the state of the art is reviewed in this Chapter. Some interesting characteristics of multi-scroll dynamical systems related to the automation of nonlinear functions as well as the Lyapunov exponent analysis are exposed in Chapter 2. The CMOS design considerations for the proposed nonlinear system is explained in Chapter 3; whereas Chapter 4 details the proposed design and simulations, treating separately the linear design from the nonlinear one. Chapter 5 concludes Chapter 3 by showing the simulations, analyzing the manufactured prototype and observing the robustness in terms of corner analysis. Conclusions and future work are given in Chapter 6.

## 1.2 Chaotic Oscillators

The relevance of the Chua's circuit has recently made possible the born of a big family of multi-scroll oscillators and techniques to control chaos. The work of Suykens had firstly presented a generalization to obtain multiple scrolls [43] in one direction (1D). Later, numerous research have shown that other chaotic systems can be generalized to exhibit multi-scroll behavior. Some of the most remarkable are the work of Yalçin [34], with a canonical third order model; Lü, with the saturated slope circuit [41], the fourth order *Jerk* circuit, and jointly with Han, with the third order hysteresis-based system [4], and by Han [5], who firstly proposed the second order hysteresis-based system.

The above cited authors have proposed circuit schemes using Opamps [9], whereas other designs based in active devices such as commercial CFOA (i. e. the Analog Devices AD844) have improved the frequency performance [34, 35]. Relevant chaotic continuous oscillator designs are summarized in Table 1.1. Here some issues are observable:

- Many new designs have been obtained by generalizing previous others, the most preferred dynamic system is the Chua's system.
- PWL-based oscillators are preferred because of the relatively simple mathematical description, dynamical analysis and circuit synthesis.
- Integrated designs are few in all cases and multi-scroll designs are scarce.
- Integrated circuit designs are done mostly by OTAs and discrete implementations use Opamps.

Table 1.1: Principal design techniques used in chaotic oscillators.

| System Name | | Nonlinear function based on | | | Reference | |
|---|---|---|---|---|---|---|
| Name | Attractor type | Function | Proposed circuit | Integrated design | Author | Year |
| Chua's circuit | double-scroll | PWL | Opamp, OTA, CFOA, UGC, CCII+ | OTA | Chua [25], Delgado [49] | 1993 |
| | 1D | PWL | Opamp | | Suykens [50] | 2000 |
| | 1D | Sinusoidal | Trigonometric function generator | | Tang [2] | 2001 |
| | 1D | PWL | Opamp | | Zhong [44] | 2002 |
| | 1D | PWL | FGMOS | FGMOS | Fujiwara [29] | 2003 |
| | 1D, 2D | PWL (saw-tooth) | Opamp | | Yu [45] | 2007 |
| Lorenz | double-scroll | Product | Multiplier | OTA, Multiplier | González [51] | 2000 |
| | multi-scroll | Complex | DSP | | Yu [52] | 2006 |
| Third order canonical system | double scroll | PWL | CFOA, Opamp | OTA, Opamp | Elwakil [47] | 2000 |
| | 1D-3D | PWL | CFOA, Opamp | | Yalcin [34] | 2002 |
| | 1D-3D | PWL | Opamp | | Lü [41] | 2004 |
| | 1D-3D | Hysteresis | Opamp, diode | | Lü [53] | 2006 |
| Second order hyst. | 1D, 2D | Hysteresis | Opamp, diode | | Han [5] | 2004 |
| NA | 1D, 2D | $tanh()$ | Differential pair, OTA | | Ozoguz [26] | 2002 |
| NA | double-scroll | $tanh()$ | LC | | Ozoguz [23] | 2005 |
| NA | 1D | PWL, $tanh()$, $t$ | CFOA, TX line | | Yalcin [3] | 2007 |
| NA | double-scroll | PWL | current mirror, C | | Ozoguz [24] | 2008 |

## 1.3 Applications of Chaotic Oscillators

In the side of applications, chaotic systems are relatively new and in some cases there is still mathematical research to be done. Most of the potential applications exploit the deterministic nature of chaotic signals [10, 11], while others are related to the random behavior. For example the synchronization and transmission of encrypted information [12–18], the use of chaotic radars [19–21] and the signal reconstruction [22] in the first case; and the noise and random bit generators [23, 24] in the second one.

For example in the case of secure communications, some of the advantages [17] are based in the complexity of the chaotic signals, which turns them suitable for message encryption, the wide spectra makes them useful as wide bandwidth communications systems and robust to narrow band disturbances. Also as the autocorrelation levels are generally low for these signals, these can be considered as orthogonal with each other and then implemented in multi-user communication schemes.

The most of chaotic communications works by first synchronizing several at least a couple of systems. Some techniques are: Master-slave synchronization, Non-autonomous synchronization, Inverse system synchronization, Adaptive control synchronization or Coupled synchronization.

A second example is in the use of chaotic radars [21], some of the main advantages are [11]: In military applications, the use of noise like signals to scan an enemy target without prevent it; the relative immunity to interference due to the natural wide bandwidth of signals; the multiple radar compatibility since the return signals can be distinguished from the other radars; and the achievement of better range ambiguity properties than by using noise signals.

Other potential applications are the chaotic power controllers [54–57], micro electro mechanical systems (MEMS) [58], and motion control [59, 60].

## 1.4 Traditional Multi-Scroll Chaotic Oscillators

Chaotic systems equations will be presented for uniformity as a set of the linear part in $\mathbf{A}$ and a nonlinear counterpart with gain $\mathbf{B}$, where $\mathbf{\Phi}(\mathbf{x})$ carries the nonlinear functions $f(\mathbf{x})$. In this sense, the nonlinear system

$$\dot{\mathbf{x}} = f(\mathbf{x}), \tag{1.1}$$

is described directly by

$$f(\mathbf{x}) = \mathbf{A}\mathbf{x} + \mathbf{B}\mathbf{\Phi}(\mathbf{x}) \tag{1.2}$$

.

Recall that in the normalized third order system, $\dot{\mathbf{x}}$ is the derivative of $\mathbf{x}$ with respect to a normalized time $\tau$.

$$\mathbf{x} = \begin{pmatrix} x_1 \\ x_2 \\ x_3 \end{pmatrix}$$

Moreover, many of the actual chaotic oscillators have started from the proposed Chua's oscillator [39, 40]. This circuit has been implemented by an RLC circuit (Fig. 1.1), and differs by the traditional Chua's circuit in the presence of the parasitic inductor resistance $R_L$ which produces the term $\gamma$ (1.3). The nonlinear part of the circuit is a negative three-segment PWL resistor which produces function (1.4). The system normalization has been done by defining all its parameters and variables (1.5). Here, $E$ is used as the excursion scaling factor.

$$\mathbf{A} = \begin{pmatrix} -\alpha & \alpha & 0 \\ 1 & -1 & 1 \\ 0 & -\beta & -\gamma \end{pmatrix} \quad \mathbf{B} = \begin{pmatrix} -\alpha & 0 & 0 \\ 0 & 0 & 0 \\ 0 & 0 & 0 \end{pmatrix} \quad \mathbf{\Phi} = \begin{pmatrix} f(x_1) \\ 0 \\ 0 \end{pmatrix} \tag{1.3}$$

$$f(x_1) = bx_1 + \frac{1}{2}(a-b)\left(|x_1+1| - |x_1-1|\right) \tag{1.4}$$

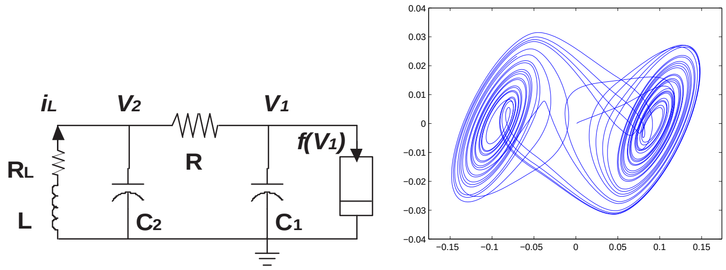


(a) (b)

Figure 1.1: Chua's oscillator, (a) circuit direct implementation, (b) double-scroll attractor observed in the $(x_1, x_2)$-plane.

The used rescaling variables are:

$$
\begin{aligned}
x_1 \triangleq \frac{V_1}{E}, \quad x_2 \triangleq \frac{V_2}{E}, \quad x_1 \triangleq \frac{i_L R}{E}, \\
\alpha = \frac{C_2}{C_1}, \quad \beta = \frac{R^2 C_2}{L}, \quad \gamma = \frac{R R_L C_2}{L}, \\
a = RG_a, \quad b = RG_b, \quad \tau = \frac{t}{RC_2}
\end{aligned}
\tag{1.5}
$$

System (1.3) describes a double-scroll attractor by using parameters and initial conditions in the neighbor of the equilibrium at the origin $\mathbf{x} = [0.001, 0, 0]$. As earlier mentioned, the Chua's system has been generalized principally by introducing more slopes in the nonlinear function to generate more equilibrium points, and eventually, multi-scroll behavior. Some of the most important systems derived in this sense are described below.

### 1.4.1 Suykens generalization

Equation (1.2) is rewritten as [43]:

$$
\mathbf{A} = \begin{pmatrix} 0 & \alpha & 0 \\ 1 & -1 & 1 \\ 0 & -\beta & 0 \end{pmatrix}, \mathbf{B} = \begin{pmatrix} -\alpha & 0 & 0 \\ 0 & 0 & 0 \\ 0 & 0 & 0 \end{pmatrix}, \mathbf{\Phi} = \begin{pmatrix} h(x_1) \\ 0 \\ 0 \end{pmatrix}, \tag{1.6}
$$

$$h(x_1) = m_{2q-1}x_1 + \frac{1}{2}\sum_{i=1}^{2q-1}(m_{i-1} - m_i)\left(|x_1 + c_i| - |x_1 - c_i|\right) \tag{1.7}$$

The nonlinear function is composed by a set of progressively small slopes, Table 1.2 summarizes the used coefficients.

### 1.4.2 Zhong generalization

As reported in [44], the system parameters are $q = 1$ for $2N$ even scrolls, and $q = 2$ for $2N-1$ scrolls. Vector $[m_0...m_9] = [-4.416, -0.276, -3.036, -0.276, -3.036, -0.276, -3.036, -0.276, -3.036, -0.276]$ represents the slopes, and vector $b$ shows the breakpoints. See Table 1.3 and:

$$\mathbf{A} = \begin{pmatrix} -\alpha & \alpha & 0 \\ 1 & -1 & 1 \\ 0 & -\beta & 0 \end{pmatrix}, \quad \mathbf{B} = \begin{pmatrix} -\alpha & 0 & 0 \\ 0 & 0 & 0 \\ 0 & 0 & 0 \end{pmatrix}, \quad \mathbf{\Phi} = \begin{pmatrix} g(x_1) \\ 0 \\ 0 \end{pmatrix}, \tag{1.8}$$

$$g(x_1) = m_{2n-1}x_1 + \frac{1}{2}\sum_{i=q}^{2N-1}(m_{i-1} - m_i)(|x_1 + b_i| - |x_1 - b_i|). \tag{1.9}$$

### 1.4.3 Yu generalization

In a first work [46], Simin Yu showed the possibility to make uniform scrolls on the original Chua's system by choosing the breakpoint $b_i$ of the PWL function and the system parameters $\alpha \approx 9.5$, $\beta \approx 14$, $a \approx -0.528$, and $b \approx -1.406$. The use of a recursive expression was proposed to find the breakpoints on the $n$-scroll function conformed by alternating slopes $a$ and $b$:

$$f(x_1) = m_{n-1}x_1 + \frac{1}{2}\sum_{i=1}^{n-1}(m_{i-1} - m_i)\left(|x_1 + b_i| - |x_1 - b_i|\right). \tag{1.10}$$

For classical circuit implementations, the gain of slopes is always $m_a = a/R$ or $m_b = b/R$. If an odd-scroll attractor has to be generated, the function starts with slope $m_a$; otherwise, the slope at the origin was $m_b$. The method to compute the breakpoints of the function starts with these slopes been defined as well as the first break point $b_1$, and applying expression:

$$b_{i+j} = \frac{2\sum_{j=1}^{i}(m_j - m_{j-1})b_j}{1+m_i} - b_i. \tag{1.11}$$

In a latter work [45] a simpler multi-scroll system was designed by using a saw-tooth like nonlinear function, see Table 1.4. There, the system parameters are $\alpha = 10$, $\beta = 16$, $\xi = 0.25$, $A_1 = 0.5$, and the rest of the system is described by Table 1.5 and:

$$\mathbf{A} = \begin{pmatrix} 0 & \alpha & 0 \\ 1 & -1 & 1 \\ 0 & -\beta & 0 \end{pmatrix}, \quad \mathbf{\Phi} = \begin{pmatrix} f_1(x_1) \\ f_2(x_2) \\ 0 \end{pmatrix} \tag{1.12}$$

### 1.4.4 A canonical model

Other non-PWL approaches have also been introduced to generalize multi-scroll systems, such as the introduction of the cubic function based Chua's system in [1] and the sinusoidal function based oscillator in [2]. Unless useful, these approaches can increase considerably, the complexity of the design. Thus, a canonical third order model $\dddot{x} = -ax - b\dot{x} - c\ddot{x} + df_1(x)$ has also been proposed in [34]. Its matrix representation is:

$$\mathbf{A} = \begin{pmatrix} 0 & 1 & 0 \\ 0 & 0 & 1 \\ -a & -a & -a \end{pmatrix}, \quad \mathbf{B} = \begin{pmatrix} 0 & 0 & 0 \\ 0 & 0 & 0 \\ 0 & 0 & a \end{pmatrix}, \quad \mathbf{\Phi} = \begin{pmatrix} 0 \\ 0 \\ f_1(x_1) \end{pmatrix} \tag{1.13}$$

Where the model was first used with step functions such as $f_1(x)$ given by

$$f_1(x) = \sum_{i=1}^{M_x} g_{\frac{(-2i+1)}{2}}(x) + \sum_{i=1}^{N_x} g_{\frac{(2i-1)}{2}}(x) \tag{1.14}$$

$$g_\theta(\varsigma) = \begin{cases} 1, & \varsigma \geq \theta \quad \theta > 0 \\ 0, & \varsigma < \theta \quad \theta > 0 \\ 0, & \varsigma \geq \theta \quad \theta < 0 \\ -1, & \varsigma < \theta \quad \theta < 0 \end{cases}$$

A similar generalization process has been made possible the generation of multiple scroll attractors in several directions in the phase plane. These are called the 1D multi-scroll for $n \times 1$ scrolls, 2D for $n \times m$, and 3D for $n \times m \times p$ scrolls. Then, for the last two cases, one has:

$$\mathbf{\Phi} = \begin{pmatrix} f_1(x_2) \\ f_1(x_3) \\ f_1(x_1) \end{pmatrix}, \quad \mathbf{B}_{2D} = \begin{pmatrix} -1 & 0 & 0 \\ 0 & 0 & 0 \\ 0 & 0 & a \end{pmatrix}, \quad \mathbf{B}_{3D} = \begin{pmatrix} -1 & 0 & 0 \\ 0 & -1 & 0 \\ 0 & 0 & a \end{pmatrix} \tag{1.15}$$

respectively, and $f_3(x)$ as described in [34]. Some other relevant designs in this context are presented in the following.

### 1.4.5 Lü saturated function series

Based on the canonical system, a saturated function approach was proposed in [41], as this may be obtained by any linear amplifier on slewing mode:

$$\mathbf{A} = \begin{pmatrix} 0 & 1 & 0 \\ 0 & 0 & 1 \\ -a & -b & -c \end{pmatrix}, \qquad \mathbf{\Phi} = \begin{pmatrix} f(x_1; k_1, h_1, p_1, q_1) \\ f(x_2; k_2, h_2, p_2, q_2) \\ f(x_3; k_3, h_3, p_3, q_3) \end{pmatrix}, \tag{1.16}$$

$$f(x; k, h, p, q) = \begin{cases} (2q+1)k, & x > qh + 1 \\ k(x - ih) + 2ik, & |x - ih| \leq 1, -p \leq i \leq q \\ (2i+1)k, & ih + 1 < x < (i+1)h - 1, -p \leq i \leq q - 1 \\ -(2p+1)k, & x < -ph - 1 \end{cases} \tag{1.17}$$

where parameters $k = 10$ is the slope of the saturated function, and $h = 4$ is the saturated *time-delay*, $a = b = c = d_1 = d_2 = d_3 = 0.7$; $p$ and $q$ are positive integers; matrix **B** is chosen to produce 1D, 2D and 3D grid scroll attractors, as follows

$$\mathbf{B}_{1D} = \begin{pmatrix} 0 & 0 & 0 \\ 0 & 0 & 0 \\ d_1 & 0 & 0 \end{pmatrix}, \quad \mathbf{B}_{2D} = \begin{pmatrix} 0 & -d_2/b & 0 \\ 0 & 0 & 0 \\ d_1 & d_2 & 0 \end{pmatrix}, \quad \mathbf{B}_{3D} = \begin{pmatrix} 0 & -d_2/b & 0 \\ 0 & 0 & -d_3/c \\ d_1 & d_2 & d_3 \end{pmatrix}. \tag{1.18}$$

### 1.4.6 A third order hysteresis model

Hysteresis based functions have been used to produce chaos as well. Some of the pioneer works belong to Saito [6], R. Newcomb and N. El-Leithy [7]. However their implementation on scroll-based attractors have been proposed later by different approaches [3, 4, 8], in fact this behavior was exploited in all the cases of step functions [34], suppose matrix **A** as described before with constants $a \approx 0.8$ and

$$\mathbf{\Phi} = \begin{pmatrix} h(x_1) \\ h(x_2) \\ h(x_3) \end{pmatrix}, \tag{1.19}$$

$$h(x, p_1, q_1) = \begin{cases} -p_1, & x < -p_1 + 1 \\ i, & i - 1 < x < i + 1, i = \{-p_1 + 1, ..., q_1 - 1\} \\ q_1, & x > q_1 - 1 \end{cases},$$

with matrix **B** simply growing like identity matrix to generate $p_1 + q_1 + 1$, $(p_1 + q_1 + 1) \times (p_1 + q_1 + 1)$, or $(p_1 + q_1 + 1) \times (p_1 + q_1 + 1) \times (p_1 + q_1 + 1)$ scrolls, respectively:

$$\mathbf{B}_{1D} = \begin{pmatrix} 1 & 0 & 0 \\ 0 & 0 & 0 \\ 0 & 0 & 0 \end{pmatrix}, \quad \mathbf{B}_{2D} = \begin{pmatrix} 1 & 0 & 0 \\ 0 & 1 & 0 \\ 0 & 0 & 0 \end{pmatrix}, \quad \mathbf{B}_{3D} = \begin{pmatrix} 1 & 0 & 0 \\ 0 & 1 & 0 \\ 0 & 0 & 1 \end{pmatrix}. \tag{1.20}$$

### 1.4.7 Transconductor based multi-scroll attractors

Another interesting nonlinear function was proposed by Özoguz [26] and is based on the trasconductance function of the *tanh()* natural response of the differential pair:

$$\mathbf{A} = \begin{pmatrix} 0 & 1 & 0 \\ 0 & 0 & 1 \\ 0 & -a & -a \end{pmatrix}, \qquad \mathbf{\Phi} = \begin{pmatrix} f(x_1) \\ 0 \\ f_1(x_2) \end{pmatrix}, \tag{1.21}$$

$$f(x) = \sum_{j=-N}^{M} (-1)^{j-1} tanhk(x - 2j), \tag{1.22}$$

with $a$=0.25, $M$ and $N$ positive integers related to the number of scrolls, and matrix $\mathbf{B}$ chosen to generate 1D or 2D scroll attractors, as follows:

$$\mathbf{B}_{1D} = \begin{pmatrix} 0 & 0 & 0 \\ 0 & 0 & 0 \\ -a & 0 & 0 \end{pmatrix}, \quad \mathbf{B}_{2D} = \begin{pmatrix} 0 & 0 & -a \\ 0 & 0 & 0 \\ -a & 0 & 0 \end{pmatrix}. \tag{1.23}$$

Nowadays, the topics related to multi-scroll oscillators and the circuits to synthesize them constitutes an important field for research, due to the high amount of works; and the existence of new material such as the multi-scroll Lorenz oscillator [61], which is too complex that requires a digital signal processor, the contrasting first order $n$-scroll system in [3]. Or the circuits reported in [62, 63], which only show simulation based results.

## 1.5 Integrated Implementations of Chaotic Oscillators

The afore-mentioned designs have been principally implemented by discrete (off-the-shelf) circuit in voltage mode and generally use Opamps for all the required operations (an exception is the classical implementation of the Chua's oscillator [39]). Moreover, the use of more recent mixed mode active devices such as the CCII [16, 64–66], CFOA [34–37] or UGC [32, 33, 67] is letting the implementation to be smaller since the variables are identified directly from the currents or voltages in the circuit indistinctly.

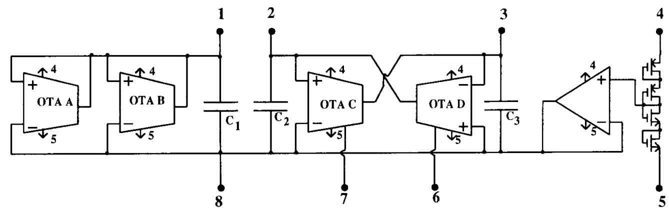


Figure 1.2: Proposed Chua's oscillator using OTAs and different supply levels [25].

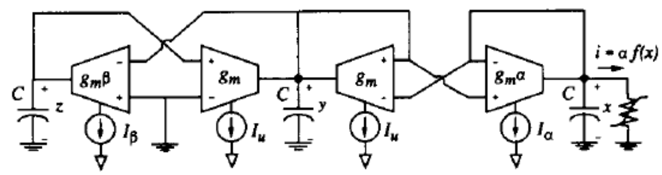


Figure 1.3: Proposed Chua's oscillator in [49].

Many is to be made in the CMOS implementation, since Opamps and OTAs are the only used active devices [9]. A brief description of the existent designs will be made below.

*Cruz and Chua Design*

One of the first monolithic implementation was the Chua's oscillator by Chua itself as shown in Fig. 1.2, [25]. The circuit is an adaptation of that in Fig. 1.1 using external resistor connected to points 1 and 2 (to adjust the nonlinear function gain). The nonlinear function was generated by two OTAs with different transconductance gains (A and B) as well as bias current capability. The inductor was obtained from the gyrator (C, D and capacitor $C_3$). Finally, an internal reference ground is used to avoid supply variations (Opamp). See Table 1.6 for more details.

*Rodríguez and Delgado Design*

A similar Chua's implementation was realized based on the state variable perspective [49] (the normalized system). Gm-C integrators have been used by arranging identical OTAs in parallel. The nonlinear function was realized by two parallel OTAs with independent bias control. A simplified version is shown in Fig. 1.3, see also Table 1.6.

*Elwakil et al. Design*

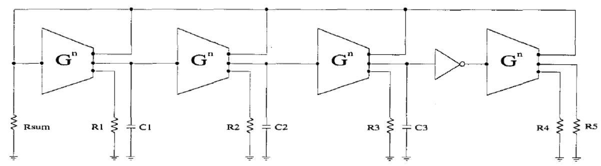


Figure 1.4: Proposed two-scroll oscillator in [47].

The two-scroll version of the originally proposed canonical system was also been realized by selecting the capacitance or resistances of the loads $Z_1$, $Z_2$ in Fig. 1.4 [47]. Thus allowing to have positive and negative integrals. All the system parameters were available since all the loads were externally connected. The nonlinear function has been made by the use of as simple inverter as a comparator, see Table 1.6.

*Fujiwara et al. Design*

The proposed circuit [29] was built as the Cruz and Chua's design, a simulated inductor was used as well as transistors in linear mode as the circuit resistor. A particular change is noted in the design of the nonlinear function, since FGMOS have been exploited as switches in the current path. In this way, the PWL design can grown by connecting several parallel cells each of them using several external controls to adjust the slope and breakpointos of the V-to-I characteristic as shows Fig. 1.5. By reporting a 3-scroll experimental attractor, a first multi-scroll oscillator was obtained by a fully integrated design, however the poor CMRR did not allow it to prove more scroll generation. Table 1.6 enumerates some technical details.

## 1.6 Thesis Objectives

The importance of continuous chaotic oscillators is principally lying in the potential applications been still on research. The need of a CMOS integrated multi-scroll design arises with the appearance of multi-scroll oscillators, and the very limited amount of integrated realizations.

A key point is that since these realizations are few, there is not enough criteria for selecting the design requirements for nonlinear systems. Also, the performance of such

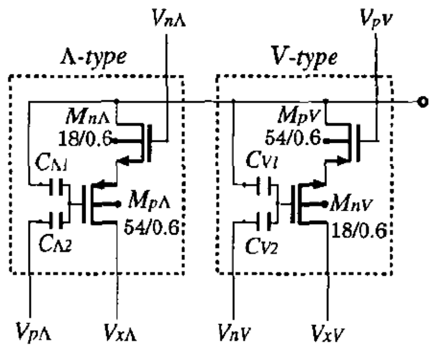


Figure 1.5: First proposed three-scroll integrated oscillator based in the use of FGMOS transistors [29].

designs based on non-traditional active devices is unknown at integrated level.

In this way, the motivation of this thesis is to stretch the gap between multi-scroll systems and the integrated circuit realization by analyzing the dynamical system, obtaining the circuit requirements, proposing innovative design based on an FGMOS-based voltage-to-current cell for realizing PWL functions, and showing the experimental results as well as parameter variation analysis.

The main goal is to design a CMOS chaotic oscillator capable to generate multi-scroll oscillators. The most relevant aspects and particular objectives are cited below.

1. Analyze the different alternatives in the selection of the chaotic system. Generate behavioral models.

2. Analyze the impact on the number of scrolls and the system chaotic regime.

3. Obtain design criteria for the synthesis of multi-scroll chaotic oscillators.

4. Design of CMOS compatible multi-scroll oscillator and analyzing the frequency limitations due to circuit parasitic effects.

5. Realization of circuit layout and simulations.

6. Validation of the design methodology by obtaining the desired behavior experimentally and with process variations.

7. Identification of further design enhancements.

Table 1.2: Suykens parameters and functions.

| Scroll type | Parameters |
|---|---|
| Even | $\alpha$=9; $\beta$=14.286; $m$=[-1/7, 2/7, -4/7, 2/7, -4/7, 2/7,...]; $c$=[1, 2.15, 3.6, 8.2, 13,...] |
| Odd | $\alpha$=9; $\beta$=14.286; $m$=[0.9/7, -3/7, 3.5/7, -2.4/7, 2.52/7, -1.68/7, 2.52/7, -1.68/7,...]; $c$=[1, 2.15, 3.6, 6.2, 9, 14, 25,...] |

Table 1.3: Zhong parameters.

| Scroll number | Parameters |
|---|---|
| $2N$ | $[b_1...b_9] = [0.1, 1.1, 1.55, 3.2, 3.85, 5.84, 6.6, 8.7, 9.45]$ |
| $2N-1$ | $[b_2...b_9] = [0.8, 1.4, 3.2, 3.9, 5.8, 6.4, 8.3, 9.2]$ |

Table 1.4: Simin Yu scroll type nonlinear functions.

| Scroll number | $f_1(x)$ | $f_2(x)$ |
|---|---|---|
| $2N$ | $\xi\{x - A_1[-sgn(x) + \sum_{i=0}^{N-1}(sgn(x + 2iA_1) + sgn(x - 2iA_1))]\}$ | $A_2[-sgn(x) + \sum_{j=0}^{N-1}(sgn(x + 2jA_2) + sgn(x - 2jA_2))]$ |
| $2N+1$ | $\xi\{x - A_1[\sum_{i=0}^{N-1}(sgn(x+(2i+1)A_1) + sgn(x-(2i+1)A_1))]\}$ | $A_2[\sum_{j=0}^{N-1}\{sgn(x + (2j + 1)A_2) + sgn(y - (2j+1)A_2)\}]$ |

Table 1.5: Simin Yu scroll type linear functions.

| Scroll type | Matrix **B** |
|---|---|
| 1D | $\mathbf{B} = \begin{pmatrix} -\alpha & 0 & 0 \\ 0 & 0 & 0 \\ 0 & 0 & 0 \end{pmatrix}$ |
| 2D | $\mathbf{B} = \begin{pmatrix} -\alpha & -\alpha & 0 \\ 0 & \beta & 0 \\ 0 & 0 & 0 \end{pmatrix}$ |

Table 1.6: CMOS oscillators: technical data.

| Parameters | Cruz and Chua [25] | Rodríguez and Delgado [48, 49] | Elwakil et al. [47] | Fujiwara et al. [29] |
|---|---|---|---|---|
| Technology ($\mu$m) | 2 | 2.4 | 1.2 | 0.35 |
| Biasing (V) | - | $\pm$2.5 | $\pm$2.5 | $\pm$1.65 |
| Center frequency (KHz) | 160 | - | 118 | 7000 |
| Nonlinear function strategy | Distinct bias currents and saturation | Distinct bias currents and saturation | Simple inverter | Switching currents by FG-MOS |

# Chapter 2

# Multi-Scroll Chaotic Oscillators

In this Chapter some important concepts on chaos are reviewed. Also, two ways for proving chaotic behavior, the analytic basis by the Shil'nikov Homoclinic and Heteroclinic Theorems and the numerical method based in the computation of the Lyapunov exponents (LE), are introduced.

A LE analysis is performed over some of the already known multi-scroll systems using forward Euler, fourth order Runge-Kutta and Matlab ODE 45 integration routines. The relation between the number of scrolls and the corresponding exponents reveal fewer interaction than with the system parameters.

The main conclusion [68] is that the number of scrolls has low relevance for the system long term complexity. Besides, it is observed that the Lyapunov exponents are independent on the number of scrolls for saw-tooth based systems, since they only have a single Jacobian. This is in agreement with entropy computations given in [69].

A new multi-scroll saw-tooth based system is presented in [67, 70], and prior analysis of the double-scroll version of this system is given in [48]. This system will be chosen to perform integrated circuit design due to the integer relation on coefficients and the modularity of the nonlinear function, while LE is considered of less relevance. However it is shown that by modulating the state space, the LE exhibit proportional scaling.

## 2.1 Continuous Chaos Definitions

Although mentioned in Chapter 1.1, some concepts of chaos have not been explicitly defined. This section is dedicated to the explanation of the main concepts which are related to continuous chaotic behavior and the appearing of such phenomena under the Shil'nikov condition.

*Chaotic system*: There is no universal definition for chaos, however, the scientific community agrees that there are some relevant characteristics of chaotic behavior [71, 72]

- Is generated from a deterministic dynamical system [73].
- No periodicity [71].
- Ergodicity [11].
- Sensitivity to initial conditions (has at least one positive Lyapunov exponent) [74, 75].

In general, many chaotic systems are represented (as seen in Section 1.4, by a $n$-order continuous nonlinear dynamical equation of the form

$$\dot{\mathbf{x}} = \mathbf{f}(\mathbf{x}) \tag{2.1}$$

where $\mathbf{x} \in \Re^n$; moreover, chaos cannot be obtained in continuous systems of *effective* order less than three, since solutions must be unique (no intersection is allowed)[71, 75]. The effectiveness is used here to avoid confusion with non-autonomous or delay-based systems, in which the required order is apparently less [3, 8, 72].

*Dynamical systems.* A system that evolves in time according to some rule or process [71].

*Deterministic system.* Dynamical system that can be described by differential equations for continuous systems; or differences equations for discrete ones. These may be linear or non-linear. In all cases, the future states (sometimes predicted and other not) will always be the same for the same initial conditions.

*Non periodicity.* It is well known that any random process will have no period. However, chaos and quasi-periodic systems can be expressed in equations and still present no period. Quasi-periodic systems, can be decomposed by a finite set of harmonics separated by frequencies with irrational relation. In contrast, chaos presents a continuous spectra, thus proving the existence of uncountable harmonic components.

*Ergodicity.* A system is considered to be ergodic if the trajectory visits all the points in the attractor ($t \to \infty$). For convenience sometimes the concept of quasi-ergodic system is used indistinctly, which implies that in a long time, the trajectory will pass arbitrarily close to any point in the attraction region.

*Sensitivity to initial conditions.* This property implies that two near initial conditions will separate as the system evolves in time and eventually generate uncorrelated trajectories no matter how short is the distance between them. In fact any set of neighboring initial conditions will spread along the attractor in a exponential way. This is the reason for the existence of positive Lyapunov exponents.

This implies that in the practice, such a system will be really unpredictable, since no initial condition can be given without an uncertainty margin (say $\parallel \delta_0 \parallel$). In such case, the prediction of the system response with some tolerance margin ($a$) may be pointless if the rate of grow ($\lambda$) is exponential, according to [71] the time of prediction will be minimal:

$$t_{horizon} \propto \frac{1}{\lambda} ln \frac{a}{\parallel \delta_0 \parallel} \tag{2.2}$$

*Lyapunov exponents.* These are used to determine the stability of periodic and non periodic solutions as well as equilibrium points and are considered to be the indicator of initial condition dependence. Furthermore, they represent the rate of expansion or contraction of the flow (the neighboring trajectories) which varies somehow along the attractor, but has an exponential feature in chaotic systems.

In linear systems, these exponents are related to the real part of the system eigenvalues. But for n-order chaotic systems, they correspond to the n-directions of growing of an n-ellipsoid of neighboring initial conditions. In order to characterize the system long therm dynamics and considering the ergodicity, the Lyapunov exponents are obtained by averaging over many points in the trajectory.

A detailed description for their obtention is found in Appendix B.

*Autonomous system.* Those that have no explicit dependence with time. The dependence on time of each state variable is implicit since the system is dynamical. However, any future state can be obtained by only the value of the present ones. In fact, any $n$-order non-autonomous dynamical system can be rewritten as a $n+1$-order autonomous counterpart by simply taking time as a new state with unity grow rate (time derivative).

*System equilibriums (Steady states).* In opposition to linear autonomous systems in which there is only one equilibrium point (the origin), the nonlinear counterpart can present a variety of equilibriums $\mathbf{x_e}$. Some of them are attractors, since all are constant solutions for the differential equation and can be calculated by solving

$$f(\mathbf{x}_e) = 0. \tag{2.3}$$

From the theory of linear systems, some equilibriums can be cited such as [74, 75]: stable nodes and stable spirals (attractive), unstable nodes or unstable spirals (repulsive), centers (in energy conservative systems) or saddle points (which have stable eigenvectors as well as unstable ones).

In this context, a dynamical system may have stable behavior whenever trajectories are associated with negative eigenvalues and eigenvectors, and unstable behavior if trajectories are governed by positive eigenvalues.

*Attractor.* Sometimes called limit set, is a set of points to which near trajectories are attracted and fulfill the following: (a) for any initial conditions on them, the solutions remain on them forever; (b) there exist an open set of initial conditions (basin of attraction for the complete set) which is attracted to them; (c) these points form the minimal set with these properties.

*Chaotic attractor.* Also called strange attractor is an attractor that also has dependence to initial conditions as well as fractional dimension. These attractors appear in the phase space (the region in which the states or solutions are plotted one against the others) and resembles complex non intersected geometries.

*Bifurcation.* Is the process of creation and destruction of equilibriums in nonlinear systems. A bifurcation diagram is sometimes the graphical representation of the place of stable and unstable equilibriums.

*Orbit diagram.* Called sloppily bifurcation diagram by a huge amount of books and articles [76], these are used to represent the stable points in the bifurcation process after the transient behavior. Along with the Lyapunov exponents, these diagrams can give an insight into the system behavior over a sweep on some parameter. See details in Appendix A.

*Homoclinic orbit.* A trajectory that connects one equilibrium point with itself. In most cases these equilibriums need to have stable and unstable trajectories (there are saddle points).

*Heteroclinic orbit.* A trajectory that connects one equilibrium point with other.

*Heteroclinic loop.* A trajectory loop made by two or more heteroclinic orbits.

*Orbital period.* This is a measure respecting to the frequency of chaotic (non-periodic) systems. It quantifies the typical time required for a trajectory to traverse the hole attractor; i.e. to visit all the equilibrium points.

### 2.1.1 Lur'e Representation

A recently proposed representation for chaotic systems is named the Lur'e representation: a linear system interconnected by feedback to a static nonlinearity that satisfies a sector condition [34]. Which is supposed to describe the circuit as a linear system with nonlinear feedback as

$$\dot{\mathbf{x}} = \mathbf{A}\mathbf{x} + \mathbf{B}\sigma(\mathbf{C}\mathbf{x}). \tag{2.4}$$

In this way, the saturated function based system is described by $\mathbf{A}$, $\mathbf{B}$ and $f()$ in (1.16), (1.17) and (1.18) is, for 1D to 3D:

$$\mathbf{C} = \mathbf{I}_{3\times 3}, \quad \sigma_{1D} = \begin{pmatrix} f_1() \\ 0 \\ 0 \end{pmatrix}, \quad \sigma_{2D} = \begin{pmatrix} f_1() \\ f_2() \\ 0 \end{pmatrix}, \quad \sigma_{3D} = \begin{pmatrix} f_1() \\ f_2() \\ f_3() \end{pmatrix}. \tag{2.5}$$

## 2.2 Homoclinic and Heteroclinic chaos

There are many process that gives birth to chaos, most of them still unknown. In this section the chaos generation is reviewed by the Shil'nikov criteria [77, 78].

First, a saddle focus equilibrium point $\mathbf{x_e}$ is taken from (2.1) by first obtaining the Jacobian derivative of $\mathbf{f}$ at $\mathbf{x_e}$ and having a real and a complex conjugate of eigenvalues:

$$\gamma,\, \sigma \pm j\omega, \quad \gamma\sigma < 0, \quad \omega \neq 0 \tag{2.6}$$

with $\gamma$, $\sigma$, and $\omega$ real numbers.

These eigenvalues are used to find a closed loop between the 2-D eigenplane corresponding to the complex conjugate and the 1-D eigenline of the real eigenvalue. Such a trajectory may be part of one or two similar equilibriums $\mathbf{x_e}$ (homoclinic or heteoclinic trajectory, respectively).

The *Shil'nikov homoclinic method* states that in a third order autonomous system (2.1) if:

1. The corresponding eigenvalues of the saddle focus equilibrium point satisfy the Shil'nikov inequality:
$$|\gamma| > |\sigma| > 0. \tag{2.7}$$
2. There exist a homoclinic orbit based at $\mathbf{x}_e$.

Then the system shows *homoclinic chaos*.

The *Shil'nikov heteroclinic method* probes *heteroclinic chaos* by using two equilibrium points $\mathbf{x}_{e1}$ and $\mathbf{x}_{e2}$. The conditions are:

1. The corresponding eigenvalues of both equilibrium points are saddle foci that satisfy the Shil'nikov inequality:

$$|\gamma_1| > |\sigma_1| > 0, \qquad |\gamma_2| > |\sigma_2| > 0, \qquad \sigma_1\sigma_2 > 0 \text{ or } \gamma_1\gamma_2 > 0. \tag{2.8}$$

2. There exist a heteroclinic orbit trough $\mathbf{x}_{e1}$ and $\mathbf{x}_{e2}$.

For further reading, a nice analysis on the Chua's oscillator homoclinic chaos is found in [78].

## 2.3 Notes on Lyapunov Exponents

Since the design of chaotic systems is highly qualified to the Lyapunov exponents of the system, some of the concerning products of this work are explained below.

### 2.3.1 Lyapunov exponents and the number of scrolls

The appearance of the attractor is greatly changed by the number of equilibrium points of the system and consequently on the number of scrolls. Previous work on the characteristics related to the number of scrolls is found in [69]. There, the chaotic signal of the canonical system with step-based PWL function [34] was sampled to obtain $1 \times 10^6$ bits and the theoretic entropy of the random stream was computed by algorithm in [79] and was observed to grow about 5%, among the 3 to 10-scroll attractors; for the rest of them, the change was about 0.5%.

Thus an analysis with respect to the Lyapunov exponents was performed to observe the sensitivity changes of other multi-scroll chaotic systems [68]. The selected systems where:

(a) the Zhong generalization of the Chua's system (Section 1.4.3),

(b) the Yu modified Chua's circuit (Section 1.4.2),

(c) the saturated function series based system (Section 1.4.4), and

(d) the saw-tooth based generalized Chua's system (Section 1.4.3).

The Lyapunov exponents of the four systems were computed using algorithm in Appendix B on around 500000 steps with initial conditions $\mathbf{x}_0 = [0.1, 0, 0]$ (observe that the ergodicity maintains a unique long term exponent). The integration was carried out by Forward-Euler (FE), fourth order Runge-Kutta (RK4), both fixed step algorithms; and the Matlab ODE45 routine with variable step. The computed positive exponent is summarized in Tables 2.1, 2.2 and 2.3. The results were in agreement for all the integration algorithms.

The results show similar conclusion than [69], the positive exponents grow less than 10% for more than 4 scrolls in (a), 3 scrolls in (b) and (c) and remain constant in (d). In all the cases the influence on the system parameters to the characteristic exponent was greater than the number of scrolls in the attractor.

Also, it was observed that the negative exponent tends to decrease in magnitude in (a) and (b), as the positive one increases. In (c) the relation goes backwards since the sum of all the system exponents keeps constant (this sum is associated with the system dissipativity [71]). Moreover, in the case of (d), there are no variations with the number of scrolls since the system is based in a single slope saw-tooth PWL function which makes the Jacobian constant and unique.

Thus, from the electronic design point of view, it could be comparable to generate few scrolls since the generation of large number of scrolls leads one to large circuits while the Lyapunov exponents are quite similar.

The exploration on these exponents is still an open field, since there is no single direction of complexity; if the local exponents [80, 81] are considered, perhaps for mixing applications, there are still many issues to be investigated.

## 2.4 On the design of a multi-scroll system

A multi-scroll system can be designed by taking the Chua's system reported by Rodriguez-Vazquez and Delgado-Restituto [48] which is expressed in (2.9). Equilibrium points may be created by breaking the nonlinear function. Chaotic behavior will arise with the appropriate selection of the system coefficients to accomplish the inequality and generate bond orbits as in [46]. This process may be performed in several forms, however, the application of saw-tooth functions has shown quick results. An example is in a variation of the Chua's system proposed by Simin Yu [45]. Other works in which this function appears are found in [62, 82].

$$\begin{aligned}
\dot{x}_1 &= \alpha x_2 + f(x_1) \\
\dot{x}_2 &= \alpha x_1 - \gamma x_2 - \alpha x_3 \\
\dot{x}_3 &= \beta x_2
\end{aligned} \tag{2.9}$$

Thus, it was proposed [70] to use a saw-tooth function such as (2.10) for $2n+1$ scrolls or (2.11) for $2n$ scrolls, $k = 1...n$:

$$f(x) = \begin{cases} -\xi x & |x| \leq B_p \\ \xi(2ksgn(x) - x) & |x| \leq B_p(2k+1) \\ & |x| > B_p(2k-1) \end{cases} \tag{2.10}$$

$$f(x) = \xi((2k-1)sgn(x) - x) \qquad \begin{array}{l} |x| \leq 2kB_p \\ |x| > 2B_p(k-1) \end{array} \tag{2.11}$$

For the system's particular nonlinear function, the Jacobian can be considered constant, this maintains mathematical simplicity while the system complexity is the same for any number of scrolls in terms of the Lyapunov exponents [68].

Thus, the dynamical system given by (2.9), with parameters $\alpha = 3$, $\beta = 4$, and $\gamma = 1$ and a saw-tooth function (based on a parallel array of comparators and a negative amplifier) will generate a multi-scroll attractor. A Lyapunov analysis reveals $\lambda_1 = 0.222$, $\lambda_2 = 0$, $\lambda_3 = -1.913$ for the selection of the slope parameter $\xi = 0.8$. Figure 2.1 reveals the chaotic behavior along with the bifurcation in variable $x_2$, the other bifurcation diagrams (most affected by the number of scrolls) are shown in Fig. 2.2 for a double-scroll attractor ($n = 1$).

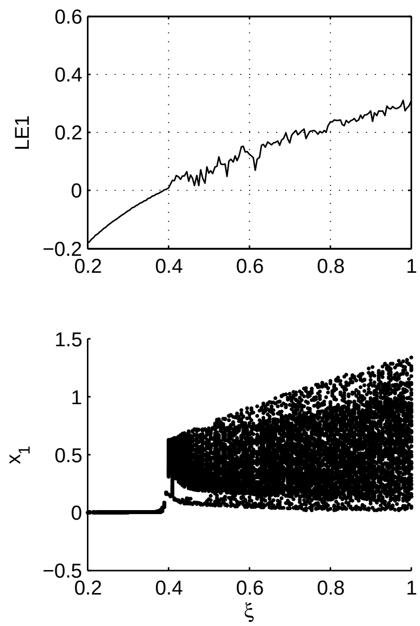


Figure 2.1: Lyapunov exponents and bifurcation diagram of the multi-scroll system.

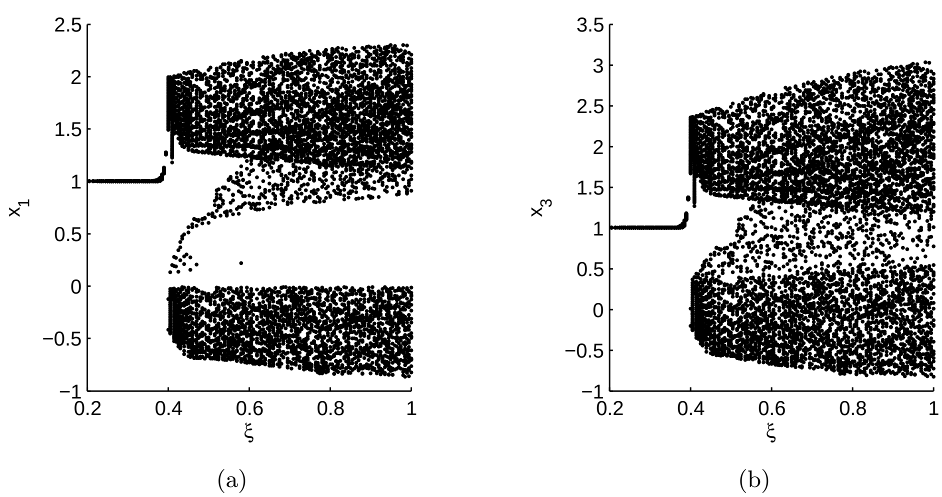


Figure 2.2: Bifurcation diagram of (a) state $x_1$, and (b) state $x_3$.

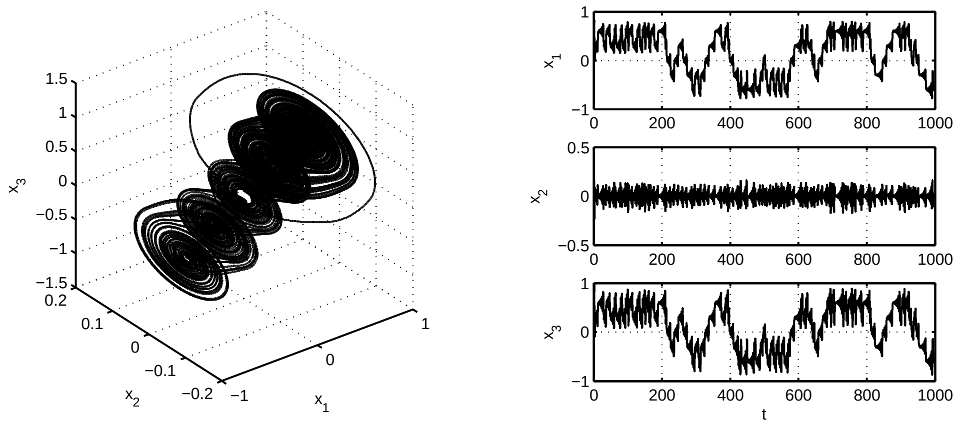


(a) (b)

Figure 2.3: The system 5-scroll attractor in (a) phase space, and (b) time.

The above description corresponds to a typical dissipative system $\dot{\mathbf{x}} = \mathbf{f}(\mathbf{x})$ with $\nabla V = \frac{\delta f_1}{\delta x_1} + \frac{\delta f_2}{\delta x_2} + \frac{\delta f_3}{\delta x_3} = -\xi - \gamma < 0$. It has the equilibrium points $[\pm(2kBp - 1), 0, \pm(2kBp-1)]$ for even scroll-number, and $[\pm 2kBp, 0, \pm 2kBp]$ for odd scroll-number. The eigenvalues (at the origin) are given by $-2.1309$ and $0.1655 \pm j2.1161$, which corresponds to saddle-foci equilibriums with 1-D stable manifold and a 2-D unstable manifolds.

A typical 5-scroll attractor ($n = 2$) may be seen in Fig. 2.3. The frequency spectra is shown in Fig. 2.4.

### 2.4.1 Increasing Lyapunov exponents

In spite of the analysis discussed above, a proposal for increasing the Lyapunov exponent independently on the number of scrolls is now examined. Considering that these exponents provide from a generalization of the system eigenvalues. Suppose a linear $n$-order system in the form:

$$\dot{\mathbf{x}} = \mathbf{A}\mathbf{x} \tag{2.12}$$

with $\mathbf{A}$ a real full-range $n \times n$ matrix. Since this matrix is linearly independent, its

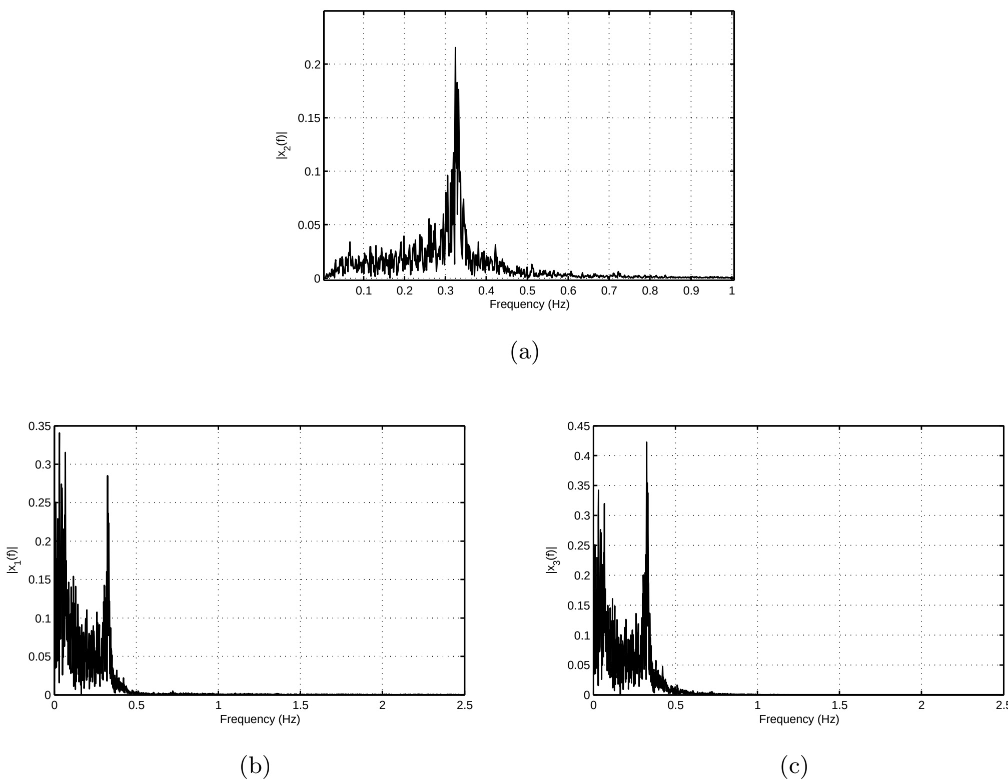


Figure 2.4: System FFT (a) $x_2$, (b) $x_1$, and (c) $x_3$.

eigenvalues may be obtained by turning it into a diagonal matrix; thus for a constant $k$, the product $k\mathbf{A}$ will scale all the eigenvalues by $k$. This constant may be regarded as the rate of change of the dynamical system. This suggests that in a chaotic system, the Lyapunov exponents can be varied if the system dynamics rate is increased.

This is in fact incorrect because the Lyapunov exponent is used to give a perspective on the rate of grow for autonomous systems [75]. The independence on time can be observed in term $\frac{1}{T}$ (with $T$ the total time used in the computation, see Appendix B and Eq. B.1) for details. However, if the term $k$ is made variable (say $k_v$), this no longer holds.

The Lyapunov exponent of an arbitrary autonomous chaotic system can be increased if the integrator gain is made variable; say, with dependence of some combination of the system states only to keep the system order. Suppose the nonlinear system $\dot{\mathbf{x}} = f(\mathbf{x})$ as given by (2.9) in two scrolls, and a variable gain $k_v$ in the form

$$\begin{aligned} \dot{\mathbf{x}} &= k_v(x_1, x_2) f(\mathbf{x}) \\ k_v(x_1, x_2) &= p(x_1 + m x_2 + q). \end{aligned} \tag{2.13}$$

If the selection of coefficients $p = w/10$, $q = 6$ and $m = 5$ is made to allow the integration gain to vary in a positive range, say roughly $k_v \in [\epsilon ... w)$ for some $\epsilon > 0$, then one have an approximate linear relation of the Lyapunov exponents to the maximum integration gain $w$, as suggests Fig. 2.5. Here, by using $w = 1$, the computed exponents were $\lambda_1 = 0.107$ and $\lambda_3 = -0.851$; by scaling $w$ to 10, a similar change was found $\lambda_1 = 0.954$ and $\lambda_3 = -8.077$. The zero exponent remained unchanged.

The system phase and time response is shown in Fig. 2.6. Note that the attractor remains unchanged since it is independent on time. Besides, it can be seen that the integration rate follows the values of signal $p(x_1 + 5x_2 + q)$. This behavior has been also observed with non-PWL chaotic systems such as the Lorenz system.

On the other hand, the FFT analysis performed in Fig. 2.7 shows that as the nonlinear signal is in fact being modulated by a linear combination of itself. Wider signal spectra can be readily achieved respecting the original system (Fig. 2.4).

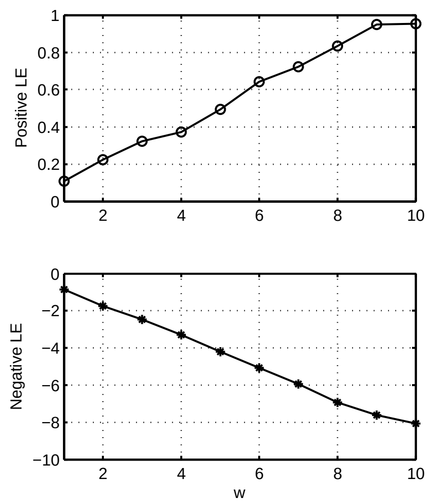


Figure 2.5: Lyapunov exponents for the proposed system as a function of the integration gain $w$.

As a conclusion, while the Lyapunov exponents prove to be hard to improve (increase) with the number of scrolls and the system chaotic behavior is restricted to a finite parametric region. The solution for higher Lyapunov exponent may be based in the use of non-constant integration rates.

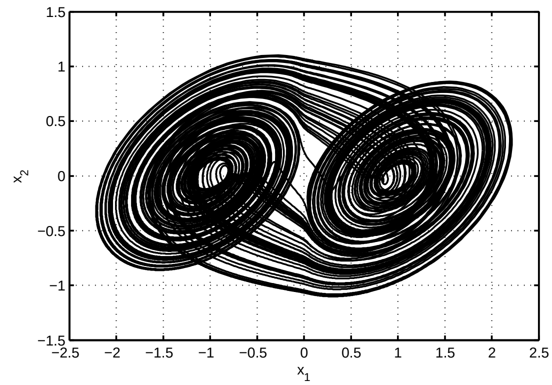


(a)

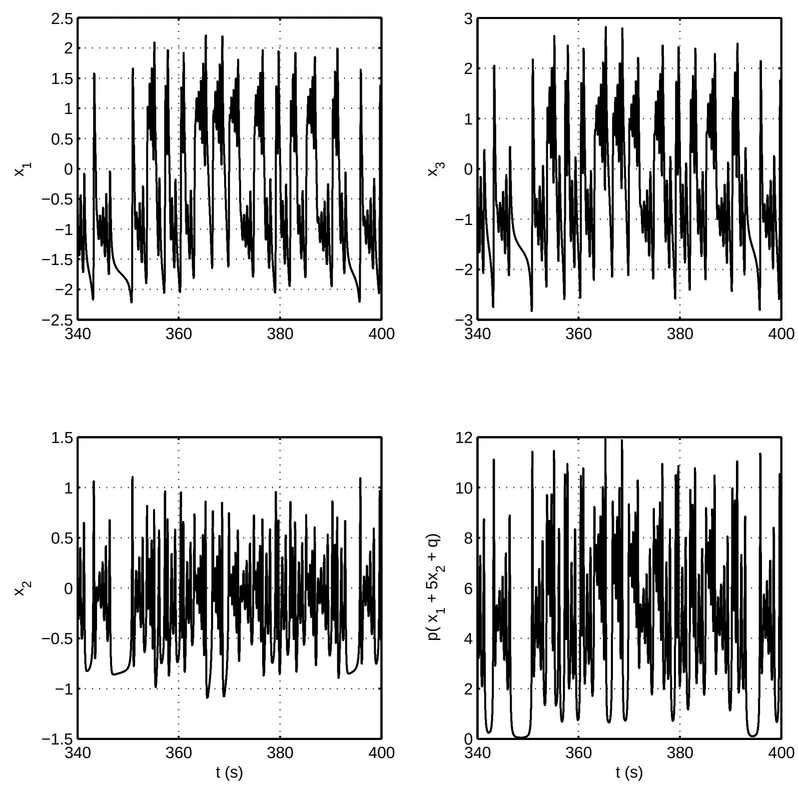


(b)

Figure 2.6: Variable integration of the proposed system for a double-scroll attractor $w = 10$ in (a) phase space, and (b) time.

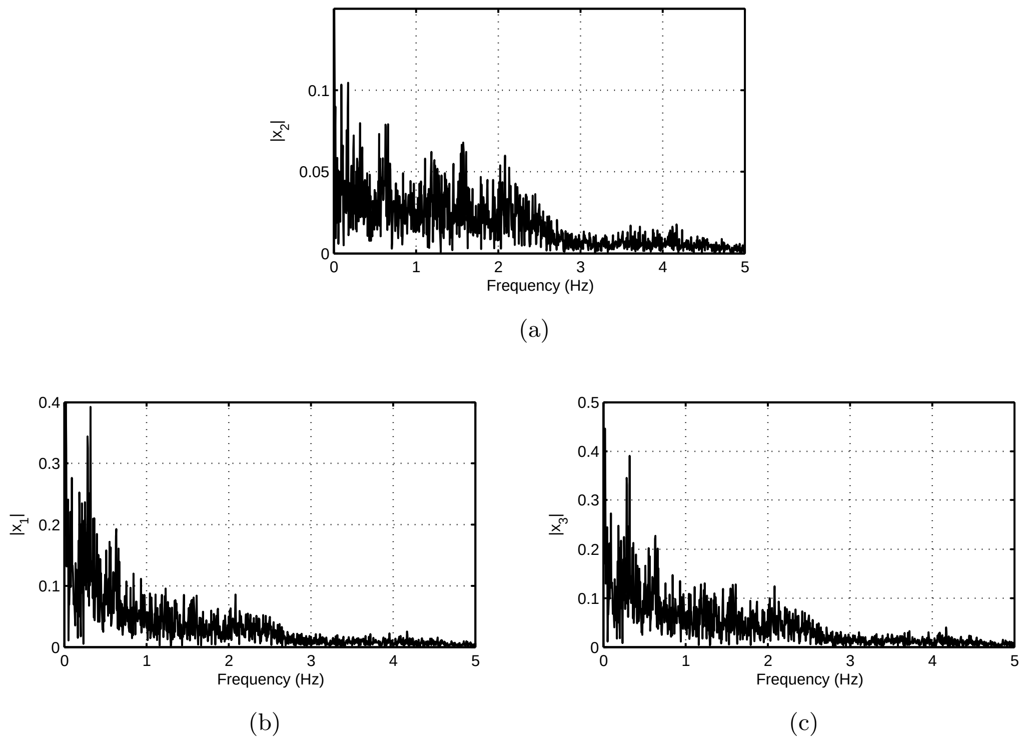


Figure 2.7: FFT analysis performed to the system (2.13) with $w = 10$ for signals (a) $x_2$, (b) $x_1$, and (c) $x_3$.

Table 2.1: Positive Lyapunov exponent for the Zhong generalization (a).

| Scrolls | FE | RK4 | ODE45 |
|---|---|---|---|
| 2 | 0.40884 | 0.23720 | 0.24144 |
| 3 | 0.49882 | 0.36999 | 0.37958 |
| 4 | 0.50620 | 0.41298 | 0.41808 |
| 5 | 0.52163 | 0.41002 | 0.41051 |
| 6 | 0.55911 | 0.44154 | 0.43760 |
| 7 | 0.57303 | 0.44652 | 0.45613 |
| 8 | 0.63320 | 0.49336 | 0.51609 |
| 9 | 0.64162 | 0.53176 | 0.51772 |
| 10 | 0.68270 | 0.52967 | 0.54934 |

Table 2.2: Positive Lyapunov exponent for the Yu generalization (b).

| Scrolls | FE | RK4 | ODE45 |
|---|---|---|---|
| 2 | 0.43009 | 0.41390 | 0.41119 |
| 3 | 0.46237 | 0.40714 | 0.41378 |
| 4 | 0.47426 | 0.42061 | 0.40292 |
| 5 | 0.48414 | 0.39354 | 0.40152 |
| 6 | 0.41400 | 0.38767 | 0.40267 |
| 7 | 0.45197 | 0.39254 | 0.38952 |
| 8 | 0.48472 | 0.41582 | 0.42209 |
| 9 | 0.47069 | 0.39259 | 0.40155 |
| 10 | 0.48958 | 0.65408 | 0.66798 |
| 11 | 0.70011 | 0.66261 | 0.66900 |
| 12 | 0.68698 | 0.65842 | 0.68653 |
| 13 | 0.69638 | 0.66850 | 0.66162 |
| 14 | 0.68121 | 0.66582 | 0.67615 |
| 15 | 0.70895 | 0.67435 | 0.68519 |

Table 2.3: Positive Lyapunov exponent for the Lü saturated approach (c).

| Scrolls | FE | RK4 | ODE45 |
|---|---|---|---|
| 2 | 0.11586 | 0.10082 | 0.10260 |
| 3 | 0.14503 | 0.12807 | 0.12819 |
| 4 | 0.15998 | 0.14171 | 0.13683 |
| 5 | 0.16647 | 0.14427 | 0.14657 |
| 6 | 0.16811 | 0.14790 | 0.14572 |
| 7 | 0.17278 | 0.14928 | 0.15382 |
| 8 | 0.17344 | 0.15335 | 0.15396 |
| 9 | 0.17319 | 0.15613 | 0.15130 |
| 10 | 0.17470 | 0.15507 | 0.16303 |
| 11 | 0.17523 | 0.15011 | 0.15540 |
| 12 | 0.17641 | 0.15614 | 0.16508 |
| 13 | 0.17373 | 0.15251 | 0.16284 |
| 14 | 0.18470 | 0.15570 | 0.16517 |
| 15 | 0.18132 | 0.15917 | 0.15232 |

# Chapter 3

# Design of Integrated Chaotic Oscillators

In PWL-based chaotic oscillators, the designs are governed by a set of slopes. This Chapter proposes a procedure to systematically obtain circuit parameters (given a circuit topology) from a nonlinear PWL function. It is based on the saturation of linear amplifiers. Some examples and experiments are given for the circuit synthesis of a CFOA-based multi-scroll oscillator [34, 35, 37, 66, 84].

Whereas this method proves to work, the importance of a high speed switching component is highlighted in the generation of PWL functions. Analysis on the electrical requirements of integrated chaotic oscillator is also presented both for the linear part (integrators, amplifiers), and the nonlinear part (PWL function).

In this way a CMOS design is sketched based on a floating gate (FGMOS) inverter, which has the ability to change the threshold by the biasing and capacitor sizes connected to the floating node. This generates an internal-referenced shift of the switching behavior, useful for multi-scroll PWL functions.

It is worth to mention that the state of the art diversity of multi-scroll designs are based on external DC references, an issue that seriously limits the reliability of integrated realizations.

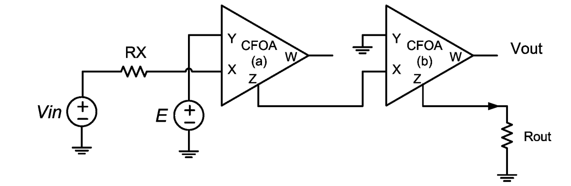


(a)

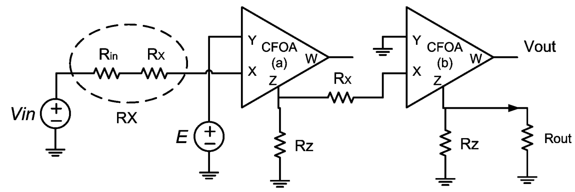


(b)

Figure 3.1: CFOA-based PWL cell (a) ideal, and (b) circuit with parasitic resistances.

## 3.1 Matching the nonlinear behavior

The circuit design of system synthesis of some nonlinear functions is critical to obtain the expected equilibriums. Suppose the required nonlinear function is described by a set of slopes as in Section 1.4.2, equation (1.9) is repeated here for convenience

$$g(x_1) = m_{2n-1}x_1 + \frac{1}{2}\sum_{i=q}^{2n-1}(m_{i-1} - m_i)(|x_1 + b_i| - |x_1 - b_i|)\,. \tag{3.1}$$

Now consider a CFOA-based topology to approach for a saturated slope [66] as shown in Fig. 3.1. A parallel array will be used for higher number of scrolls, consider the case of $q = 1$, $n = 1$ for a double-scroll. The CFOA has the following port relationships: $V_y = 0$, $V_x = A_vV_y$, $I_z = A_iI_x$ and $V_w = A_vV_z$. Where $A_v$ and $A_i$ are the voltage and current gains, respectively and the most dominant parasitic is the resistance at X-port ($R_X$).

Basically, we assume that the saturated response of a CFOA amplifier can be linearized for all the range of the output signal which is beyond the last breakpoint of the respective PWL function. The circuit response is controlled by saturating the current follower of terminal Z; besides, a parallel connection results in a direct addition of signals. This makes the CFOA, a suitable circuit for the generation of PWL functions. The linearizing approximation will depend on the circuit topology and technology [83].

In real applications, parasitic elements will degrade the nonlinear function. Resistance $R_x$ for example, is around 50Ω for the commercial CFOA AD844. Routine analysis of Fig. 3.1a leads to (3.2). Where $R_X = R_{in} + R_x$ according with parasitics shown in Fig. 3.1b, the non-ideal gains will be taken into account later. First, it is shown how the saturated circuit works to produce PWL functions

$$V_{out} = R_{out}(V_{in} - E)/R_X. \tag{3.2}$$

By assuming that the signal in terminal Z is saturated when it reaches some threshold bias-dependent voltage $V_{Zsat}$, and if the output current remains constant (ideal case), then (3.2) is locally valid between boundaries

$$\begin{aligned} V^+ &= \frac{R_X}{R_{out}} V_{Zsat} + E, \\ V^- &= -\frac{R_X}{R_{out}} V_{Zsat} + E. \end{aligned} \tag{3.3}$$

The response of the proposed CFOA-based PWL cell shown in Fig. 3.1a, is described by

$$V_{out}(V_{in}) = \begin{cases} \frac{R_{out}(V^- - E)}{R_X} & \text{if } V_{in} < V^-, \\ \frac{R_{out}(V_{in} - E)}{R_X} & \text{if } V^- < V_{in} < V^+, \\ \frac{R_{out}(V^+ - E)}{R_X} & \text{if } V_{in} > V^+. \end{cases} \tag{3.4}$$

If nonideal gains ($A_v$, $A_i$) and parasitics from Fig. 3.1b are taken into account, one can consider $a_W = A_i^2 A_v$ the total gain at port W, and the ratios $\frac{R_z}{R_x+R_z}$ and $\frac{R_z||R_{out}}{R_{out}}$ at Z terminal of CFOA(a) and CFOA(b), respectively. However, for the saturated output Z, which is not able to follow the current signal, a linearized saturated output can be considered by the experimental value $a_{off} \approx 25 \times 10^{-3}$ [84].

The nonlinear behavior of the proposed CFOA-based PWL cell can be described by

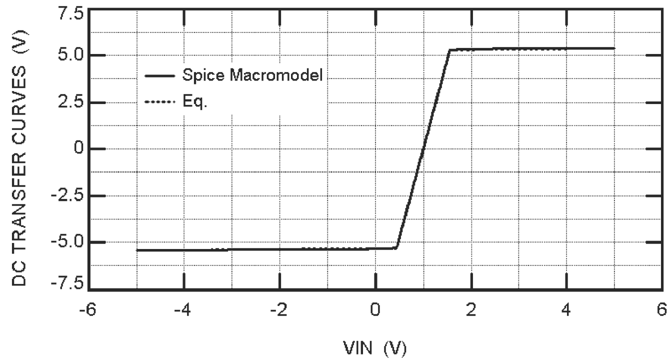


Figure 3.2: Comparison between (3.5) and the Spice macro-model with parameters $E = 1$, $R_X = 5K\Omega$ and $R_{out} = 50K\Omega$.

$$
\begin{aligned}
V_{out}(V_{in}) &= \begin{cases} \frac{a_W R_{out}}{R_X}(V^- - A_v E) + a_W a_{off}(V_{in} - V^-) \\ \text{if } V_{in} < V^-, \\ \frac{a_W R_{out}}{R_X}(V_{in} - A_v E) \\ \text{if } V^- < V_{in} < V^+, \\ \frac{a_W R_{out}}{R_X}(V^+ - A_v E) + a_W a_{off}(V_{in} - V^+) \\ \text{if } V_{in} > V^+, \end{cases} ; \\
V^- &= \frac{-V_{Zsat} R_X}{A_i^2 R_{out}} + A_v E, \\
V^+ &= \frac{V_{Zsat} R_X}{A_i^2 R_{out}} + A_v E. \qquad (3.5)
\end{aligned}
$$

A comparison between (3.5) and the proposed cell using the Spice macro-model of the CFOA AD844 is shown in Fig. 3.2, where $V_{Zsat} = 5.3V$ for $V_{bias} = \pm 10V$ (different supply dependent values can be expected in the experiment).

To accurately approach the described nonlinear function. A technique can be applied to produce in general, even or odd PWL functions from the saturated function modeled before. These are composed by a set of contiguous arbitrary slopes $m$, each one delimited by a set of breakpoints $b_p < b_q$, where $E$ is the middle point $E = b_p + Sat = b_q - Sat$ and $Sat = \frac{1}{2}(b_q - b_p)$.

To generate the nonlinearities required in multiscroll circuits one starts from the

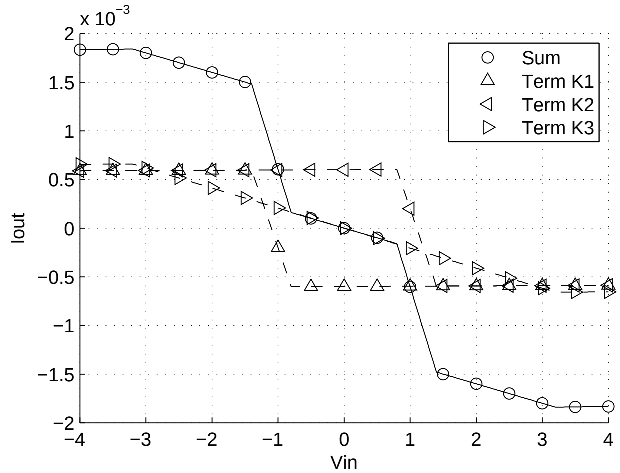


Figure 3.3: $v - i$ characteristic of Chua's diode to generate 3-scroll attractors showing each component.

current mode nonlinear response of the PWL cell shown in Fig. 3.1a, which output current is seen in the resistance $R_{out}$, considering a latter gain of $A_V R_{out}$ for the voltage response. Notice that the slopes described by (3.5) can be expressed as

$$\frac{\partial}{\partial V_{in}} \frac{V_{out}}{A_V R_{out}} = \begin{cases} \frac{A_i^2}{R_X} & \text{if } V^- < V_{in} < V^+, \\ \frac{a_{off}}{R_{out}} & \text{otherwise.} \end{cases} \tag{3.6}$$

A PWL function can be generated by adding several bounded slopes as shown in Fig. 3.3. The technique for parameterizing these cells is based on shifting the $V_{in}$ axe by $E$ starting from left to right for each block and using an extra block to adjust the slope of all the used range. For generating PWL functions, a system is formulated with the local slopes, which are function of either $R_X$ or $R_{out}$, once $E$ and $Sat$ are known (taken as $Sat = \frac{1}{2}(V_{in}^+ - V_{in}^-)$). Depending on the region of each $K$-cell (active or saturated) one has:

$$\begin{aligned} m_1 &= f_1(R_{K1},..,R_{Kg+1}) \text{ for } \{K_1, K_{g+1}\} \text{ active} \\ \vdots \quad &\vdots \qquad \vdots \qquad \vdots \\ m_g &= f_g(R_{K1},..,R_{Kg+1}) \text{ for } \{K_g, K_{g+1}\} \text{ active} \\ m_{g+1} &= f_{g+1}(R_{K1},..,R_{Kg+1}) \text{ for } \{K_{g+1}\} \text{ active} \end{aligned} \tag{3.7}$$

where $g = n$ for odd scrolls, and $g = n - 1$ for even scrolls. To solve (3.7) coefficients are chosen according to (3.6), depending on the operation region and the relation for the parameters given by

$$\frac{R_X}{R_{out}} = \frac{A_i^2 Sat}{V_{Zsat}}. \tag{3.8}$$

The following normalization variables are proposed:

$$K_i = \frac{Sat_i}{R_{Xi}}, \qquad j_i = \frac{A_i^2}{Sat_i}, \qquad c = \frac{a_{off} A_i^2}{V_{Zsat}}.$$

Thus, (3.7) is normalized as

$$\begin{pmatrix} m_1 \\ m_2 \\ \vdots \\ m_{g+1} \end{pmatrix} = \begin{pmatrix} -j_1 & c & \dots & -j_{g+1} \\ c & -j_2 & \dots & -j_{g+1} \\ \vdots & \vdots & \ddots & \vdots \\ c & c & \dots & -j_{g+1} \end{pmatrix} \begin{pmatrix} K_1 \\ K_2 \\ \vdots \\ K_{g+1} \end{pmatrix}. \tag{3.9}$$

### 3.1.1 Example: 3-Scroll, PWL Function

Consider again Fig. 3.3 with PWL cells 1 to 3 described by the values in Table 3.3, and the set of slopes

$$\begin{pmatrix} m_a \\ m_a \\ m_b \end{pmatrix} = \begin{pmatrix} -j_1 & c & -j_3 \\ c & -j_2 & -j_3 \\ c & c & -j_3 \end{pmatrix} \begin{pmatrix} K_1 \\ K_2 \\ K_3 \end{pmatrix}. \tag{3.10}$$

Values $m_a$, $m_a$, and $m_b$ correspond to the slopes presented among the limits $[-b_3, -b_2]$, $[b_2, b_3]$, and $[-b_4, b_4]$, respectively. By solving (3.10) one reaches

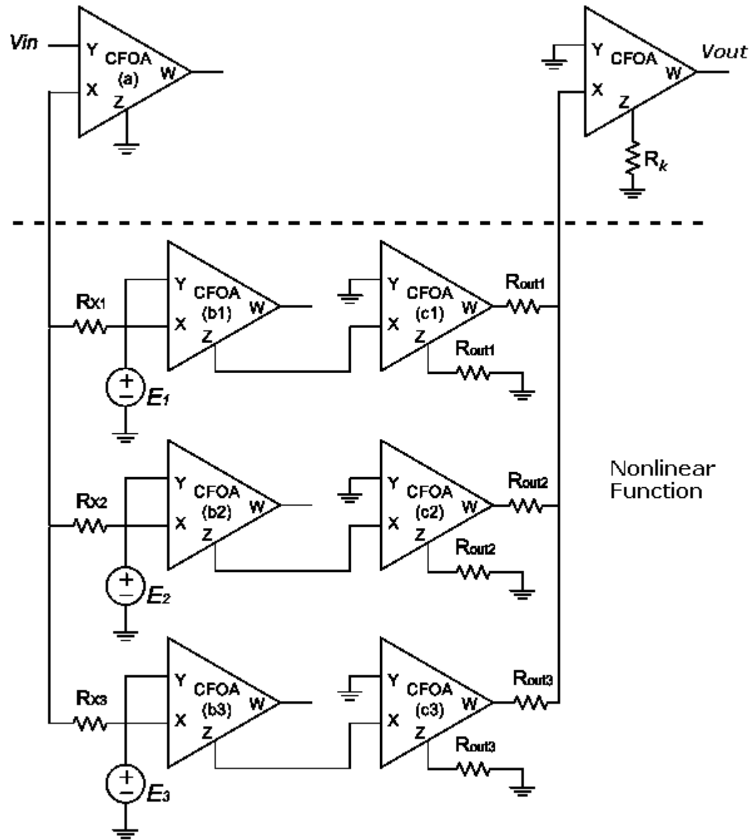


Figure 3.4: Parallel connection of CFOA-based nonlinear cells for a $v - v$ PWL-characteristic (Fig. 3.3) to generate 3-scroll attractor.

$$\begin{aligned} K_1 &= \frac{m_b - m_a}{c + j_1}, \\ K_2 &= \frac{m_b - m_a}{c + j_2}, \\ K_3 &= \frac{c^2(2m_a - m_b) + cm_a(j_2 + j_1) + m_b j_1 j_2}{(c + j_2) j_3 (c + j_1)}. \end{aligned} \tag{3.11}$$

As a result, the circuit of Fig. 3.4 is obtained with the parameters given in Table 3.2 for $V_{Zsat} = 5.3$V and a reduction of 14300 times for practical current levels. This is applied to a CFOA-based Chua's circuit to obtain a 3-scroll attractor.

By applying similar approach, the required PWL function (3.1) was observed to be identical to the proposed behavioral function (3.5) in the attractor region, thus allowing the generation of up to 6-scroll attractors by Spice simulation as shows Fig. 3.5. For experimental observations the chaotic oscillator was built directly by interconnecting integrator stages using CFOAs, see Fig. 3.6. An important issue for physical implementation is the characterization of the bias dependent parameter $V_{Zsat}$ in spite of the different values shown by the simulation model and the real device.

## 3.2 Integrated design approach

As seen in Table 1.1 in Section 1.2, the generation of PWL functions allows to obtain several multi-scroll oscillator schemes. To design many of these functions a switching component may be used, direct applications will achieve stair-like or saw-tooth functions; also, by controlling the biasing of some linear active cell, other PWL functions can be generated. From the previous discussion it can be established that the generation of the nonlinear function is a critical issue [70, 85, 86], because the behavior must be accurate enough to keep the relations of the dynamical system equilibrium points simultaneously.

This means that the design of nonlinear functions has several dimensions of difficulty compared to a simple linear one. It has several input and output offset points on each segment, the slew rate affects the bandwidth capacity in different manners (according to the specific PWL function), the hysteresis effects may produce more than two different signal paths.

In this Chapter, the most relevant aspects are discussed to settle design requirements and propose a circuit topology, for example.

*Impedance coupling.* Coupling is essential for signal transmission and the good integrator performances. For simplicity in the actual design, one can use gate input for voltage signals and source input for current signals. The cascode configuration was also used to achieve good output coupling. The design of the active devices has been in this way calculated to contribute by 1% of the system coefficient.

The other effects are analyzed by the linear and nonlinear parts separately. Let us consider the $n$-order nonlinear system of the Lur'e form described by (3.12), it can be

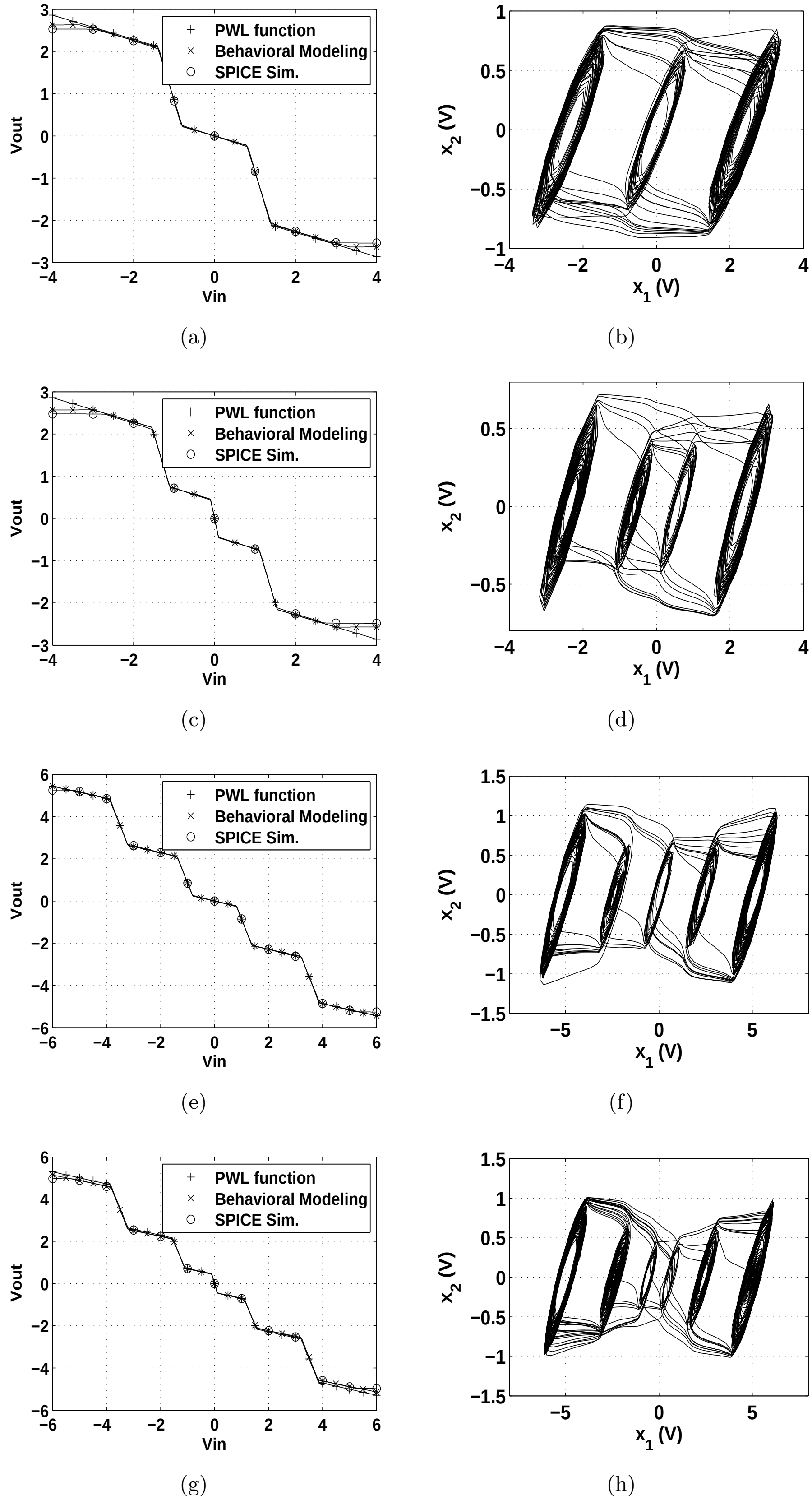


(a) (b) (c) (d) (e) (f) (g) (h)

Figure 3.5: Spice simulations for 3, 4, 5, and 6-Scroll attractor. Nonlinearities comparisons are shown in: (a), (c), (e), and (g). Phase diagrams of the $n$-scroll attractor are shown in: (b), (d), (f), and (h).

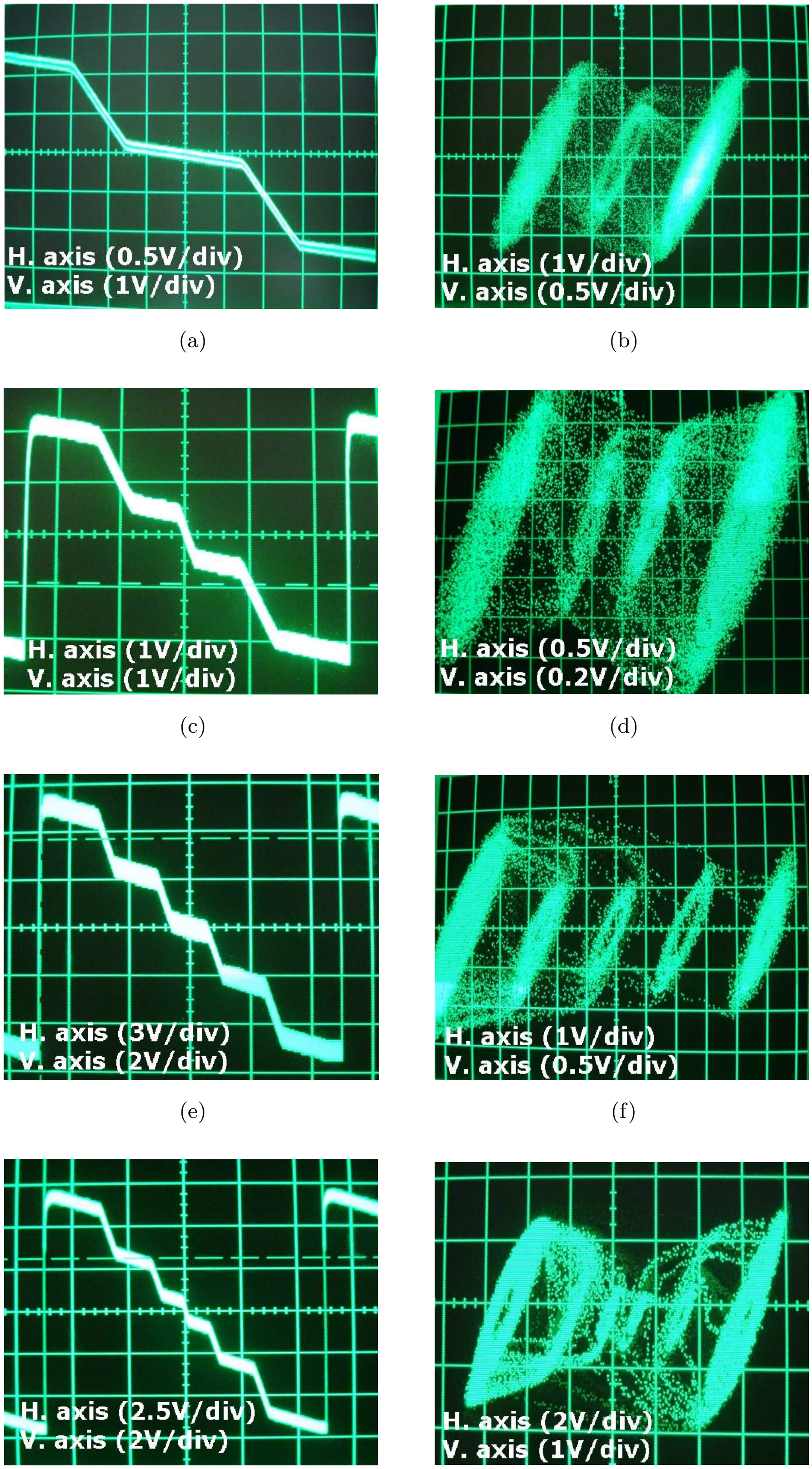


(a) (b)

(c) (d)

(e) (f)

(g) (h)

Figure 3.6: Experimental results for 3, 4, 5, and 6-Scroll attractor. Nonlinearities are shown in: (a), (c), (e), and (g). Phase diagrams of the $n$-scroll attractor are shown in: (b), (d), (f), and (h). Horizontal axis is variable $x_1$ and vertical axis is $x_2$.

simply implemented as shown in the conceptual diagram in Fig. 3.7. Note the matrix **A** stands for the system linear part and the rest is used for the nonlinear feedback,

$$\dot{\boldsymbol{x}} = \boldsymbol{A}\boldsymbol{x} + \boldsymbol{B}\boldsymbol{\sigma}(\boldsymbol{C}\boldsymbol{x}) \qquad \boldsymbol{x}, \boldsymbol{\sigma} \in \mathbb{R}^n. \tag{3.12}$$

## 3.3 Linear design requirements

*Swing.* Since the IC design is focused to generate multi-scroll attractors, the increase on the number of scrolls on the same dynamic range will eventually cause the loss of the chaotic behavior due to the noise and circuit fault tolerances. The topology selection must be made in order to maximize swing, as well as to provide a suitable circuit biasing.

*Bandwidth.* Since the linear part is in charge of the signal integration and other linear operations, the linear circuit bandwidth can be much lower than the nonlinear counterpart.

Chaotic oscillators have a wide frequency spectra, which can be scaled by the integrator gain ($A_{int}$, generally the $RC$ constant). If the spectrum is known a priory, the active devices bandwidth are set in accordance to this gain. In our proposed first integrated design, the capacitor will be externally chosen allowing the spectrum to be scaled.

In the proposed system (2.9), a dominant frequency is observed in state $x_2$, see Fig. 2.4a. This follows the empirical relation (see Fig. 2.4) given below

$$f_{x2} \approx \frac{3A_{int}}{10} \tag{3.13}$$

*Gain.* Evidently, different gains will affect the final system parameters letting it to loose the chaotic behavior. However, by decomposing the signal path into several matched trajectories such as in [48], the overall effect will be a little modification on the value of $A_{int}$. In our design we propose that if unity gain cells have a fixed gain near the unity ($<2\%$ of difference), the system parameters are given mainly by the matched resistors.

*Parameter relation.* This part is a big issue on the design of integrated chaos generators because of the high parameter sensitivity that most autonomous chaotic systems exhibit. A parameter space analysis can be used as a first glance to locate the appropriate values. Recently, several software programs have been built to calculate and analyze chaotic regions [1]. If a chaotic region is known over some tolerances, the parameter relations may be kept by using circuit matching techniques adequately.

*Offset.* The influence of offset on autonomous systems is a complex issue that has not been addressed. The use of low offset linear cells is imperative knowing that further effects can be compensated by the adjustable output of the nonlinear part. However, the use of non-autonomous systems has surmount this effect.

*Linearity.* Very high linearity of any system term will not be required in an essentially nonlinear system.

## 3.4 Nonlinear design requirements

*Swing.* The saturated behavior that is typically designed, implies that an active cell may use different biasing than the rest of the circuit which has to process the signal beyond saturation. In fact, some approaches have suggested this [35, 41]; however, the circuit construction becomes very impractical as the number of desired scrolls grows. A typical solution is the use of V-I nonlinear cells, due to the natural gain of the signal from voltage to current. In this mode, lower currents can be easily handled while the associated voltages remain low and in the same dynamic ranges for all the oscillator.

*Bandwidth.* Among the numerous research on experimental designs, it is well know that autonomous chaotic behavior is severely limited in frequency. The diverse active cells, generally have a very high bandwidth than the observed in the oscillation spectra. in fact, the delay response exhibited by the active devices is directly degrading the PWL function [86], thus changing critically the dynamical system properties.

[1] Sprott JC, Rowlands G. Chaos Data Analyzer (http://sprott.physics.wisc.edu/cda.htm) and Hegger R, Kantz H, Schreiber T. Nonlinear Time Series Analysis TISEAN (http://www.mpipks-dresden.mpg.de/~tisean).

Consider, the time response for the circuit saturations that the PWL function requires. Several nonlinear cells has to surmount large signal changes and also change on/off states continuously as the system solutions change the region of the function behavior. Roughly, if the signal highest dominant frequency is $f_{max}$, and the PWL function has a continuous transition which is a $k < 1$ portion of the entire input swing, then the nonlinear cell saturation delay must be $k/f_{max}$. However, the cell bandwidth is higher than the inverse of this delay, since this last also accounts for the time for turning it on and off. The dependence on the PWL function delay is then obvious.

*Gain.* If the PWL saw-tooth function is considered, the gain is actually scaling parameter $\xi$, which may allow to control the system behavior. At this point, it is found convenient to work with adjustable design to control the chaotic bahavior.

*Offset.* This is well known to be one of the main drawbacks in comparator designs; thus, the comparator output offset is proposed to be adjustable. Furthermore, the nonlinear function may suffer from input offset.

*Modularity.* Since the change on the number of scrolls is desirable on multi-scroll oscillator circuits and this effect depends directly on the applied nonlinear function; a desirable nonlinear function may be built to grow in a systematic mode. A voltage-to-current nonlinear function grows by simply connecting cells in parallel.

*Transition.* Since this is a system bandwidth conditional issue, a good and simple approach has been found to be the selection of an inverter circuit as the heart of the proposed nonlinear cell.

*DC references.* Most of the multi-scroll designs base their nonlinear function on external voltage references. This means that the number of external components grow inadmissibly by extending the number of scrolls. The use of voltage dividers as suggest [41] is not an alternative for integrated design. Instead, capacitor values are known to be implemented with relatively high accuracy and good matching properties. FG-MOS technology uses capacitive gates of MOS transistor to combine signals. In this Thesis, this CMOS compatible technology is proposed to eliminate the need of external references as will be detailed in Chapter 4.

*Adjustability.* By using the FGMOS technology, some parameters of the nonlinear cell can be adjusted to match correctly to its counterpart. for example, the output offset and the stair gain are adjusted by a parallel FGMOS transistor which gate is mainly biased by the capacitor sizes and a fine tuning is allowed by the compression effect.

*Low hysteretic.* While there exist some hysteresis and delay-based multi-scroll chaotic systems [3, 4, 8]; hysteretic control is an important issue to generate accurate nonlinear functions. The proposed voltage-to-current cell has low hysteresis due to the intrinsic low hysteresis of the properly biased inverter.

However, the nonlinear parasitic capacitances in the inverter may cause input offsets that will produce hysteretic behavior. These variations are tolerated by the oscillator, since the total desired capacitance is 10pF and the highest parasitic capacitor is 200 times lower.

## 3.5 Final description

For a first prototype of the chaotic oscillator, the considerations on area have been relaxed; the oscillator bandwidth is been work in two modes: the low-frequency design (for the integrated circuit detailed in Chapter 4) and the high frequency design (observed in simulations). Recall from Table 1.6 that the highest frequency reported by a multi-scroll design is about 7MHz.

The proposed design is based in the use of FGMOS to change the threshold of an inverter in accordance with the biasing and capacitor sizes. This implies that the response is flat all over the dynamic range and shows a fast transition at an internally fixed voltage reference. A slewing transconductance structure is later used for the nonlinear comparator as will be shown in the next Chapter.

As a summary, the circuit realization of (3.12), requires that each active device fulfills the performances shown in Table 3.3 and classified according to their relevance, regarding our proposed design procedure. In the next Chapter, the design of the linear and nonlinear part is explained in detail and adapted to the Saw-tooth based multi-scroll approach proposed in Chapter 2.

Table 3.1: Values required.

| Cell | $Sat$ | $E$ |
|---|---|---|
| 1 | $\frac{1}{2}(b_3 - b_2)$ | $-b_2 - \frac{1}{2}(b_3 - b_2)$ |
| 2 | $\frac{1}{2}(b_3 - b_2)$ | $b_2 + \frac{1}{2}(b_3 - b_2)$ |
| 3 | $b_4$ | 0 |

Table 3.2: Circuit parameters.

| E(V) | $R_X(\Omega)$ | $R_{out}(\Omega)$ |
|---|---|---|
| -1.1 | 4586 | 88458 |
| 1.1 | 4586 | 88458 |
| 0 | 44534 | 80536 |

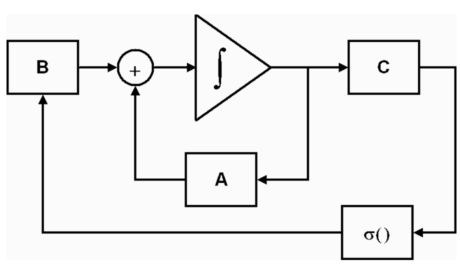


Figure 3.7: Conceptual diagram of the electronic implementation of (3.12).

Table 3.3: Design requirements.

<table>
<tr><td></td><td>Linear circuit</td><td>PWL circuit</td></tr>
<tr><td rowspan="2">Required</td><td>Swing<br>Parameter relation<br>Low offset</td><td>Modularity<br>Fast transition<br>DC references<br>Adjustability<br>Low hysteresis</td></tr>
<tr><td colspan="2">High $Z_{in}$<br>High $Z_{out}$</td></tr>
<tr><td rowspan="2">Not necessary</td><td colspan="2">Area</td></tr>
<tr><td>High Bandwidth<br>Exact gain<br>High linearity</td><td></td></tr>
</table>

# Chapter 4

# FGMOS Based Multi-Scroll Oscillators

A chaotic oscillator is designed in this Thesis from the state space equations using unity gain cells (UGCs) for linear amplification and integration and a particular switching block for the nonlinearity required by a multi-scroll constant-Jacobian system 2.9. The design for linear and nonlinear parts is in accordance with the requirements reviewed in the previous Chapter.

First, the macro-model generates an extended state space system. For adequate circuit coupling, the maximum output resistance of the cells is examined as well as the transfer V-to-I gain; thus, a bias current is selected and the design of the voltage follower (VF), the current follower (CF), and the current mirror (CM) cells is presented.

On the other hand the nonlinear function is given by the FGMOS circuit as proposed. First, a discussion over the failure effects such as the trapped charges from the manufacture process, the tunneling effect and the hot electron injection is given to clarify the design tolerance. An overview of the floating gate (FG) voltage calculation is given. Also the gate voltage is generated by the capacitance of poly 1 to poly 2 and the substrate. The capacitance ranges are obtained in accordance to the parasitics an the coupling constraints. In this way a shifted inverter is designed.

Then, a FGMOS V-I comparator topology is proposed and the transient response is examined in detail to calculate the time transition in both cases. The cell maximum transient time is found to be around 2ns. However, it is also suggested an optimization to reach the same time of a simple inverter (about 0.25ns in its technology).

The computation of the nonlinear function breakpoints (threshold shifts) is now introduced from the point of view of the layout capacitors. Both stair and saw-tooth functions are designed taking into account the circuit V-to-I gain, the dynamic range, the breakpoints and the slope system parameter.

❏

Given the circuit considerations, in the two different domains (linear and non-linear). The system synthesis is now carried out by integrating the signal in current mode trough user defined capacitors. This allows for the selection of the operating spectrum and the system coupling whenever such capacitors are external.

Moreover, capacitive loads are widely preferred to integrate signals on this kind of oscillators due to the fact that inductive loads are not this simple to have on chip and the system is highly sensitive to the low $Q$.

As observed in Chapter 1, the selected active devices are diverse and the state of the art is still young to define the dominance of one particular cell over the others. This is due to the fact that the differences on the cells are also used as design advantages. For example typical integrated designs make use of the OTA [25, 48, 49] as a block of construction, thus synthesizing gm-C integrators, others use the versatility of the CFOA to synthesize compact designs.

Whereas the design and application of OTAs is very popular and specially needed on compensated schemes, the selection of unity gain cells (UGCs) for chaotic oscillators is also possible as shown in [30–33]. The motivation in the use of these cells, is the simplicity of the realization procedure.

## 4.1 Linear Design: UGCs

The set of UGCs is conformed by a voltage follower [87–91] (VF), a voltage mirror [91, 92] (VM), a current follower [90, 93] (CF) and a current mirror [93, 94] (CM). The

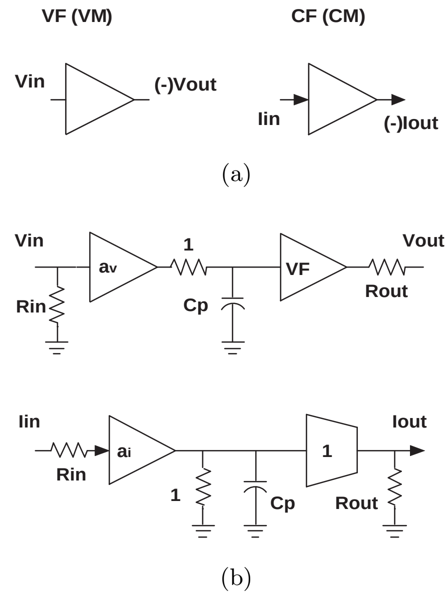


Figure 4.1: UGC's representation, (a) ideal behavior, (b) with parasitics.

behavior of each cell consists in copying the voltage or current as shown in Fig. 4.1a. The main parasitics that are considered in the model are also shown in Fig 4.1b. Here $a_v$ and $a_i$ represent the cell voltage and current gain respectively. More specifically there will be called $a_{VF}$, $a_{VM}$, $a_{CF}$ and $a_{CM}$ for the corresponding UGC. By similar reasoning, there are input resistances $R_{inVF}$, $R_{inVM}$, $R_{inCF}$, $R_{inCM}$; output resistances $R_{outVF}$, $R_{outVM}$, $R_{outCF}$, $R_{outCM}$; and pole capacitors $C_{VF}$, $C_{VM}$, $C_{CF}$, $C_{CM}$. These last are represented as $C_p$ along with the unitary resistances. Thus, the cell dominant pole will be $f_{-3dB} = \frac{1}{2\pi C_p}$.

Having the circuit considerations in mind, the developed UGCs use cascode configurations. The linear transfer is made by the connection of a VF in series with a resistance and a summing node at the input of a CF or CM (depending on the parameter sign) as shows Fig. 4.2.

Since all these cells have a single gain, a resistance bank is proposed. Thus for a parameter $a$, a signal will be transmitted by a $\frac{R}{a}$ resistance. Where $R$ is the current-to-voltage scaling and it also conforms the integration gain $\frac{1}{RC}$ at the end of the current-mode cell (CF or CM). Thus, the proposed system (2.9) is realized by connecting the

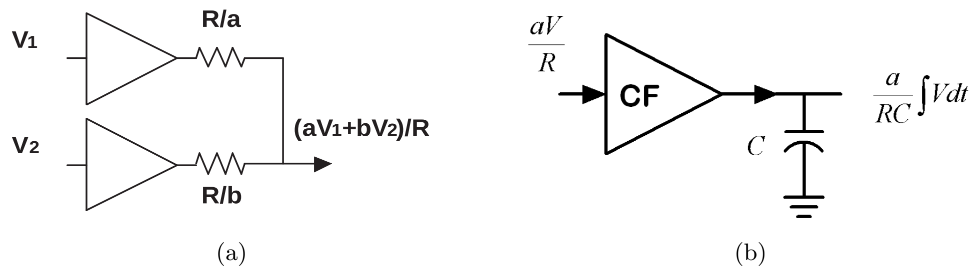


Figure 4.2: Signal transfers with UGCs, (a) scaling and summing, (b) integrating.

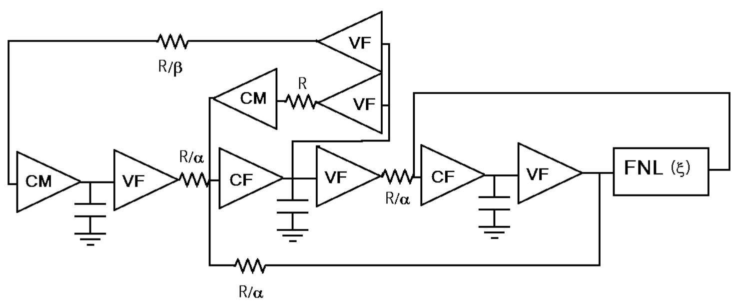


Figure 4.3: Circuit realization of the proposed multi-scroll chaotic oscillator.

cells as shown in Fig. 4.3.

The real values of integrated resistances may vary over the fabrication process, thus a pseudo common centroid is used to keep the relative values and consequently the system coefficients. The absolute variations can be seen as a constant term on the dynamical system (2.9) which is a deviation on the system spectra. This may be undesirable in some applications, but it may not show any remarkable effect in chaotic signals because of their wide spectrum.

Considering the parasitics described in Fig. 4.1b, and the circuit block realization of (2.9) the system macro-model is derived as:

$$
\begin{aligned}
C\frac{d}{dt}V_{x1} &= V_{x11} - \frac{V_{x1}}{R_F}, \\
C\frac{d}{dt}V_{x2} &= V_{x6} - \frac{V_{x2}}{R_E}, \\
C\frac{d}{dt}V_{x3} &= V_{x4} - \frac{V_{x3}}{R_D}, \\
C_{CM}\frac{d}{dt}V_{x4} &= a_{CM}\frac{V_{x10}}{R_A} - V_{x4}, \\
C_{VF}\frac{d}{dt}V_{x5} &= a_{VF}V_{x3} - V_{x5}, \\
C_{CF}\frac{d}{dt}V_{x6} &= a_{CF}\frac{V_{x17}}{R_{inCF}} - V_{x6}, \\
C_{VF}\frac{d}{dt}V_{x7} &= a_{VF}V_{x2} - V_{x7}, \\
C_{CM}\frac{d}{dt}V_{x8} &= a_{CM}\frac{V_{x9}}{R_B} - V_{x8}, \\
C_{VF}\frac{d}{dt}V_{x9} &= a_{VF}V_{x2} - V_{x9}, \\
C_{VF}\frac{d}{dt}V_{x10} &= a_{VF}V_{x2} - V_{x10}, \\
C_{CF}\frac{d}{dt}V_{x11} &= a_{CF}\frac{V_{x16}}{R_{inCF}} - V_{x11}, \\
C_{VF}\frac{d}{dt}V_{x12} &= a_{VF}V_{x1} - V_{x12}, \\
C_{VF}\frac{d}{dt}V_{x13} &= a_{VF}V_{x1} - V_{x13}, \\
C_{inNLF}\frac{d}{dt}V_{x14} &= \frac{C_{x13} - V_{x14}}{R_{outVF}}, \\
C_{NLF}\frac{d}{dt}V_{x15} &= NLF - V_{x15},
\end{aligned}
\tag{4.1}
$$

with

$$\begin{aligned}
R_A &= R/\beta + R_{inCM} + R_{outVF}, \\
R_B &= R/\gamma + R_{inCM} + R_{outVF}, \\
R_C &= R/\alpha + R_{outVF}, \\
R_D &= R_{outCM}||R_{inVF}, \\
R_E &= R_{outCF}||R_{inVF}||R_{inVF}||R_{inVF}, \\
R_F &= R_{outCF}||R_{inVF}||R_{inVF}, \\
\frac{V_{x17}}{R_{inCF}} &= \frac{R_{outCM}}{R_{outCM}+R_{inCF}}\left(V_{x8} + \frac{V_{x5}+V_{x12}-2V_{x17}}{R_C}\right), \\
\frac{V_{x16}}{R_{inCF}} &= \frac{R_{outFNL}}{R_{outFNL}+R_{inCF}}\left(V_{x15} + \frac{V_{x7}-V_{x16}}{R_C}\right).
\end{aligned} \tag{4.2}$$

Where the V-I nonlinear function is $NLF$, with dominant electrical parameters $C_{inNLF}$, $R_{outNLF}$, and $C_{NLF}$. The transistor design is explained as follows.

### 4.1.1 Voltage follower

Consider the current trough active cells given by the system parameters and the voltage-to-current scaling given by the nominal circuit resistance $R$. If we choose $R = 120k\Omega$ and the system described in (2.9). The highest gain is given by parameter $\beta = 4$. Naturally the circuit dynamic range ($DR$) is to be known, in this case we choose $\pm 1$ which is easily achievable in a 5V-bias technology.

Then the current handling capacities are calculated for active devices controlling one signal transmission path from the required maximum current

$$I_{max} = \frac{DR\beta}{R} = 33\mu A. \tag{4.3}$$

A possible choice for the bias current is $I_D = 60\mu$A. The circuit schematic has been derived from a translinear VF [89]; however, nodes 13 and 12 have diode connected transistors which improves the cell offset as shown in Fig. 4.4. Here terminals 10 and 11 are input and output, respectively; terminals 1 to 4 are generated by the cascode

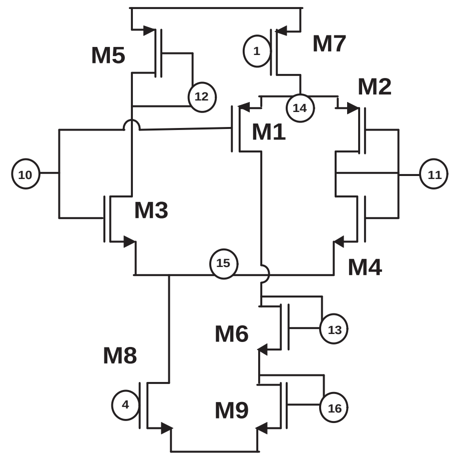


Figure 4.4: Voltage follower.

bias circuit in Fig. 4.12. The bulk terminals are all connected to the bias in all the schematics unless specifically pointed.

As it is planed to work with symmetrical biasing, both PMOS and NMOS transistors must be matched, thus the transconductance $gm_N = gm_P = gm$, and the circuit output resistance is approached by

$$R_{outVF} \approx \frac{2}{gm_N} || \frac{2}{gm_P} \approx \frac{1}{gm}. \tag{4.4}$$

In this way, the system gains will be affected by the series resistance. A low conservative choice is to set $R_{outVF} = 1\%R$. Thus having a maximum variation of 8% in the gain given by $\beta$ and 6% for the gain of $\alpha$ for both sides considered. Thus the transistor sizes are obtained by considering $K_N = c_{oxN}\mu_0$ and $K_P = c_{oxP}\mu_0$ (For the particular technology parameters are $K_N = 57.6\mu A/V$ and $K_P = 18.6\mu A/V$), this gives

$$gm = \frac{1}{120K\Omega} \times 1\% = 83.3\mu A/V, \tag{4.5}$$

$$\frac{W}{L}_N = \frac{gm^2}{4K_N I_D} = 50.2, \tag{4.6}$$

$$\frac{W}{L}_P = \frac{gm^2}{4K_P I_D} = 155.6. \tag{4.7}$$

Thus, the saturation voltage is $V_{sat} \approx 0.15$. The final adjusted sizes are summarized

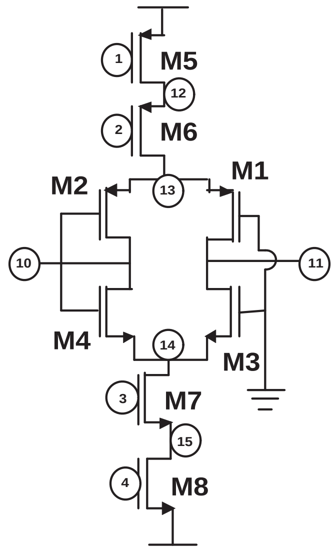


Figure 4.5: Current follower.

in Table 4.1 and the cell electrical parameters are found in Table 4.2.

### 4.1.2 Current follower

Following the translinear topology and the same biasing, the CF circuit schematic is shown in Fig. 4.5. Transistor dimensions are also summarized in Table 4.1 and the cell electrical performance is described in Table 4.2.

### 4.1.3 Current mirror

The CM circuit schematic is shown in Fig. 4.6. This particular topology uses matched transistors to copy the ground voltage to both terminals, obtaining low offset. Transistor dimensions are summarized in Table 4.1 and the cell electrical performance is described in Table 4.2.

## 4.2 Nonlinear: FGMOS Comparator Based Design

It may found every where in literature that chaotic multi-scroll PWL-based oscillators are all dependent on voltage DC references to generate the used nonlinear functions.

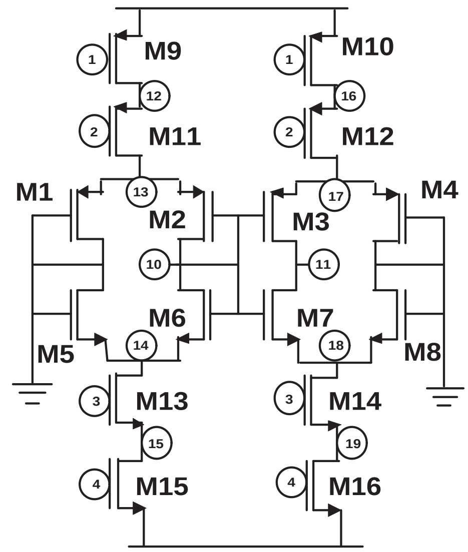


Figure 4.6: Current mirror.

The central idea on the design of a multi-scroll oscillator is to reduce such explicit dependence. A first approach is to use resistors as voltage dividers [41]. However, a multi-scroll design would not be reliable if the actual variance of the integrated resistances were taken into account.

Floating gate MOSFETs (FGMOS) attract the attention for their novel applications on fully CMOS compatible design based in the capacitive structure of the transistor gates. Recall that integrated capacitors have minor variations than resistors. A principal drawback in their use are the charges that can appear for different causes:

- The most dominant effect is the charging during the manufacture process. A typical cause is the antenna effect that occurs due to the high electrical fields used in dry etching, in which large geometries are vulnerable to the collected ionized particles [95]. If these structures are not connected to any diffusion, the trapped charges can damage the circuit.

  A common layout solution for these structures such as the transistor gates, is to temporally isolate the biggest geometries form the sensible areas by using interconnections of higher levels such as metal 2 or 3, which are know to be connected to a diffusion somewhere in the die.

- Charge injection during the device operation is related to the Fowler-Nordheim tunneling effect, which allows electrons to flow trough a barrier by a high electric field. This process has shown to occur only if the floating gate potential is biased at programming voltages [96]. In fact, for 10nm of oxide thickness the required potential is about 15V [97]. Typical thickness in the 0.5$\mu$m technology are $t_{ox}$=13.9nm.

- Hot electron injection is an effect of carriers displacement into a saturated transistor due to increase in their instantaneous velocities. This effect can lead the gate to collect some of the carriers that are passing trough. Two conditions that allow and increase this effect are the high drain voltages as well as the high channel current.

  This is not the case of the current design since the current in the inverter is only used to charge the capacitance of the switching MOS gate, which is lower than some of the parasitic capacitances of the inverter itself. In addition, the switching transistors are usually operating in linear or cutoff regions. In the case of the saturated current adjustable sources, the drain voltage is always near the minimum $V_{dsat}$.

The trapped charge of the manufacturing process can be canceled by a simple layout technique which has shown experimentally good performance for 0.5$\mu$m technology [98]. It consist in adding vias contacts to the floating gate to connect it directly to the upper metal of the current technology. In this way the possible charges generated during manufacturing process of all the lower layers will flow to the vias contacts and discharge trough the last metal layer. Finally, this layer is etched and the gate is isolated [98].

### 4.2.1 FGMOS and tresholding

The gate voltage $V_{DC}$ of the FGMOS can be simply set by choosing adequate capacitors and biasing. The total capacitance connected to this node is considered $C_T = C_1 +$

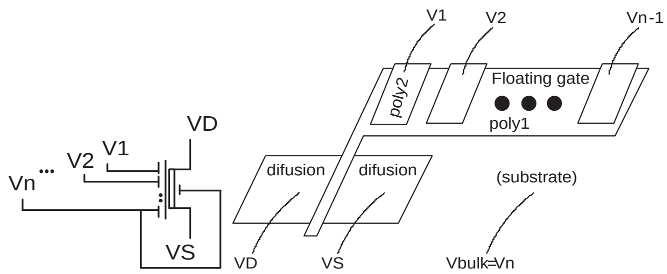


Figure 4.7: The used FGMOS transistor, (a) electrical diagram, (b) physical device.

$C_2 + ... + C_n$, as well as each of the used bias voltages ($V_2$ to $V_n$). Here, $C_1$ is the input capacitor, thus $V_1 = V_{in}$ will not contribute to the DC reference. The bias set of capacitors will be called $\mathbf{C}_b = \{C_2, C_3, ..., C_n\}$, their existence will produce the overall input signal to be compressed by the ratio $k = \frac{C_1}{C_T}$ (see Fig. 4.7),

$$V_{DC} = V_2 \frac{C_2}{C_T} + V_3 \frac{C_3}{C_T} + ... + V_n \frac{C_n}{C_T}. \tag{4.8}$$

As the bulk capacitance $C_n$ in this large structure is taken into account. The bulk contribution given by (4.9) has been calculated by the technology dependent parameter $f_{cpcb}$[1] which is the ratio of the Poly1 to bulk capacitance to the Poly2 to Poly1 capacitance [98],

$$C_n = f_{cpcb}(C_1 + C_2 + ... + C_{n-1}). \tag{4.9}$$

According to Fig. 4.7, if the total capacitance $C_T$ and the compression factor $k$, $(1 > k > 0)$ are chosen, the other capacitors may be calculated using (4.9) and (4.10), this last expression is derived form (4.8):

[1] The parameter was reported as $f_{cpcb} = 0.14$ [98] for the $0.5\mu$m ON semiconductor process; however, the authors agreed that a more accurate value for this constant is $f_{cpcb}$=0.1333, as used in this Thesis.

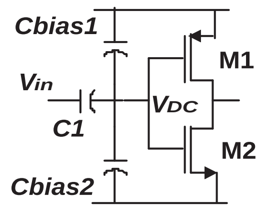


Figure 4.8: FGMOS simple shifted inverter.

$$\begin{aligned} C_1 &= kC_T, \\ C_2 &= \left( C_T \frac{V_3 + V_b f_{cpcb}}{f_{cpcb}+1} - C_1 (V_3 - V_1) - C_T V_{DC} \right) \frac{1}{V_3 - V_2}, \\ C_3 &= (C_T - C_1 - C_2 - f_{cpcb}(C_1 + C_2)) \frac{1}{f_{cpcb}+1}. \end{aligned} \tag{4.10}$$

FGMOS technologies can be used in low voltage design for the ability to set the transistor threshold voltage. In this work, other remarkable characteristics have been exploited. The signal compression inherent to these transistors is used for external adjusting; and the variation on the threshold makes possible the generation of PWL functions.

Consider the inverter in Fig. 4.8. Since NMOS and PMOS are matched transistors with symmetrical biasing, the gate threshold voltage is around zero in the conventional inverter. By using FGMOS, the circuit threshold can be accurately changed to $V_{DC}$. See Fig. 4.9 for an example of equidistant spaced inverter responses $V_{inv}$ given with an input signal in the interval of -2.5V to 2.5V.

Here, it is desired to have a large factor $k$ to have low compression. However, for the selection of the total capacitance $C_T$, two bounds must be considered. First, the capacitance $\mathbf{C}_b$ (and therefore $C_T$) must be sufficiently high to avoid the effects of the nonlinear parasitic capacitances of gate to source (M1, M2). As a rule of thumb, this means about ten times the value of the higher parasitic capacitance $C_{max}$. Roughly, M1 and M2 saturated:

$$C_{max} \approx \frac{2}{3} C_{ox}(W_{M1}L_{M1} + W_{M2}L_{M2}) + C_{ov\_P}W_{M1} + C_{ov\_N}W_{M2} = 88.4fF \tag{4.11}$$

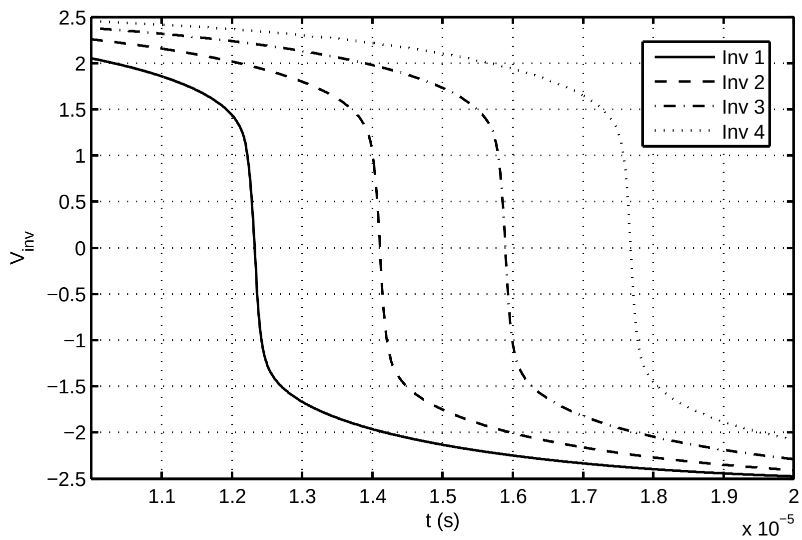


Figure 4.9: Transient response of several shifted inverters. Input signal varies from rail to rail in the time interval.

Second, if $h$ FGMOS inverters are to be connected in parallel (for generating each break point of the nonlinear function) $\mathbf{C}_b$ must be low enough to prevent the effect given by the parasitic low frequency pole formed by the equivalent input capacitance, say $C_{in}(h, C_1, C_T)$, and the output resistance of the preceding buffer $R_{out}$.

$$f_p = \frac{1}{2\pi R_{out} C_{in}}. \tag{4.12}$$

### 4.2.2 FGMOS comparator design

A fixed threshold V-I comparator using the input FGMOS inverter is used for the construction of stair-like nonlinear functions. A first approach is shown in Fig. 4.10. Here, a source follower (M7) was used to handle the switching transistor M3. The whole oscillator was prove to work as expected generating up to 6-scroll attractors [70]. However, the transient behavior of the function may lead to instabilities because of the feedback in the source of M3 and the nonlinear behaviors of M4 and M5 when turning from saturation to triode operation.

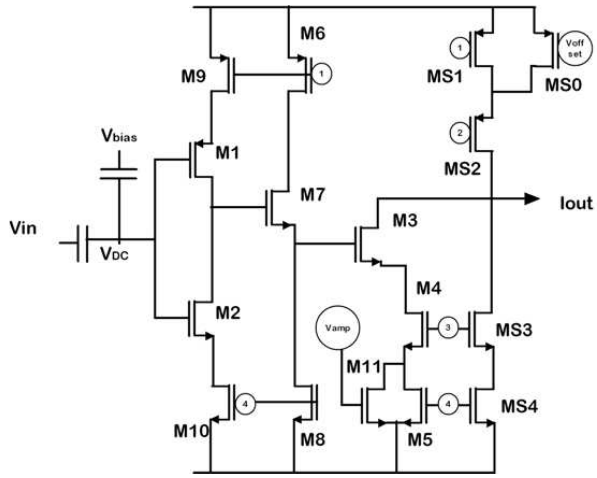


Figure 4.10: A first FGMOS V-I comparator.

Thus, an improved V-I comparator has been developed, see Fig. 4.11b. The first stage is the inverter designed with FGMOS (i.e. M1 and M2 transistors), which drives the gate of M3, allowing the bias current (branch M5 to M7) to be switched between M3 and M4. The output branch is conformed by transistors MS0-MS4. FGMOS transistors M6 and MS0 are used to control the amplitude and offset of the output signal, respectively. $V_A$ and $V_B$ are playing the role of $V_{bias}$ to preset adequate control voltages at the gates of M6 and MS0.

All bulk connections are made to the corresponding bias voltages $V_{dd}$ or $V_{ss}$, where $V_{dd} = -V_{ss} = 2.5$V. Voltages Vb1 to Vb4 are obtained by using the cascode biasing circuit shown in Fig. 4.12 which was developed exclusively for this design. The transistor sizing of the voltage-to-current cell is shown in Table 4.3.

The transient behavior can be analyzed by means of the simplified stages shown in Fig. 4.11c, 4.11d and 4.11e. The approximations used herein for roughly describing the circuit behavior are supported by the simulations. The transition time is divided into $t_1$ (Fig. 4.11c), $t_2$ (Fig. 4.11d) and $t_3$ (Fig. 4.11e) for each stage. First, the value of equivalent capacitors is calculated.

The inverter load capacitance $C_{L1}$ is mainly given by the capacitance $C_{gd}$ of both PMOS and NMOS transistors, which is calculated considering the Miller effect and using the overlap capacitances $C_{ov}$; and the capacitance at the gate of M3 connected to ground $C_{gs\_M3}$, which considers the overlap and gate capacitance in a single term $c_{ox}M_{M3}L_{M3}$, thus, [2]

$$C_{L1} \approx C_{gd\_M1} + C_{gd\_M2} + C_{g\_M3} = 2C_{ov\_P}W_{M1} + 2C_{ov\_N}W_{M2} + c_{ox}M_{M3}L_{M3} \approx 14.4fF. \tag{4.13}$$

For time $t_2$, it will be seen that the value of $C_{L2}$ only matters when both transistors of the differential pair are in cutoff region, thus ignoring capacitance from the cascode current source, one have,

$$C_{L2} \approx 2C_{ov\_N}W_{M3} = 1.56fF. \tag{4.14}$$

For the time $t_3$, the capacitors connected to the cell output are all in saturation and all the gates are fixed. Thus, the total capacitance is given by $C_{L3} \approx C_{gd\_MS2} + C_{gd\_M4} + C_{gd\_MS3}$ as

$$C_{L3} \approx C_{ov\_P}W_{MS2} + C_{ov\_N}(W_{M4} + W_{MS3}) \approx 6fF. \tag{4.15}$$

Call $t_{HL}$ the total time required for the output current signal to fall from $I_{off}$ to $-I_{bias}$ (similar to a digital circuit) and $t_{LH}$ the total time required to raise the output current from $-I_{bias}$ to $I_{off}$. Both cases are analyzed separately.

### Transition $t_{HL}$

Figure 4.11c corresponds to the FGMOS inverter, its decreasing output controls transistor M3 (second stage) by turning it to cutoff when its value is below $V_{tN} + 2V_{dsat} - Vss$. For simplicity, a basic approximation is used for the inverter excursion time as $t_1$ since this transition is relatively fast [99]

$$t_1 = t_{pHL} = \frac{C_{L1}(Vdd - Vss)}{K_N(Vdd - Vss - V_{thN})^2}, \tag{4.16}$$

[2]Using the values of ON 0.5$\mu$m technology: $C_{ov\_N} = 0.2fF/\mu m$, $C_{ov\_P} = 0.29fF/\mu m$, $C_{ox} = 2.548fF/(\mu m)^2$.

Thus one have $t_1 \approx$0.071ns.

In the second stage described by Fig. 4.11d, M3 and M4 are both in cutoff, since node $V_x$ has been initially set by voltage $V_{GS}$ of M3 to the cascode fixed current $I_{bias} = 2\mu$A when only M3 is conducting; and now, this current is simply discharging the node $V_x$ until transistor M4 starts conducting this same current. The overall voltage change on the node is

$$\Delta V_x = V_x(t = t_2) - V_x(t = 0) = Vdd - V_{GS}(I_{bias}) - (0 - V_{GS}(I_{bias})) = Vdd. \quad (4.17)$$

Thus, if both transistors are in cutoff, the time is found by integrating the constant current through $C_{L2}$, then

$$t_2 \approx C_{L2}\frac{\Delta V_x}{I_{bias}} = 1.95nF. \quad (4.18)$$

According to the third stage described by Fig. 4.11e, a current $I_{bias}$ will suddenly discharge the output node from $V_{out}(t = 0) = 0.5 I_{bias} R_{load}$ to $V_{out}(t = t_3) = 0$ (50% of excursion) through the parallel RC circuit given by the output load $R_{load} << R_{cascode}$ and $C_{L3}$. Thus

$$t_3 \approx -R_{load}C_{L3}ln\left(\frac{V_{out}(t_3) - I_{bias}R_{load}}{V_{out}(0) - I_{bias}R_{load}}\right) = 0.005ns \quad (4.19)$$

This generates $t_{HL}$ =2.026ns, which is in close accordance with the simulation shown in Fig. 4.13. It can be noticed that (4.18) points to the highest delay. As a comment on optimization, the drain terminal of transistor M3 can be biased to a voltage as low as ground in order to reduce (4.17) and make $t_2$ negligible with respect to $t_1$. In this way, the comparator delay can be similar to a single inverter delay (most influenced by $C_L$ and technology). See Fig. 4.14.

### Transition $t_{LH}$

Following Fig. 4.13, it can be observed the close relation on this transition time to the inverter transition time which is $t_1 \approx$0.242ns [99],

$$t_1 = t_{pLH} = \frac{C_L(Vdd - Vss)}{k_P(Vdd - Vss - |V_{thP}|)^2}. \tag{4.20}$$

This is due to the second stage described by Fig. 4.11d. As node $V_x$ has a low voltage fixed by the saturated transistor M4. When M3 leaves the cutoff region, the current flows from M3 to M4 and the transfer is direct, the fast adjustment of $V_x$ is due to the instant high transconductance of M3 (roughly $t_2 = 0$).

At the third stage described by Fig. 4.11e, the calculation reaches the same value of transition $t_{HL}$. Thus, the total time is $t_{LH}$ =0.250ns, which is in accordance with the simulation.

### 4.2.3 *Sign()*–based PWL functions

The generation of stair-type PWL functions with the V-I comparator is now shown from the point of view of integrated circuit. Later, the design is extended to saw-tooth-type functions.

#### Stair-type functions

A symmetric function respecting to the origin $V_{in} = 0$ in the form of (4.21) for odd number of steps or (4.22) for even number of steps is to be built,

$$g(x) = \begin{cases} 0 & |x| \leq B_p \\ 2ksgn(x) & \begin{matrix} |x| \leq B_p(2k+1) \\ |x| > B_p(2k-1) \end{matrix} \end{cases}, \tag{4.21}$$

here $k = 1, 2...$ accounts for $n = 1 + 2k$ number of steps and spaced by $B_p$ or

$$g(x) = (2k-1)sgn(x) \qquad \begin{matrix} |x| \leq 2kB_p \\ |x| > 2B_p(k-1) \end{matrix}, \tag{4.22}$$

for $n = 2k$ even number of steps.

Thus, there will be two parallel V-I comparators with opposed capacitive biasing. For each of the V-I comparators assume only two capacitors connected to the floating node ($C_1$ and $C_2$). Since the approximate break point $Bp$ is known the capacitor values are computed by (4.23) to (4.25)

$$\begin{aligned} C_2^q &= C_T \left( \frac{B_p^q}{V_{bias}} \right), && (4.23)\\ C_1^q &= C_T - C_2^q, && (4.24)\\ B_p^{q+1} &= \frac{C_1^q}{C_T} B_p^q. && (4.25) \end{aligned}$$

Observe that it is actually iterated since the signal compression changes the breakpoint, this process is followed for a few $q$ steps until the value of $B_p$ converges (it is sightly changed from the original).

For symmetry, the bias capacitor $C_2$ is connected to Vdd or Vss in each case. Now, other stairs can be added to the designed 3-stair function by choosing other values for the original $Bp$ and iterate it again. If the new breakpoint is a multiple of the first one, a convenient selection of the original parameter must produce bias capacitors multiples of the ones firstly computed.

Besides, since the value of $Bp$ will determine the attractor excursion (the size of scrolls), it must be chosen in accordance with the available dynamic range $DR$ and the desired number of steps $n$,

$$Bp < \frac{DR}{n}. \quad (4.26)$$

For $n = 5$ steps, one have the values for the inner stairs (see Fig. 4.15b). The additional two outer stairs are computed by replacing the value of $B_p$ by $3B_p$ as can be inferred by Fig. 4.15a in (4.23). By choosing $Bp = 147$mV, one have the set $\{C_2, 3C_2\}$ as the corresponding bias capacitors.

Note that having different values of the bias capacitor means a different compression of the received signal. To avoid these non-uniformities, ground capacitors $C_g$ are connected to the floating nodes of the cells in charge of the inner stairs (see Fig. 4.15b). This reduces the size of the input capacitor for breakpoint $Bp$ to the size of the same capacitor for $3Bp$.

In this way, with the selection of $C_T = 10$pF, $k = 0.92$, Equations (4.10) lead to $C_1 = 8.236$pF, $C_2 = 0.588$pF for 3-segment. Capacitor $C_3 = 2C_2$ will be used grounded. Besides, since the bulk capacitance is for this selection also equals $2C_2$, the layout design may be realized as a set of uniform capacitors as shown in Fig. 4.16 for 3 and 5-segment functions. This will also avoid mismatch effects since the perimeter to area relation is kept.

Observe that in practice, each step is set according to the circuit bias current which is to be switched $I_{bias}$ (adjustable amplitude through M7); thus, expression (4.21) and (4.22) are in fact scaled by the circuit factor $I_{bias}$. Figure 4.17a shows it with an extra scaling of $\xi = 0.8$.

Note also that for an even number of stairs, a non-biased V-I comparator is added ($Bp = 0$) to change the behavior at the origin. This will also need grounded capacitive bias to have the same signal compression factor as the others.

### Saw-tooth-type functions

A saw-tooth-type nonlinear function with slope $\xi$ can be generated by using a stair-type function with gain $\xi$ connected in parallel (summing) with function $h(x) = -\xi x$ as describes (4.27) for odd functions or (4.28) for even functions.

$$f(x) = \begin{cases} -\xi x & |x| \leq B_p \\ \xi(2ksgn(x) - x) & \begin{array}{l} |x| \leq B_p(2k+1) \\ |x| > B_p(2k-1) \end{array} \end{cases} \tag{4.27}$$

$$f(x) = \xi((2k-1)sgn(x) - x) \qquad \begin{array}{l} |x| \leq 2kB_p \\ |x| > 2B_p(k-1) \end{array} \tag{4.28}$$

For the circuit implementation, the gain of $h(x)$ may be given by $-\frac{\xi}{R}$, in this case it is required to fulfill the relation

$$\frac{\xi}{R} = \frac{I_{bias}}{B_p}, \tag{4.29}$$

where $I_{bias}$ is the amplitude of the step current given by the voltage-to-current cell and $1/R$ stands for the linear circuit gains. To properly couple these values, the amplitude is tuned by M6. The circuit response is shown in Fig. 4.17b.

Table 4.1: UGC transistor sizes.

| Cell | Type | Transistor | W ($\mu$m) | L ($\mu$m) |
|---|---|---|---|---|
| VF | NMOS | M3, M4 | 50.4 | 1.2 |
| | | M8 | 50.4 | 2.4 |
| | | M6, M9 | 100.8 | 3.9 |
| | PMOS | M1, M2, M5 | 148.8 | 1.2 |
| | | M7 | 148.8 | 2.4 |
| CF | NMOS | M3, M4 | 50.4 | 1.2 |
| | | M7, M8 | 50.4 | 2.4 |
| | PMOS | M1, M2 | 170.4 | 2.4 |
| | | M5, M6 | 148.8 | 2.4 |
| CM | NMOS | M5-M8 | 50.4 | 1.2 |
| | | M13-M16 | 50.4 | 2.4 |
| | PMOS | M1-M4 | 170.4 | 2.4 |
| | | M9-M12 | 148.8 | 2.4 |

Table 4.2: UGCs electrical parameters.

| Parameter | VF | CF | CM | Units |
|---|---|---|---|---|
| DR | $> \pm 1$ | $> \pm 100$ | $> \pm 100$ | V, $\mu$A |
| Gain | 0.985 | 1.00 | 0.989 | - |
| $f_{-3dB}$ ($C_L$=1pF) | 100 | 70 | 55 | MHz |
| $R_{in}$ (1MHz) | $\infty$ | 1.4 | 1.4 | k$\Omega$ |
| $R_{out}$ (1MHz) | 1.2 | 2470 | 290 | k$\Omega$ |
| Offset | 25 | -90 | <1 | $\mu$V, pA |

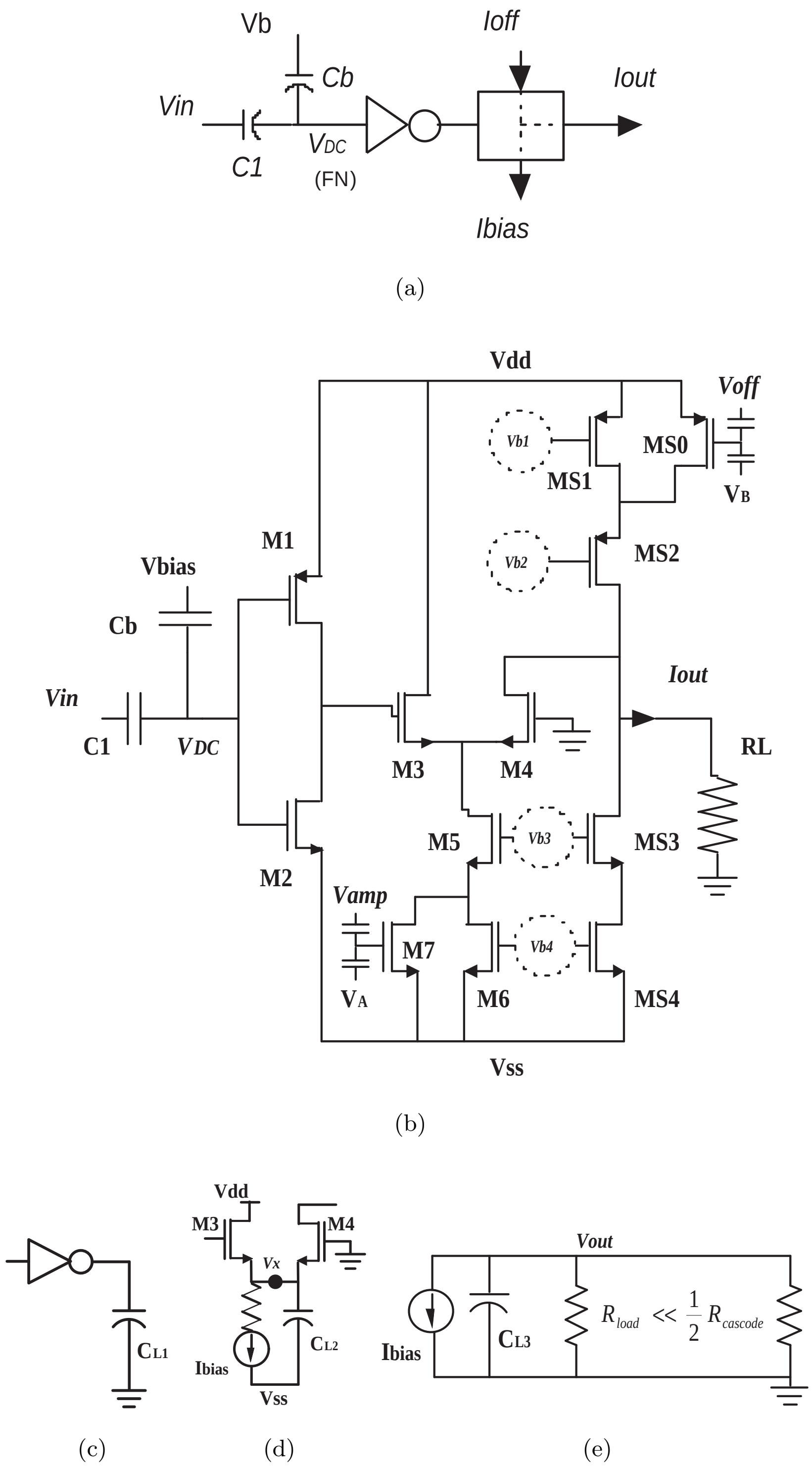


Figure 4.11: FGMOS based voltage-to-current cell, (a) simplified schematic, (b) CMOS design, and simplified stages: (c) inverter stage, (d) comparator stage, (e) output stage.

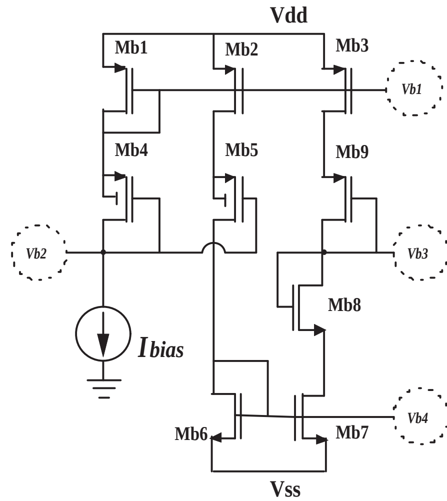


Figure 4.12: Cascode biasing of the proposed nonlinear cell.

Table 4.3: Nonlinear cell transistor dimensions.

| Transistor | Width ($\mu$m) | Length ($\mu$m) |
|---|---|---|
| M1 | 12.6 | 3.9 |
| M2 | 3.9 | 3.9 |
| M3, M4 | 1.8 | 1.2 |
| M5, M6, Ms3, Ms4 | 5.4 | 3.6 |
| M7 | 3 | 4.2 |
| Ms0 | 15 | 1.5 |
| Ms1, Ms2 | 15 | 3.6 |
| Mb1 to Mb5 | 15 | 1.2 |
| Mb6 to Mb8 | 5.4 | 1.2 |
| Mb9 | 5.4 | 6 |

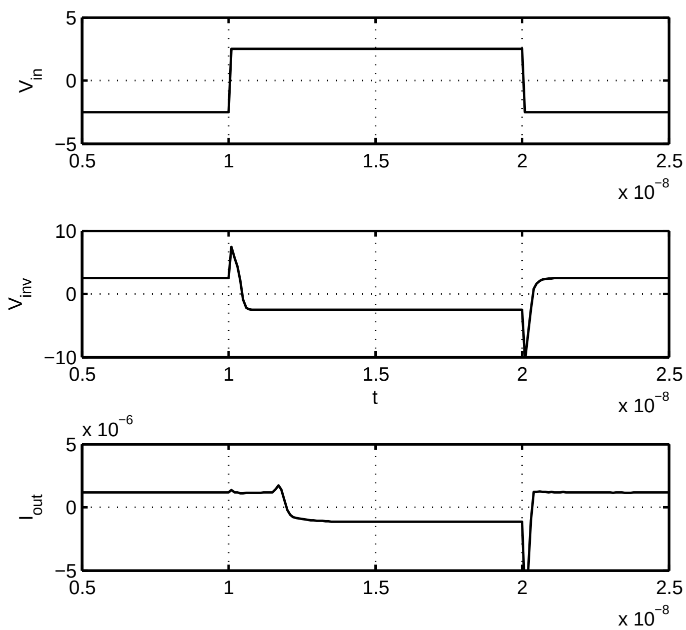


Figure 4.13: Hspice transient simulation for the high to low transition $t_{HL}$ at 10ns, and the low to high transition $t_{LH}$ at 20ns. Upper, middle and lower windows show the inverter input (Fig. 4.11c), the second stage input (4.11d), and the voltage-to-current cell output (4.11e), respectively.

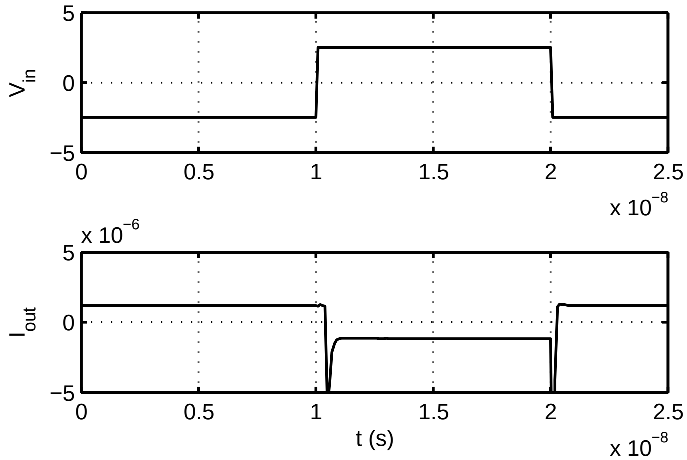


Figure 4.14: Hspice transient simulation for the voltage-to-current cell output optimized high to low transition $t_{HL}$ (near 10ns), and the low to high transition $t_{LH}$ (near 20ns).

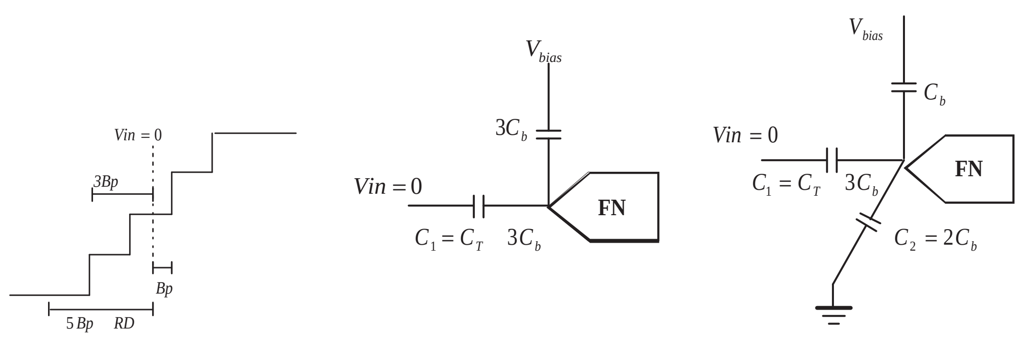


(a) (b)

Figure 4.15: Stair-type $n = 5$ function, (a) function basic relations, (b) bias capacitors connected to the FN.

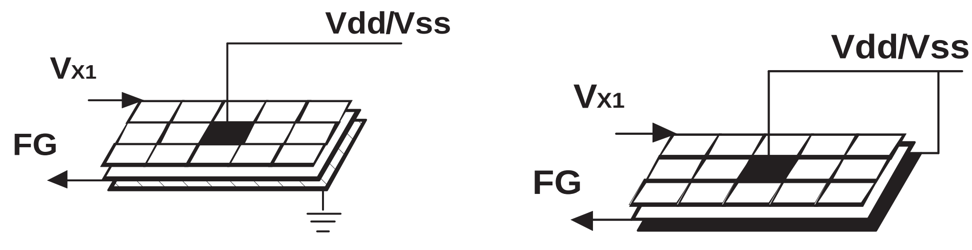


(a) (b)

Figure 4.16: Detail of the floating gate layout for the outer side (a) 3-segment function and, (b) 5-segment function.

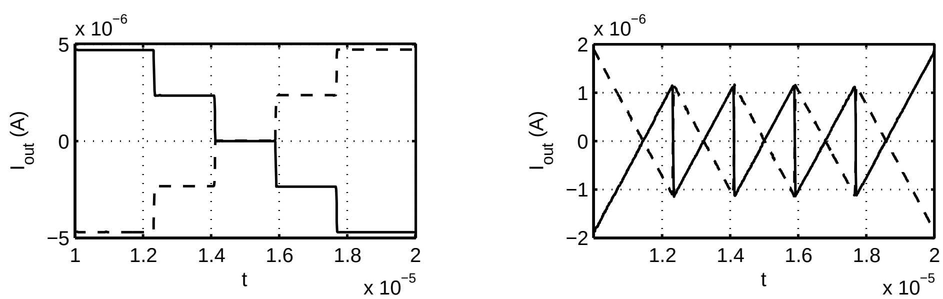


(a) (b)

Figure 4.17: PWL V-I functions CMOS transient simulation, input signal is -1V to 1V (dashed line), and 1V to -1V (solid line); (a) stair-type function, (b) saw-tooth-type function.

# Chapter 5

# Design performance and experimental results

A 3- and 5-scroll chaotic oscillator is designed for user control of the integrator gain. In this way a central $x_2$ dominant frequency of 100KHz is achieved in simulation with external capacitors of 22pF. The design frequency limitations is examined in terms of the linear buffers gain, the nonlinear cell delay (by a LE analysis), the parasitic capacitance of the external feedback (the attractor select), and the accumulated capacitance at the FGMOS comparator.

This last gives a very accurate description of the trade-off between the number of scrolls and the circuit frequency limit. In this way, simulations with the used 0.5$\mu$m technology reach up to 3.5MHz dominant frequency attractor, which is comparable with the maximum reported frequency for these systems, 7MHz in a 0.18$\mu$m technology.

The whole circuit layout shown in Fig. 5.1 allows comparing pre- and post-layout simulations of the design. These are in good agreement with the registered experimental behavior of the integrated prototype. It is worth to remark that the 5-scroll behavior is observed in integrated mode for the first time.

Additionally, the circuit robust behavior is discussed in terms of PVT analysis. This reveals the good performance of the designed UGCs, and the usefulness of the adjusting controls on the V-I comparator. These common controls change the PWL function

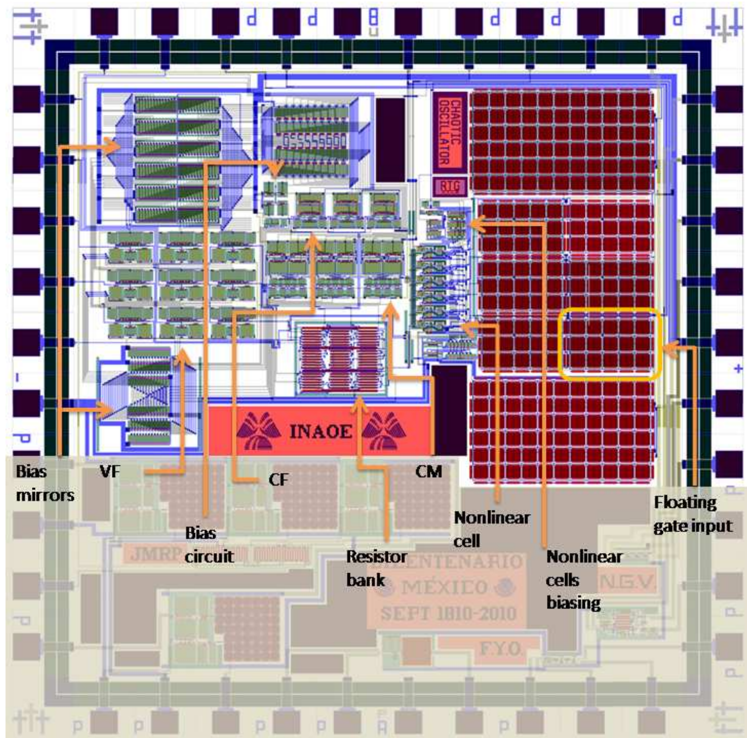


Figure 5.1: Layout of the multi-scroll chaotic oscillator as proposed in 4.3.

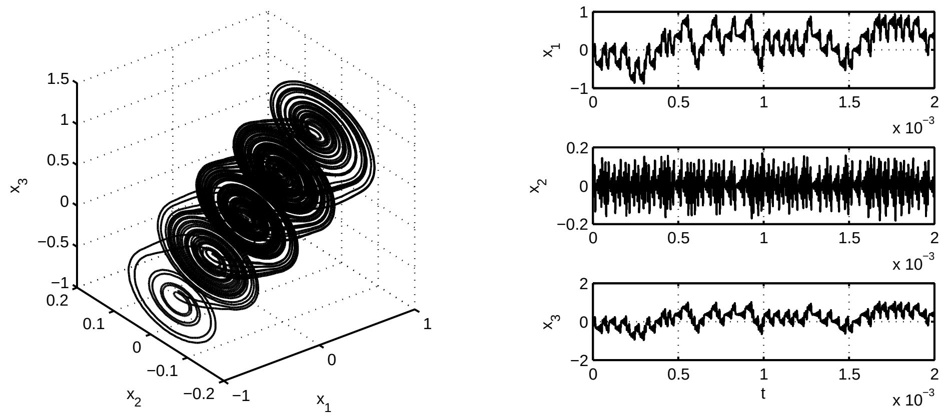


(a) (b)

Figure 5.2: Hspice simulation of the ≈100KHz chaotic oscillator in (a) phase space, and (b) time.

amplitude and offset. The nonlinear function is then presented and re-adjusted. The 5-scroll attractor is observed in each case for a 100x the period of the dominant frequency, in some cases the system orbital period has grown greater than this and a scroll seems as been lost. However, in the great majority of the cases, the attractor integrity is conserved over all the variations.

## 5.1 Simulation Results

The complete oscillator designed following the scheme shown in Fig. 4.3 and the nonlinear saw-tooth function design generating 3- and 5-scroll attractors. External integration capacitances are used to control the spectra scaling of the system. A 10pF parasitic capacitance has been supposed in the buffered output of variable $x_1$ which is feedback to the desired PWL function input. Hspice simulations before layout are shown in Fig 5.2 for integrator capacitance of $C = 22$pF, this correspond to a 100KHz dominant frequency $f_{x2}$.

In order to know the frequency limits of this design, the dominant parasitics effects

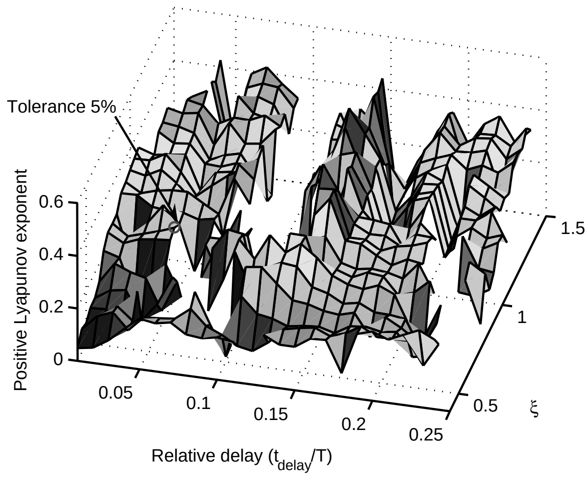


Figure 5.3: The positive Lyapunov exponent as a function of slope $\xi$ and the relative delay ($t_{delay}/T$) of the comparator response.

are now revisited:

*Linear cells dominant pole*

Considering the system spectra and the electric parameters given in Table 4.2, it is reasonably to assume that with the selection of the integrator capacitors, the dominant frequency $f_{x2}$ can raise up to 25MHz approximately due to the CM pole.

*Nonlinear cell delay*

The nonlinear function delay can be represented as a fraction of the dominant period $T$ of the system. In this way, as the period decreases, the relation is changed. Call this relation ($t_{delay}/T$), a Lyapunov analysis of the system is made to found the limits on the system stability and chaotic behavior. Figure 5.3 suggest that for the selection of coefficient $\xi = 0.8$, the maximum delay to period relation tolerated is 5%. Now, as explained in Chapter 4, if the 2ns delay time is used, this gives a frequency limit of 25MHz.

*External attractor selection*

If external connection is used to choose the attractor, a typical experimental setup may have a 5pF parasitic capacitance which will combine to the output VF resistance to limit the dominant frequency to less than 13MHz. This is surmounted by the high frequency design which has no external inputs except for the biasing.

*The amount of scrolls*

Another dominant pole occurs on the input of the nonlinear function since the FG-MOS structure grows in capacitance with the number of scrolls (i.e. parallel connected comparators). Recall form the design of the nonlinear comparator that the used capacitors are notably higher than the parasitics and consider these only. The input capacitance of a single comparator is then $C_{comp} = C_1||(C_T - C_1) = 1.455pF$, thus a low frequency pole is formed with the output resistance of the precedent buffer $R_{outVF}$. Call $n_s$ the number of scrolls, then eq. (4.12) is rewritten as

$$f_p = \frac{1}{2\pi R_{outVF}(n_s - 1)(C_1||(C_T - C_1))}. \tag{5.1}$$

Thus for a 2-scroll oscillator, this leads to 91MHz, this will divide by $(n_s - 1)$ according to the scroll number, for 3-scroll one the dominant frequency will be limited to about 22MHz.

However, the signal transmission by the clustering of such high capacitance at the input of the nonlinear function is also limited by the slew rate (SR) of the VF. Consider the highest SR function given by the delivered current and the load capacitance $C_L = (n_s - 1)C_{comp}$ as

$$\frac{V_{out}}{\Delta t} = \frac{I_{max}}{C_L}. \tag{5.2}$$

To this point the shape of the chaotic input signal $x_1$ is approximated by a sinusoidal with peak amplitude $V_p = 2n_s Bp$, in dependence with the number of scrolls, and frequency $f$. Thus, by using its derivative, maximum slope $2\pi f V_p$ is obtained. Therefore, (5.2) can rewritten to show the dominant frequency limit for the $x_2$ variable as

$$f_{x2} \approx \frac{I_{max}}{2\pi k_s n_s Bp(n_s - 1)C_{comp}}. \tag{5.3}$$

Factor $k_s > 1$ is used to approach the relation between the whole significative spectra and frequency $f_{x2}$. Also, $Bp = 0.147$, and the maximum bias current of the active devices is $I_{max} = 30\mu$A. Thus Fig. 2.4a suggests that the maximum dominant frequency

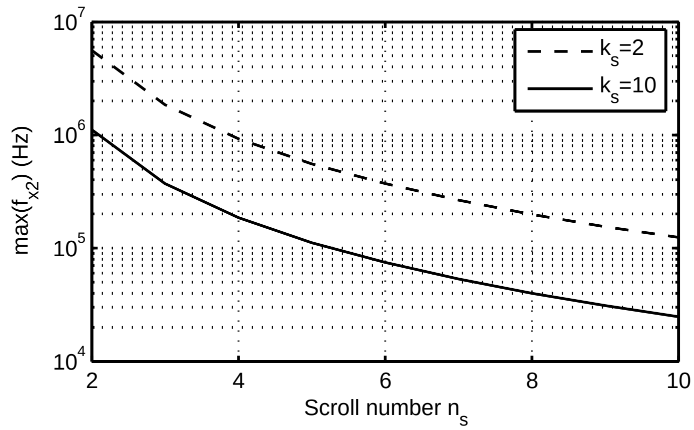


Figure 5.4: Possible limits for the highest dominant frequency $f_{x2}$ according to the limited slew rate and the equivalent capacitance of the nonlinear function showing the dependence on the number of scrolls. Coefficient $k_s$ accounts for the relation between the system spectra and the dominant frequency $f_{x2}$.

may be located around the curve $k_s = 2$ in Fig. 5.4 and certainly above the curve $k_s = 10$.

Note that the dominant frequency in $x_2$ has been taken in the place of $x_1$, this is valid for the cases in which the PWL function region is being switched by the farthest region, i.e. signal $x_1$ is changing from one of the extreme scroll to the other extreme scroll, thus both frequencies will be similar.

In accordance to this derived limit, a fully integrated version of the oscillator in 3-scroll was observed in simulations to achieve up to 2.6MHz dominant frequency $f_{x2}$, as depicted Fig. 5.5 and Fig. 5.6. By changing system coefficient $\xi = 1$, the dominant frequency was observed to achieve 3.5MHz. This is a similar result to the reported by Fujiwara [29] for a design on 0.18$\mu$m technology, recall that the actual technology is 0.5$\mu$m.

The oscillator layout was made by using Tanner suite version 13. Postlayout simulations resemble the attractor characteristics for 3- and 5-scrolls, as show Figs. 5.7 and 5.8 respectively. Similar results are observed in the frequency analysis for both attractors as show Fig. 5.9.

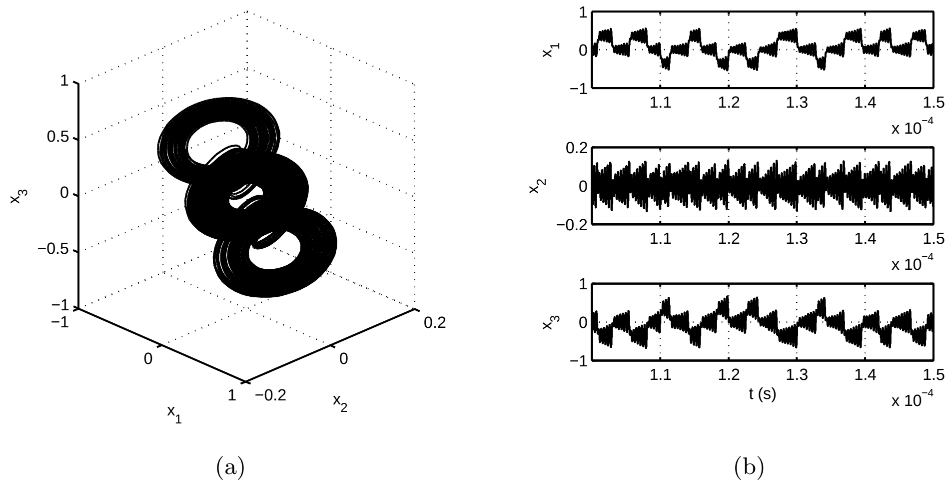

Figure 5.5: Hspice simulation of the ≈2.6MHz chaotic oscillator in (a) phase space, and (b) time.

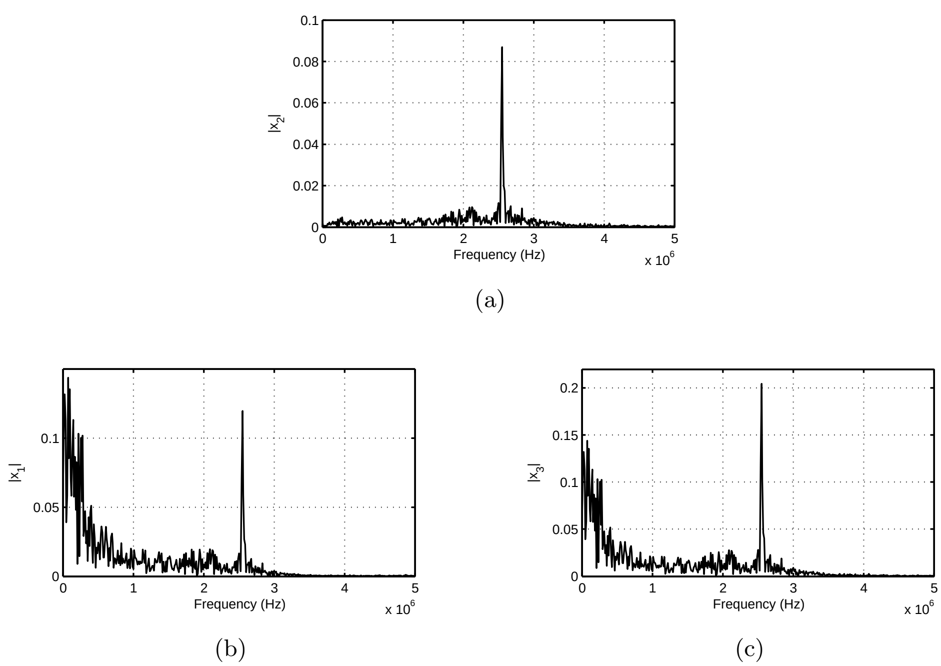

Figure 5.6: FFT analysis of the signals, (a) $x_2$, (b) $x_1$, and (c) $x_3$.

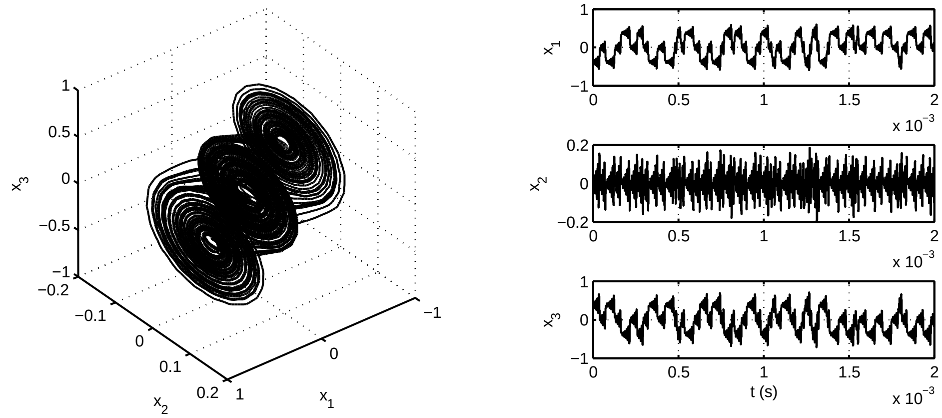


(a) (b)

Figure 5.7: Hspice postlayout simulation of the prototype chaotic oscillator showing 3-scrolls in (a) phase space, and (b) time.

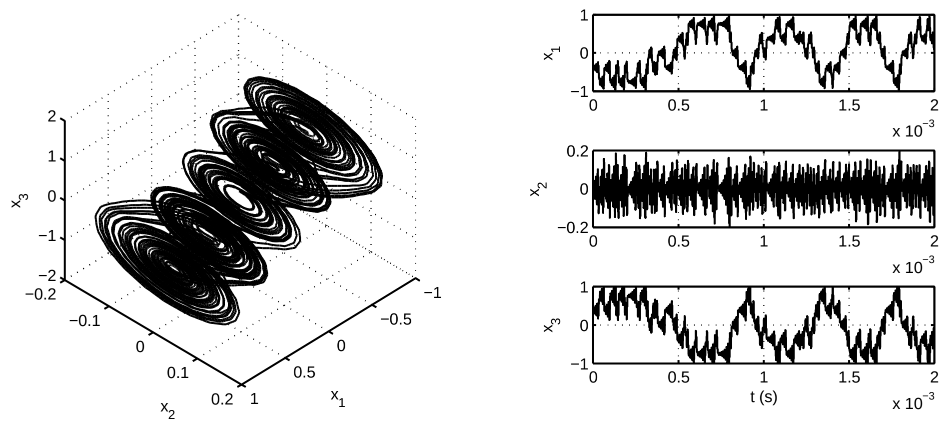


(a) (b)

Figure 5.8: Hspice postlayout simulation of the prototype chaotic oscillator showing 5-scrolls in (a) phase space, and (b) time.

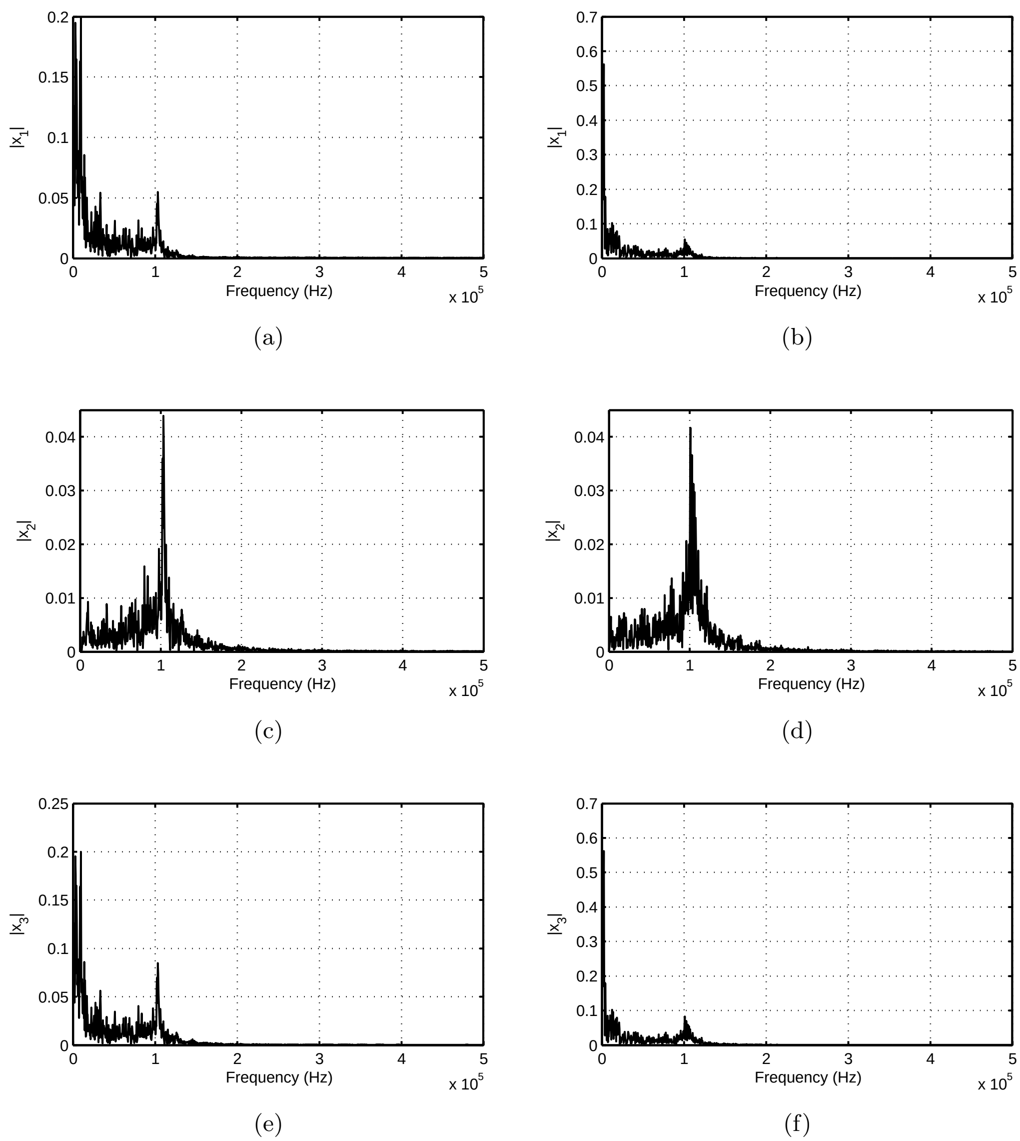


Figure 5.9: FFT analysis of the extracted signals for, (a,c,e) the 3-scroll attractor, and (b,d,f) the 5-scroll attractor.

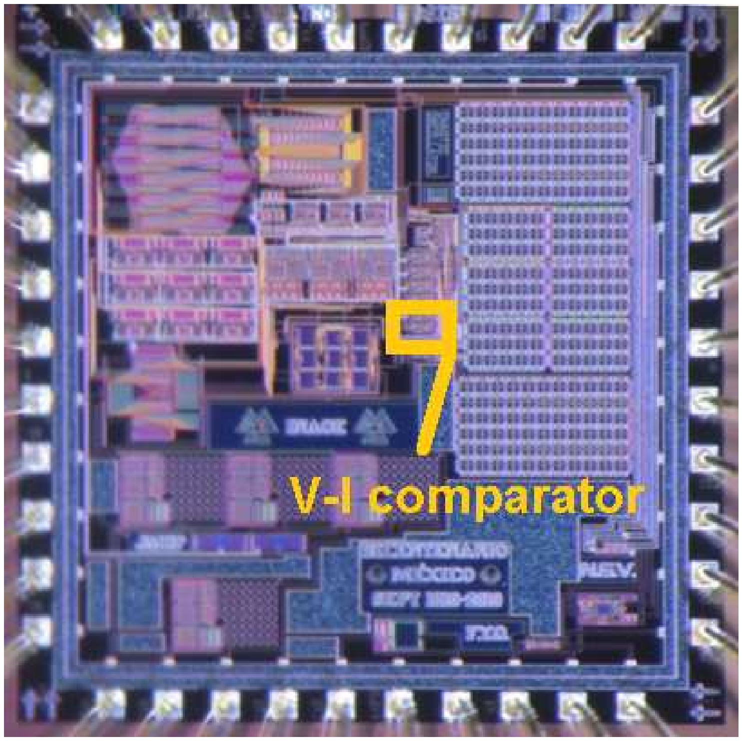


Figure 5.10: Chip microphotography.

## 5.2 Experimental Results

The proposed design was fabricated using 0.5$\mu$m ON semiconductor technology, the chip microphotography is shown in Fig. 5.10. Technical details and pin connection sheet are found in Appendix C. The system output signals $x_1$ and $x_2$ are shown in time in Fig. 5.11 for a 3 and 5-scroll behavior. The attractor is observed in Fig. 5.12 for 3- and 5-scrolls respectively.

The maximum dominant frequency $f_{x2}$ was performed within parasitic capacitances over 10% of the used integration capacitors. In the experimental setup, these were approximately 5pF, then the lowest capacitor used was $C$=47pF, thus a dominant frequency of about $f_{x2}$=50kHz was obtained. Figure 5.13 shows the spectrum of $x_1$ and $x_2$ for 3 and 5-scroll attractors.

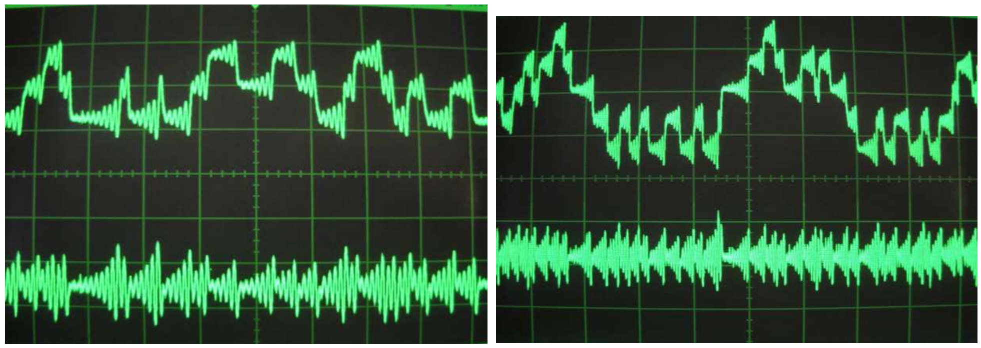

(a) (b)

Figure 5.11: Observed signals $x_1$ and $x_2$ in time for (a) 3-scroll attractor (X-axis 500$\mu$s/div, Y-axis 500mV/div for $x_1$, and 200mV/div for $x_2$), and (b) 5-scroll attractor (X-axis 1ms/div, Y-axis 500mV/div for $x_1$, and 200mV/div for $x_2$).

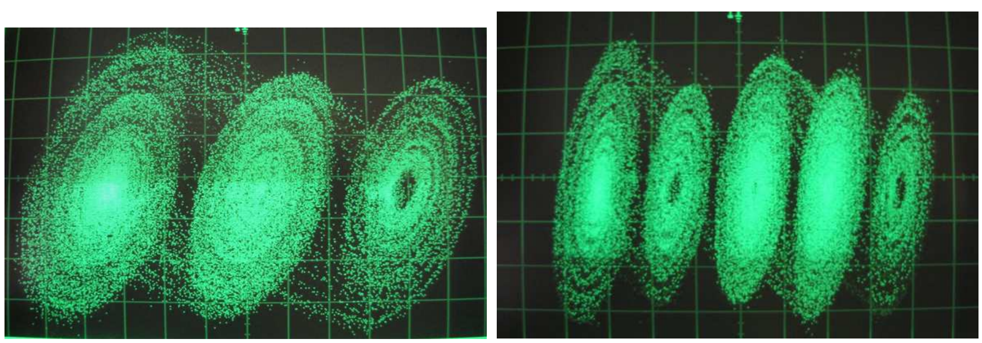

(a) (b)

Figure 5.12: Observed signals $x_1$ and $x_2$ in phase showing (a) the 3-scroll attractor (X-axis 100mV/div, Y-axis 50mV/div) and (b) the 5-scroll attractor (X-axis 200mV/div, Y-axis 50mV/div).

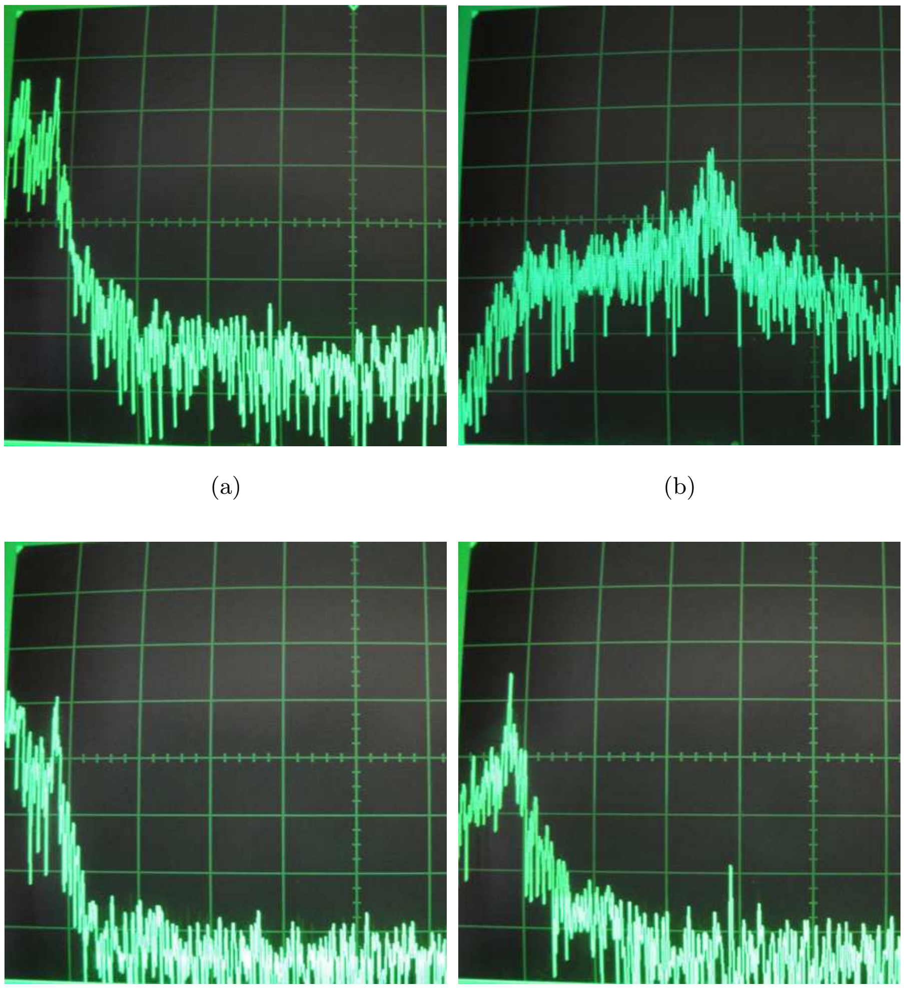

(a) (b) (c) (d)

Figure 5.13: Spectrum of experimental signals for a 3-scroll attractor (a) $x_1$, (b) $x_2$; and for a 5-scroll attractor (c) $x_1$, (d) $x_2$. X-axis 50kHz/div, Y-axis 10dB/div, center 250kHz, offset -40dB in subfigures a,c,d; and X-axis 10kHz/div, Y-axis 10dB/div, center 50kHz, offset -40dB in subfigure b.

Table 5.1: PVT maximum variations of the UGCs electrical parameters.

| Cell | Absolute offset (mV/$\mu$A) | Relative -3dB frequency (%) | Relative gain (%) |
|---|---|---|---|
| VF | 5.993 | 16.6 | 0.3 |
| CF | 2.489 | 20.2 | 0.6 |
| CM | 0.020 | 12.6 | 0.07 |

## 5.3 Design for Robust Behavior

The whole oscillator design is now analyzed from the perspective of process variations. First the linear active cells are observed. Hspice simulations over the BSIM3v3 model have been made by using the typical process and the four corners: (NMOS-PMOS) typical-typical, fast-fast, fast-slow, slow-fast, slow-slow (TT, FF, FS, SF, SS, respectively) of the actual technology. The temperature has been sweep between $-20\,^{\circ}$C and $100\,^{\circ}$C. For the case of the linear cells, the supply voltages has been also changed in $\pm 10\%$ of its nominal value. Electrical parameter variations of the PVT analysis are summarized in Table 5.1.

Despite the topology and functionality differences of the linear and the nonlinear part of the oscillator, another not less important is the independent biasing which is carried out in scaled designs of the same circuit topology shown in Fig. 4.12. This makes imperative the use of adjusting controls for achieving good matching between these two parts.

To further prove the nonlinear design robust behavior, the usefulness of the controls $Vamp$ and $Voff$ in the generation of accurate nonlinear functions is now observed. Recall from the previous Chapter that these controls are used to change the amplitude and the output offset respectively. The maximum absolute deviations for the comparator output offset and amplitude were observed in the temperature limits, these are summarized in Table 5.2.

Recall that the exponential behavior allows the adjusting of such variations by ad-

Table 5.2: Maximum deviations of the adjusted signals.

| Process | Amplitude ($\mu$A) | Offset ($\mu$A) |
|---|---|---|
| TT | 0.34 | -1.89 |
| FF | 1.08 | -6 |
| FS | 0.95 | 9.93 |
| SF | -0.94 | -6.65 |
| SS | -0.92 | -1.41 |

justing the control input. Thus, All the corners showed that the desired offset can be reached by tuning it except for the offset in the fast-fast case at $-20\,^{\circ}$C. The analysis is shown in Fig. 5.14.

The amplitude variations are controlled in a similar manner by M7, thus they grows with the increase of $Vamp$. The corner analysis was also performed and is shown in Fig. 5.15. In all cases, the desired amplitude is easily reached.

Although, the saw-tooth function for a 5-scroll attractor is shown in Fig. 5.16 in the process corners TT, FF, FS, SF and SS. The effect of the common adjusting inputs $Vamp$ and $Voff$ is noted by comparing Fig. 5.16a with the rest. Another important effect is the observed excessive hysteresis for the cases fast-slow and slow-fast (Figs. 5.16d and 5.16e, respectively). This is clearly the most remarkable failure in the inverter operation. Despite this effect, the whole oscillator simulations show the ability to perform multi-scroll behavior over the process variations with proper adjust of the offset and amplitude of the proposed nonlinear function.

A 5-scroll attractor was then obtained in a 1ms simulation using a 110KHz $x_2$-dominant frequency in all the cases except for FF $60\,^{\circ}$C, SF $60\,^{\circ}$C and $100\,^{\circ}$C, and SS $20\,^{\circ}$C (see Fig. 5.17), where the nonlinear function has loose its original form. The figure shows the consequently loose of some scroll whenever the orbital period grows over the simulation time. This does not imply the completely loss of a scroll, but points

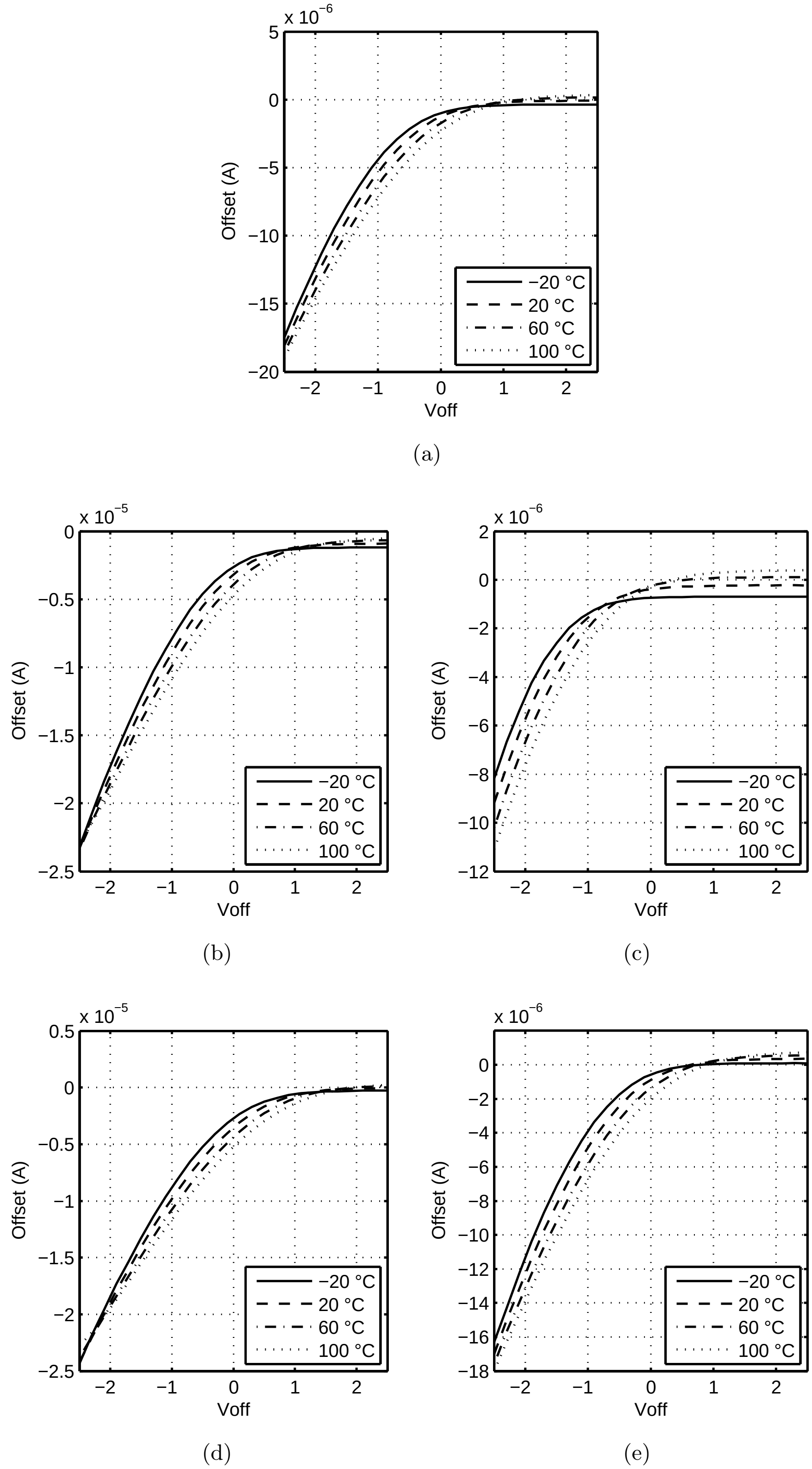


Figure 5.14: Total output offset variations of the comparator in process (a) TT, (b) FF, (c) FS, (d) SF and (e) SS.

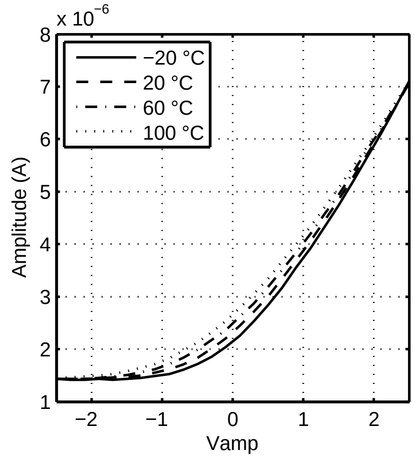


(a)

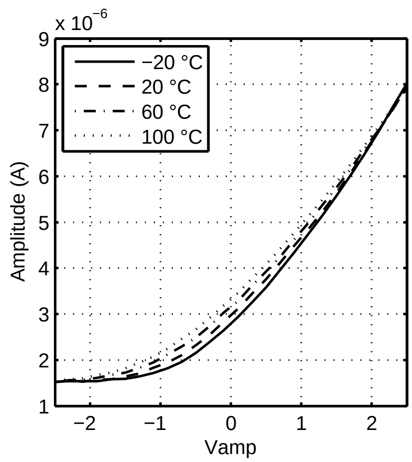


(b)

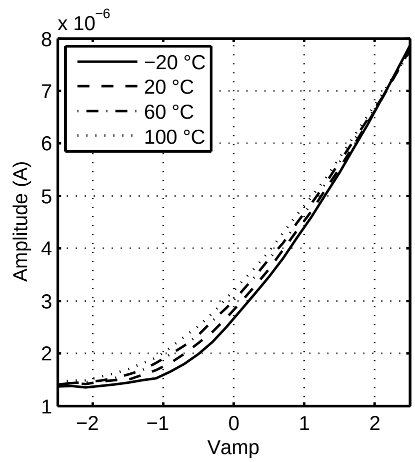


(c)

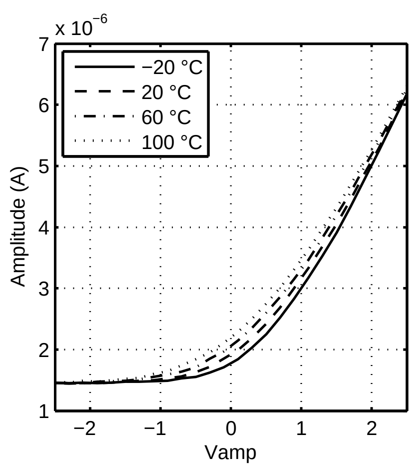


(d)

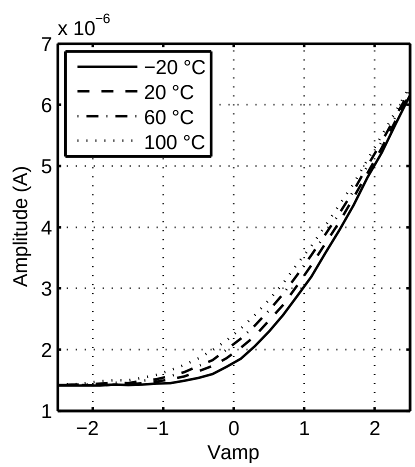


(e)

Figure 5.15: Peak-to-peak output amplitude variations of the comparator in process (a) TT, (b) FF, (c) FS, (d) SF and (e) SS.

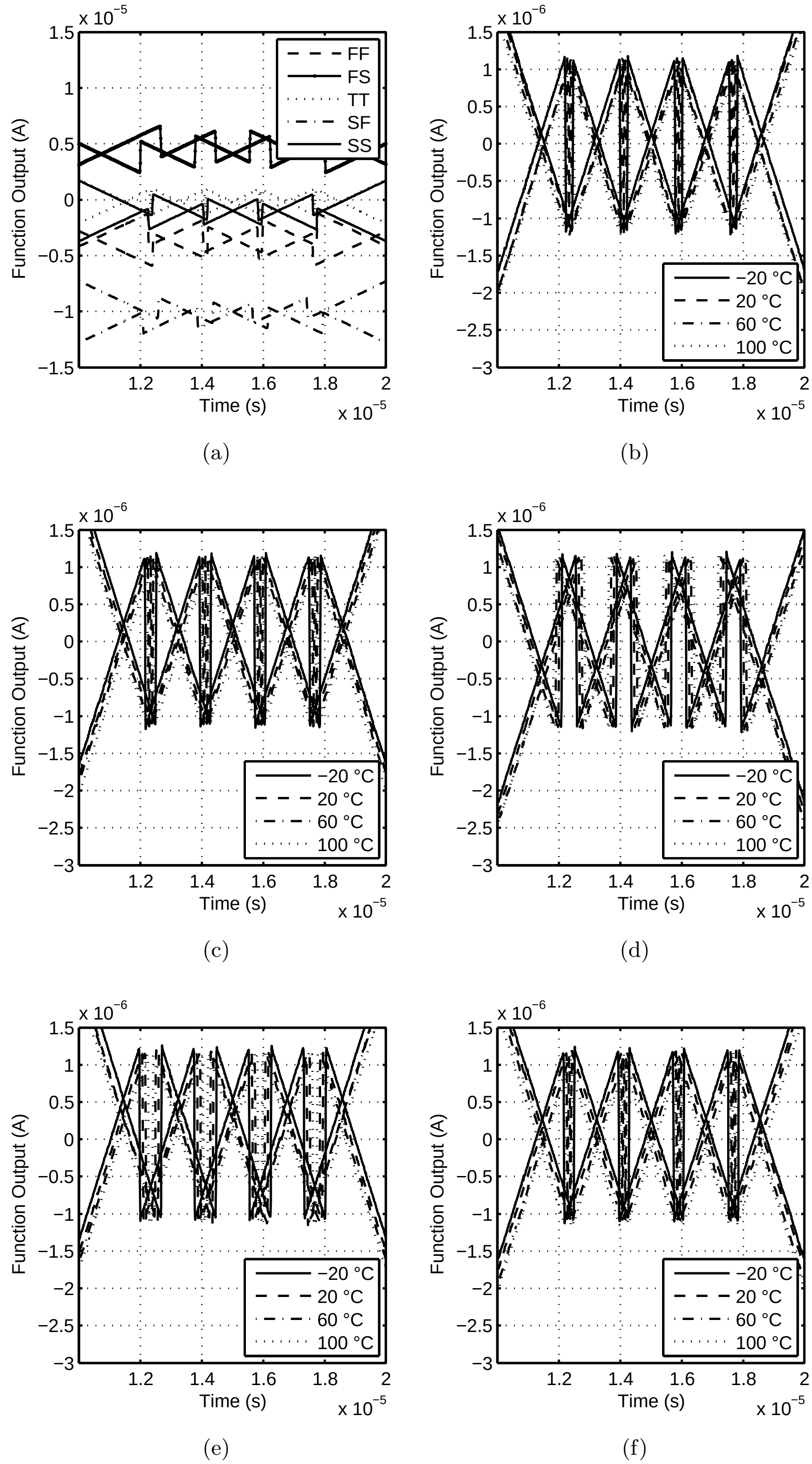


Figure 5.16: The 5-scroll function variations over the process corners: (a) without adjustment, at 20 °C; and with adjustment for each process: (b) typical-typical, (c) fast-fast, (d) fast-slow, (e) slow-fast and (f) slow-slow cases.

the weakness on the generation of the corresponding equilibriums.

The variations over the supply voltages have not been considered in the simulation analysis, since the actual circuit has no external input signals (the system is autonomous) and thus internal offset can be compensated by the tuning of $Voff$. The experimental results confirm this issue since the zero reference seems to be slightly different than the external ground.

The analysis made on this section suggest that to improve the efficiency of the inverters on nonlinear functions generation, process compensation techniques should be used. In addition, the use of non-autonomous systems for chaotic signal generation may be more advantageous.

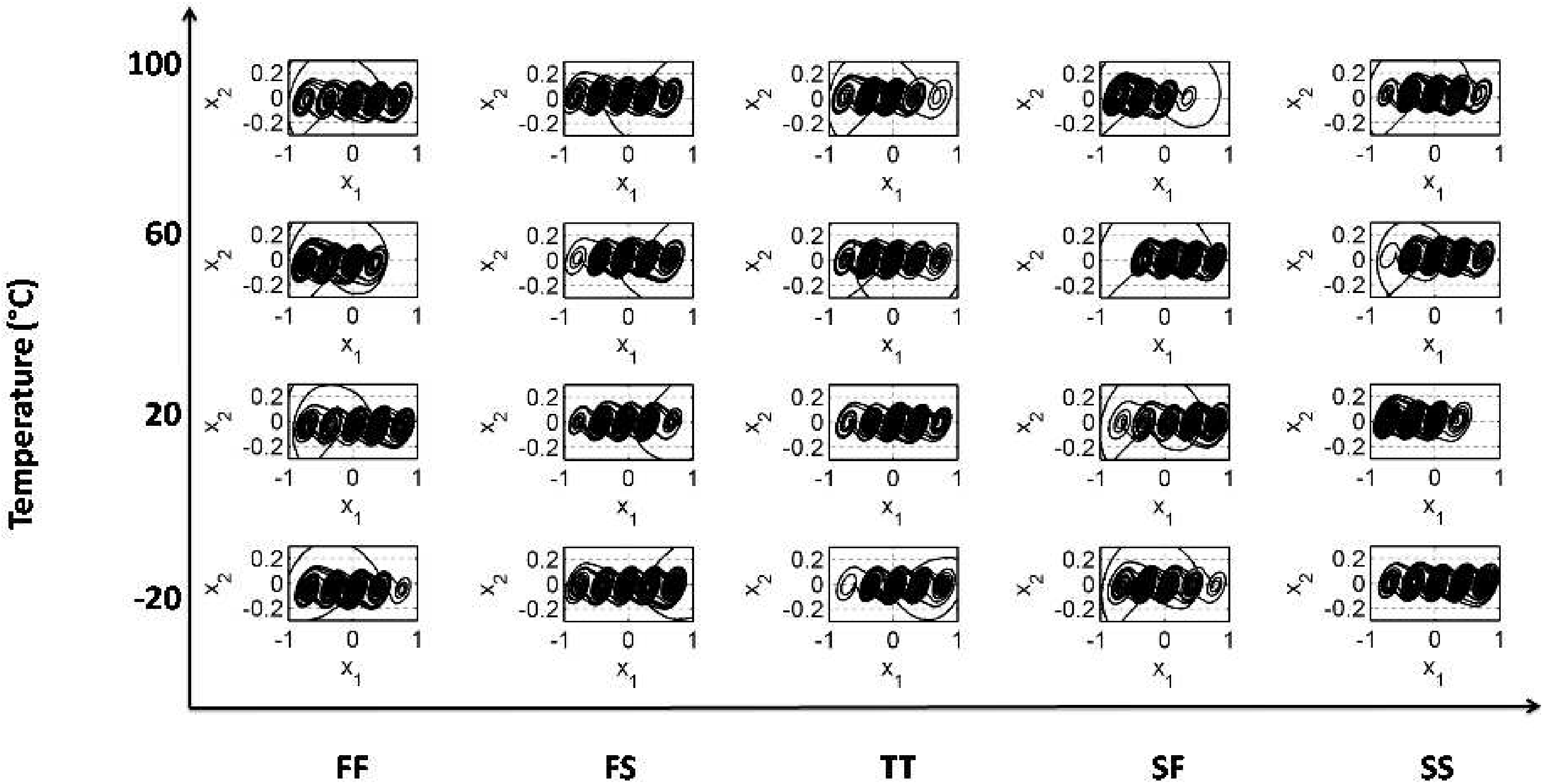


Figure 5.17: Hspice simulations of the 5-scroll attractor, the nonlinear function has been tuned over the process and temperature variations. Some of the chaotic attractors show orbital period higher than 1ms for a 110KHz $x_2$-dominant frequency or lost a scroll.

# Chapter 6

# Conclusions

The main products of this Thesis are described in brief:

The introduction of macro-models allows one to observe the effectiveness of the diverse approaches for synthesizing chaotic oscillators. However, the integrated realizations requires a set of considerations which are devoted mainly to:

- Keep the value of the system parameters by observing carefully the signal coupling.
- Choose and differentiate the required bandwidth of the active devices in the circuit, since it has different demanding.
- Allow the offset control (for the case of the comparator), which is essential in these autonomous systems.
- The generation of nonlinear functions is a complex problem that has several degrees of freedom (such as the amplitude, offset, spacing, delay), and thus the need of several adjustment controls is mandatory. Nowadays, external adjustments are numerous in all the known cases as [9, 29, 63] just to mention the most relevant. In this Thesis, the realization of the nonlinear functions allows a simplified obtention and verification of the circuit behavior.

FGMOS-based adjustments were introduced in two modes:

- Internal, since the function breakpoints were efficiently keep by the relative sizes of the integrated FGMOS capacitors.

- External, in which the compression effect was used to adjust the switched current amplitudes and then to match it to the integrated resistor values. Besides, it makes possible the adjust of the function offset.

A new strategy was developed to generate PWL-sign-based functions (largely used in chaotic systems) in systematic way, this showed its usefulness in the simplified circuit settling, and also, establish a new potential approach in the design of integrated self-adjusting controls for the generation of these functions.

FGMOS based chaotic oscillators were proposed earlier [29], but experimental 2- and 3-scroll attractors were the only results. In this Thesis, an organized an systematic approach allows the generation of multiple scrolls plus the advantage of having a minimal set of external controls, and a well estimation of the frequency limits.

Corner-based analysis was performed to confirm the robustness of the approach in that sense. This kind of analysis has been reported here for the first time. Also, this test has revealed some of the design weak points which come principally from the simple inverter. This points to future enhancements in the design of these kind of oscillators.

In summary, this investigation has surveyed the development of multiple scroll chaotic oscillators from the point of view of dynamical systems, the circuit design and modeling, and the CMOS compatible integrated level. The prototype behavior has been observed accordingly and with the corner analysis, the effectiveness of the proposed design approach is proven. Although there are still some issues to enhance, this Thesis has been organized also to be a guide in the integrated realization of multi-scroll chaotic systems.

## 6.1 Future Work

In order to use fully integrated solutions for the generation of chaotic signals, the issue of self-adjustment of the amplitude and offset can be treated in future work. At this point it is suggested to change the effective width of some of the transistors conforming the inverter to automatically match its counterpart. This change must be sensible to temperature and process variations and can also be applied for other non-chaotic circuits.

The principle in the generation of nonlinear functions by step responses was developed; however, the functionality of the proposed V-I comparator can be proved in the design of other nonlinear functions by controlling the bias switching of a CF for example. In this case the final offset would be determined entirely by the linear cell.

In the generation of integrated chaotic oscillators in general, autonomous systems have proven to work at large frequencies [11], however, some issue is found in the complexity. Some approaches uses intrinsic states just as those found in discrete systems, thus the physical implementations are reduced. For example, if the hysteresis-based nonlinear functions are considered, chaotic dynamical systems close to order one shows to be possible. In this way, to generate complex behavior by means of an area and frequency-optimized oscillator systems may not be strictly continuous, while they will never be completely discrete.

If the need is in the increase of exponential divergence (positive Lyapunov exponents), all the system coefficients must be analyzed in order to attempt for the scale control of each in uniform manner, and then to be able to increase Lyapunov exponents and the frequency spectrum as described in this work.

Also, the analysis on Lyapunov exponents in an unfinish task, since no analytical expression may be always obtained. But a more detailed analysis in the relation of these exponents with the Jacobian eigenvalues can be used to search for empirical expressions at least in some chaotic systems.

Respecting the frequency, expressions for the lowest poles and the number of scrolls have been given for the proposed approach, however, the is not yet any clear relation between the circuits offset (which affects the output resistance), and the frequencies.

The chaotic synchronization is made by multiple approaches and one of the most attractive applications is in the encryption and decryption of information. Solutions to enhance the transmission rate of these approaches to make it comparable to the discrete counterpart have not yet been given. However, real parasitics and channel effects must be studied in order to concrete ideas and guide the integrated design in this field.

Synchronization may also be used in order to give insight in the differences between ideal and real system signals by statistical analysis. In this way, a tool for measuring the quality of a system synthesis (or the nonlinear distortion) may be achieved.

Further interesting contributions may be made in the field of fractionary chaotic systems, since the introduction of fractional calculus and fractional passive elements may lead to compact integrated realizations of chaotic oscillators [100, 101], due to the high order approximations that these fractional devices simulate.

After all, one must agree that nowadays, continuous chaotic oscillators have not been fully exploited and practical potential applications remain still hidden. Humanity is barely understanding the complexity that takes to the explanation of dynamics in life, and there are many process suitable for partnering with chaos.

# Appendix A

# Bifurcation diagram

One way of analyzing chaotic long term motion in discrete systems, is by recording every point on the trajectory respecting to a particular parameter which is been sweep. This technique has been generalized for continuous systems by changing the term "every point" by "local maxima".

Thus, long term dynamics are been observed as a line for periodic behavior. This line will divide into several branches as the harmonic peaks grows in number and changes amplitude (period-doubling); and eventually the field for a particular parameter value is being spread of many different signal amplitudes which are indicating chaotic behavior. It is important to remark that following this procedure, quasi-linear dynamics would present finite amount of amplitudes (while there are infinite number of frequency peaks) and then would be distinguished easily from chaotic dynamics by the bifurcation diagrams. However, system dependent variations must be considered for avoiding register extra local peaks for the same cycle [75].

The general procedure to obtain such diagrams is based on the integration of the system (by some user defined method such as the Rouge-Kutta based Matlab ODE45) and to register every local peaks of the time function after a initial condition transient is been passed. In our study, the second half of the time series required to reach a Lyapunov exponent within the 0.1% of uncertainty has been used to this record.

The procedure is repeated for each value of the sweep parameter and is plotted as set of points which disengages as the system enters in chaotic region. Some times, islands of stability may appear for some values which will be followed by the corresponding downhill of the Lyapunov exponent. This reason motivates the application and presentation of both analysis in tiled plots.

## A.1 Matlab code

The following Matlab code *picos(a)* was used to find local peaks in a solved dynamical system which is parsed by string *a*.

The solving process may have time as a separate vector, thus to effectively locate the corresponding points in time, one may use the call: *timeloc=usertimevector(picoloc);*.

```
function [picoloc,picoval] = picos(a)


% Fuction to find local peaks on a string Nx1
% This simple function is not available in some existing versions of Matlab
% Copyright Rodolfo Trejo G. and Esteban Tlelo C. INAOE 2011
%
%Example of usage:
%a=rand(50,1);
%a=[1 1 2 3 2 3 3 4 3 3 2 4 4 4 4 3 3 2 3 2 2 1];
%[picoloc,picoval] = picos(a);
%plot(a);
%hold on
%plot(picoloc,picoval,'ro');
%
%To change location reference use
%timeloc=usertimevector(picoloc);
```

```
%--------inicializaciones
min=0; loc=0; picoloc=[]; picoval=[];
dejasubir=diff(diff(a)>0)<0;
dejasubir=[dejasubir;0];
comienzabajar=diff(a)<0;
n=length(a);

%---------localizacion de maximos
for i=1:n-1

  if dejasubir(i)
    min=i+1;
  end;

  if comienzabajar(i) && min
    loc=floor((i+1+min)/2);
    picoloc=[picoloc,loc];
    picoval=[picoval,a(loc)];
    min=0;
  end

end  % i
```

# Appendix B

# Lyapunov Exponents Computation

The Lyapunov exponents can be computed by applying the methods given in [9]-[12]. They provide information on the average exponential rate of divergence or convergence of trajectories which are very close in phase space. The number of Lyapunov exponents equals the number of state variables, and if at least one is positive, this is an indication of chaos. Furthermore, by having more positive Lyapunov exponents, a system is called to be hyperchaotic.

A method independent of integration process is been designed in Matlab, allowing the computation by several integration algorithms. The default which is written here in the code calls Matlab routine ODE45 (a variable step fourth order Runge-Kutta based integration method). The method is summarized as follows [23]:

(a) Initial conditions of the system and the variational system are set to $\mathbf{X}_0$ and $\mathbf{I}_{nxn}$ respectively.

(b) The systems are integrated by several steps until the orthonormalization period $TO$ is reached. The integration of the variational system $\mathbf{Y} = [y1, y2, y3]$ depends on the specific Jacobian that the original system $\mathbf{X}$ is using in the current step.

(c) The variational system is orthonormalized by using the standard Gram-Schmidt method [24], the logarithm of the norm of each Lyapunov vector contained in **Y** is obtained and accumulated in time.

(d) The next integration is carried out by using the new orthonormalized vectors as initial conditions. This process is repeated until the full integration period $T$ is reached.

(e) The Lyapunov exponents are obtained by using

$$\lambda_i \approx \frac{1}{T}\sum_{j=T0}^{T} ln\|\mathbf{y}_i^j\|. \tag{B.1}$$

Time step selection was made by using the minimum absolute value of all the eigenvalues of the system $\lambda_{min}$ [25], and $\Psi$ was chosen well above the sample theorem as 50.

$$t_{step} = \frac{1}{\lambda_{min}\Psi} \tag{B.2}$$

We choose to give an orthogonalization period $TO$ of about 95 tstep, which is a third of the period corresponding to the maximum central frequency of the chaotic system. The integration time can be varied by parameter $T$. Initial conditions were $\mathbf{x}_0 = [0.1, 0, 0]$ in all cases, where the ergodicity property implies that $\lambda_i$ is unique as $T \to \infty$.

## B.1 Matlab code

Below is shown the routine to compute Lyapunov exponents *restitsaw()* which is based in the integration algorithm of function *fresaw()*.

```
function [EL] = restitsaw(xi, conti)
%COMPUTE LYAPUNOV EXPONENTS (LE), SPECIFY t_total=tt
%
limax=10; h2=0.70; n=3; alfa=3; beta=4; BP1=1;
```

```
% xi=0.8;
% conti=0.05;
%
%INITIALIZING
x=[0.1,0,0]; Y=[1,0,0, 0,1,0, 0,0,1]; CI=[x,Y]; xgraf=[x,0];
rgsm=zeros(n,n); normas=[0,0,0]; exlya=[0;0;0];
%
% TOTAL TIME IN SECONDS
tt=400; itera=floor(tt/h2);
%iNTEGRATION STEP PSI=25
ch=[-alfa*xi, alfa, 0; 1, -1, 1; 0, -beta, 0]; u=min(abs(eig(ch)));
ch=[-alfa*xi*(conti-BP1)/conti, alfa, 0; 1, -1, 1; 0, -beta, 0];
u=min(u,min(abs(eig(ch)))); h1=1/(2*u*25);
%
%INTEGRATION OF THE 12 EQUATIONS
for i=1 : itera
%
    [Xver,XY]=fresaw(alfa,beta,xi,BP1, conti, CI, h2, h1);
    if abs(XY(1:3))>limax
        EL=[NaN;NaN;NaN];
        return;
    end;
    Xver=Xver(2:length(Xver),:);
    Xver(:,4)=Xver(:,4)+(i-1)*h2;
    xgraf=[xgraf;Xver];
%
    %RENORMALIZATION
    Vgsm(:,1)=transpose(XY(4:6));
    Vgsm(:,2)=transpose(XY(7:9));
    Vgsm(:,3)=transpose(XY(10:12));
    for v=1:n
        rgsm(v,v)=norm(Vgsm(:,v),2);
        Qgsm(:,v)=Vgsm(:,v)/rgsm(v,v);
```

```
        for vv=v+1:n
            rgsm(v,vv)=transpose(Qgsm(:,v))*Vgsm(:,vv);
            Vgsm(:,vv)=Vgsm(:,vv)-rgsm(v,vv)*Qgsm(:,v);
        end
        normas(v)=log(rgsm(v,v));
    end
    CI=[XY(1:3),transpose(Qgsm(:,1)),transpose(Qgsm(:,2)),transpose(Qgsm(:,3))];
    %EXPONENT ACCUMULATION
    for j=1:n
        exlya(j,i+1)=exlya(j,i)+normas(j);
    end
    %RETURNING FOR ALL EXPONENTS NEGATIVE AT ITERATION 71
     if (i==71) & (exlya(1,i+1)<0.0)
         EL=[NaN;NaN;NaN];
         return;
     end;
end  % LOOP i
%
%TIME NORMALIZATION
for i = 2:length(exlya)
    exlya(:,i)=exlya(:,i)/(h2*(i-1));
end EL=exlya(:,i);
%
% LYAPUNOV EXPONENTS PLOT
tiempo=(0:h2:tt); figure hold on; plot(tiempo,exlya(1,:),'-r')
plot(tiempo,exlya(2,:),'-g') plot(tiempo,exlya(3,:),'-b') hold off;
grid; ylabel('Lyapunov Exponents'); xlabel('time (s)');
%
end   %FUNCTION
```

The integration algorithm is shown below, however, this function may be rewritten to use any custom integration routine. The algorithm has been written to compute the trajectories of a third order PWL-function-based n-scroll attractor system.

```
function [Xver,XY]=fresaw(alfa, beta, xi, BP1, conti, x0,tmax,step1)
```

```
%Chaotic saw-tooth system integration routine based in ODE45
%
%Slope infinity is conti=0.01;
m0=-(0.5*BP1-conti)*xi/conti;
m1=xi*(conti-BP1)/conti;
%
options=odeset('RelTol',1e-3,'AbsTol',1e-6,'MaxStep',step1,'InitialStep',step1);
[T,X] = ode45(@rigid,[0 tmax],x0,options); XY=X(length(X),:);
Xver=[X(:,1:3),T];
%
%ODE SYSTEM
function dx = rigid(t,x) dx = zeros(12,1);
[f1,f2,f3,f4]=fpwl(x(1),x(4),x(7),x(10));
dx(1) = alfa*x(2)-f1;
dx(2) = alfa*x(1)-x(2)-alfa*x(3);
dx(3) = beta*x(2);
% x(1) CONTROLLED VARIATIONAL SYSTEM Y
dx(4) = alfa*x(5)-f2; dx(5) = alfa*x(4)-x(5)-alfa*x(6);
dx(6)=beta*x(5); dx(7) = alfa*x(8)-f3;
dx(8)=alfa*x(7)-x(8)-alfa*x(9); dx(9) = beta*x(8); dx(10) =
alfa*x(11)-f4; dx(11) = alfa*x(10)-x(11)-alfa*x(12); dx(12) =
beta*x(11);
%
%  function PWL (2 scroll)
   function [o1 o2 o3 o4] = fpwl(x1,x4,x7,x10)
        if x1 < -conti
            o1=xi*(x1+BP1); o2=xi*x4; o3=xi*x7; o4=xi*x10;
        elseif x1 < conti
            o1=m1*x1; o2=m1*x4;
            o3=m1*x7; o4=m1*x10;
        else
            o1=xi*(x1-BP1); o2=xi*x4; o3=xi*x7; o4=xi*x10;
        end
```

```
    end         %fpwl
%
end             %rigid
%
end             %fsaw
}
```

# Appendix C

# Device Technical Details

The device was manufactured by MOSIS 0.5$\mu$m process under the name 84284, and the following parameters [1]:

- Design name: bicentenario
- Technology: SCN3ME_SUBM, lambda = .3
- Fill to be added: No
- Fabricated on run V09M (AMI_C5F) as ¡TBD¿
- Bonding pads: 40
- Layout size: 1498 x 1498 microns; area: 2.244 sq millimeters
- Layers found (and densities): ACTIVE, CONTACT, GLASS, HI_RES_IMPLANT, METAL1 (41.6%), METAL2 (36.2%), METAL3, N_PLUS_SELECT, N_WELL, PADS, POLY (28.3%), POLY2, P_PLUS_SELECT, VIA, VIA2
- Requested packaging: DIP40 (40 parts)
- Maximum die size: 7620 x 7620
- Die Size: 2004 (+0 / -72) x 2477 (+0 / -72) $\mu$m
- Die Rotation in Cavity: None
- Cavity Size: 7874 $\mu$m x 7874 $\mu$m

[1] MOSIS Reply Id 00370537-001-003 / 30-SEP-2010 13:33:54

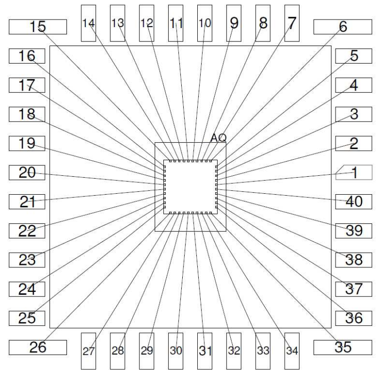


Figure C.1: Bounding diagram for MOSIS 84284 circuit.

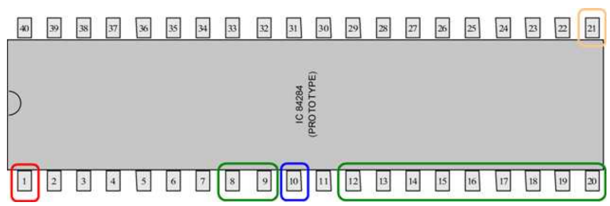


Figure C.2: Device pin diagram.

- A total of 40 parts are ordered with 40 to be packaged in DIP40

The final bounding diagram provided by the manufacturer is shown in Fig. C.1

## C.1 Device Pin Connections

According to the previous association, the device pin connections are shown in Fig. C.2. The description for each of the pins related to the project design is given in Table C.1.

Note: The connected integration capacitance $C_{integration}$ will vary the peak frequency of $x_2$ as explained in Section 3.3.

Table C.1: Device pin description.

| Pin | Description | Connecting |
|---|---|---|
| 1 | Vdd | 2.5V |
| 8 | The 5$\mu$A bias used for the nonlinear function. This pin is connected to ground trough a precision resistor | $R_{5\mu} = 68795\Omega$ |
| 9 | The 60$\mu$A bias used for the linear circuitry. This pin is connected to ground trough a precision resistor | $R_{60\mu} = 5582\Omega$ |
| 10 | Ground connection | 0V |
| 12 | Comparator response amplitude adjust, its value affects transistor M7 (Fig. 4.11b) | Adjust |
| 13 | Comparator response offset adjust, its value affects transistor MS0 (Fig. 4.11b) | Adjust |
| 14 | Buffered $x_1$ output | |
| 15 | External integration capacitance connection $C_1$ | $C_{integration}$ |
| 16 | External integration capacitance connection $C_2$ | $C_{integration}$ |
| 17 | External integration capacitance connection $C_3$ | $C_{integration}$ |
| 18 | Nonlinear 3-scroll function input for $x_1$ | pin 14 or gnd |
| 19 | Nonlinear 5-scroll function input for $x_1$ | gnd or pin 14 |
| 20 | Buffered $x_2$ output | |
| 21 | Vss | -2.5V |

# Appendix D

# Published Works

## D.1 Book Chapters

C. Sánchez-López, J. M. Muñoz-Pacheco, Victor Hugo Carbajal-Gómez, Rodolfo Trejo-Guerra, Cristopher Ramírez-Soto, Oscar S. Echeverría-Solis and Esteban Tlelo-Cuautle (2011). Design and Applications of Continuous-Time Chaos Generators, *Chaotic Systems*, Esteban Tlelo-Cuautle (Ed.), ISBN: 978-953-307-564-8, InTech.

R. Trejo-Guerra, E. Tlelo-Cuautle, J. M. Muñoz-Pacheco, C. Cruz-Hernández, C. Sánchez-López; Operating Characteristics of Mosfets in Chaotic Oscillators in *Transistors: Types, Materials and Applications*, Ed. Benjamin M. Fitzgerald: Nova Publishers, pp. 97–118, 2010.

## D.2 International Journals

Trejo-Guerra R, Tlelo-Cuautle E, Jiménez-Fuentes M, Sánchez-López, J. M. Muñoz-Pacheco, *Multiscroll Floating Gate Based Integrated Chaotic Oscillator*. International Journal of Circuit Theory and Applications (2011), doi: 10.1002/cta.821.

V. H. Carbajal-Gómez, E. Tlelo-Cuautle, R. Trejo-Guerra, C. Sánchez-López, J. M. Muñoz-Pacheco, *Experimental Synchronization of Multiscroll Chaotic Attractors using Current-Feedback Operational Amplifiers*. Nonlinear Science Letters B, vol. 1, no. 1, pp. 37–42, 2011.

Trejo-Guerra R, Tlelo-Cuautle E, Muñoz-Pacheco JM, Sánchez-López C, Cruz-Hernández C. *On the relation between the number of scrolls and the Lyapunov exponents in PWL-functions-based n-scroll chaotic oscillators*. International Journal of Nonlinear Sciences & Numerical Simulation **11**(11), 903–910, 2010.

R. Trejo-Guerra, E. Tlelo-Cuautle, C. Sánchez-López, J. M. Muñoz-Pacheco, and C. Cruz-Hernández, *Realization of Multiscroll Chaotic Attractors by using Current-Feedback Operational Amplifiers.* Revista Mexicana de Física, vol. 56, no. 4, pp. 268-274, 2010.

C. Sánchez-López, R. Trejo-Guerra, J. M. Muñoz-Pacheco, and E. Tlelo-Cuautle, *N-scroll chaotic attractors from saturated functions employing CCII+s.* Nonlinear Dynamics, vol. 61, no. 1-2, pp. 331-341, 2009.

Trejo-Guerra R, Tlelo-Cuautle E, Cruz-Hernández C, Sánchez-López C. *Chaotic communication system using Chua's oscillators realized with CCII+s.* International Journal of Bifurcations and Chaos **19**(12): 4217-4226, 2009.

## D.3 International Congress

R. Trejo-Guerra, E. Tlelo-Cuautle, J. M. Muñoz-Pacheco, and C. Sánchez-López, *Frequency Limitations from the Circuit Realization of Saw-tooth bassed Multi-Scroll Oscillators.* Joint 3rd Int'l Workshop on Nonlinear Dynamics and Synchronization (INDS) & 16th Int'l Symposium on Theoretical Electrical Engineering (ISTET), 2011.

C. Sánchez-López, J. M. Muñoz-Pacheco, E. Tlelo-Cuautle, V. H. Carbajal-Gómez, and R. Trejo-Guerra, *On the Trade-Off Between the Number of Scrolls and the Operating Frequency of the Chaotic Attractors.* IEEE International Symposium on Circuits and Systems (ISCAS) 2011.

Trejo-Guerra R, Tlelo-Cuautle E, Jiménez-Fuentes M, Sánchez-López C. *Multiscroll Oscillator based on Floating Gate CMOS Inverter.* IEEE International Conference on Electrical Engineering, Computing Science and Automatic Control (CCE): 541–545, 2010.

C. Ramírez-Soto, A. Salas-Cristóbal, R. Trejo-Guerra, O. S. Echeverría-Solís, V. H. Carbajal-Gómez, E. Tlelo-Cuautle, J. M. Muñoz-Pacheco, C. Sánchez-López, *Realización del circuito de Chua con inductores simulados basados en CCII+.* Congreso Internacional de Ingeniería Electrónica (ELECTRO 2008), Chihuahua.

# List of Figures

# List of Tables

# Bibliography


[1] Zhong G., *Implementation of Chua's circuit whit cubic nonlinearity*, IEEE Transactions on Circuits & Systems I, 41(12), pp. 934–941, 1994.

[2] Tang K. S., Zhong G. Q., Chen G., and Man K. F., *Generation of n-Scroll Attractors via Sine Function*, IEEE Transactions on Circuits & Systems I, 48(11), pp. 1369-1372, 2001.

[3] Yalcin M. E., and Özoguz S., *n-Scroll Chaotic Attractors From a First-Order Time-Delay Differential Equation*, Chaos 17, 2007.

[4] Han F., Lü J., Yu X. and Chen G., *Dynamical Behaviours of a 3D Hysteresis-Based System*, Chaos, Solitons and Fractals 28, pp. 182–192, 2006.

[5] Han F., *Multi-scroll Chaos Generation via Linear Systems and Hysteresis Function Series*, Ph.D thesis, RMIT University, Melbourne, Australia 2004.

[6] Saito T., *On a hysteresis chaos generator*, Proc. IEEE International Symposium on Circuits and Systems (ISCAS 1985), pp. 847–849.

[7] Newcomb R. W., and El-Leithy N., *Chaos Generation using Binary Hysteresis*, Circuits, Systems, and Signal Processing 5(3), pp. 321–341, 1986.

[8] Han F., Lü J., Yu X., Chen G., and Feng Y., *Generating Multi-scroll Chaotic Attractors via a Linear Second-Order Hysteresis System Dynamics of Continuous, Discrete and Impulsive Systems Series* Applications & Algorithms 12 pp. 95–110, 2005.

[9] Lü J., and Chen G., *Generating Multiscroll Chaotic Attractors: Theories, Methods and Applications*, International Journal of Bifurcations and Chaos, 16(4), pp. 775–858, 2006.

[10] Silva C. P., and Young A. M., *Introduction to Chaos-based Communications and Signal Processing*, Aerospace Conference Proceedings IEEE 1, pp. 279–299, 2000.

[11] Silva C. P., *Nonlinear Dynamics and Chaos: From Concept to Application*, Editor Henry Helvajian, Emerging Technologies 12(1), Spring 2011.

[12] Sira-Ramírez H., and Cruz-Hernández C., *Synchronization of Chaotic Systems: A Generalized Hamiltonian Systems Approach*, International Journal of Bifurcation and Chaos, 11(5), pp. 1381–1395, 2001.

[13] Posadas-Castillo C., Cruz-Hernández C., and López-Gutiérrez R. M., *Experimental realization of synchronization in complex networks with Chuas circuits like nodes*, Chaos, Solitons & Fractals, 40(4), pp. 1963–1975, 2009.

[14] Aguilar-Bustos A. Y., Cruz-Hernández C., López-Gutiérrez R. M., Tlelo-Cuatle E., and Posadas-Castillo C., Hyperchaotic encryption for secure e-mail communication, in *Emergent Web Intelligence: Advanced Information Retrieval, Series: Advanced Information and Knowledge Processing*, Springer-Verlag, pp. 471–486, 2001.

[15] Gámez-Guzmán L., Cruz-Hernández C., López-Gutiérrez R. M., García-Guerrero E. E., *Synchronization of Chua's circuits with multi-scroll attractors: application to communication*. Communications in Nonlinear Science and Numerical Simulation, 14(6), pp. 2765–2775, 2009.

[16] Trejo-Guerra R., Tlelo-Cuautle E., Cruz-Hernández C., and Sánchez-López C. *Chaotic communication system using Chua's oscillators realized with CCII+s*, International Journal of Bifurcations and Chaos, 19(12), pp. 4217–4226, 2009.

[17] Abel A., and Schwarz W., *Chaos Communications- Principles, Schemes, and System Analysis*, Proceedings of the IEEE, 90(5), pp. 691–710, 2002.

[18] Shuh-Chuan T., Chuan-Kuei H., Wan-Tai C., and Yu-Ren W. *Synchronization of Chua Chaotic Circuits with Application to the Bidirectional Secure Communication Systems*, International Journal of Bifurcations and Chaos, 15(2), pp. 605–616, 2005.

[19] Liu Z., Zhu X., Hu W., and Jiang F., *Principles of Chaotic Signal Radar*, International Journal of Bifurcations and Chaos, 17(5), pp. 1735–1739, 2007.

[20] Venkatasubramanian V., Leung H., and Xiaoxiang L., *Chaos UWB Radar for Through-the-Wall Imaging*, IEEE Transactions on Image Processing, 18(6), pp. 1255–1265, 2009.

[21] Qiao S., Shi Z. G., Chen K. S., Cui W. Z., Ma W., Jiang T., and Ran L. X., *A new Architecture of UWB Radar utilizing Microwave Chaotic Signals and Chaos Synchronization*, Progress In Electromagnetics Research, PIER 75, pp. 225–237, 2007.

[22] Dedieu H., and Ogorzalek M., *Chaos-Based Signal Processing*, International Journal of Bifurcations and Chaos, 10(4), pp. 737–748, 2000.

[23] Özoguz S., Ates Ö., and Elwakil A. S., *An Integrated Circuit Chaotic Oscillator and its Application for High Speed Random Bit Generation*, Proc. IEEE International Symposium on Circuits and Systems (ISCAS 2005), pp. 4345–4348.

[24] A. S. Demirkol, S. Özoguz, V. Tavas and S. Kilinc, *CMOS Realization of a Double-Scroll Chaotic Circuit and its Application to Random Bit Number Generation*, Proc. IEEE International Symposium on Circuits and Systems (ISCAS 2008), pp. 2374–2377.

[25] Cruz J. M., and Chua L. O., *An IC Chip of Chua's Circuit*, IEEE Transactions on Circuits & Systems II, 40(10), pp. 614–625, 1993.

[26] Özoguz S., Elwakil A. S., and Salama K. N., *N-Scroll Chaos Generador using Nonlinear Transconductor*, Electronic Letters, 38(14), pp. 685–686, 2002.

[27] Tavas V., Dermikol, A. S., Özoguz S., Zeki A., Toker A., *Integrated Cross-Coupled Chaos Oscillator Applied to Random Number Generation*, IET Circuits, Devices & Systems, 3(1), pp. 1–11, 2009.

[28] Xing-Yun L., *A new 3D Four-Wing Chaotic System with Cubic Nonlinearity and its Circuit Implementation*, Chinese Physics Letters, 26(9), pp. 1–4, 2009.

[29] Fujiwara T., Horio Y., and Aihara K. *An Integrated Multi-Scroll Circuit with Floating-Gate Mosfets*. Proc. IEEE International Symposium on Circuits and Systems (ISCAS 2003), pp. 180-183.

[30] Gupta S., and Senani R., *New Single-Resistance-Controlled Oscillators Configurations Using Unity-Gain Cells*, Analog Integrated Circuits and Signal Processing, 46(2), pp. 110–119, 2006.

[31] Gupta S. S., and Senani R., *New voltage-model/current-mode universal biquad filter using unity-gain cells*, International Journal of Electronics, 93(11), pp. 769-775, 2006.

[32] Sánchez-López C., Trejo-Guerra R., and Tlelo-Cuautle E., *Simulation of Chua's chaotic oscillator using unity gain cells*, Proceedings of the 7th International Caribbean Conference on Devices, Circuits and Systems, ISBN 978-1-4244-1957-9, México, 2008.

[33] Sánchez-López C., Castro-Hernández A., and Pérez-Trejo A., *Experimental verification of the Chua's circuit designed with UGCs*, IEICE Electron. Express, 5(17), pp. 657–661, 2008.

[34] Yalçin M. E., Suykens J. A. K., and Vandewalle J., *Families of Scroll Grid Attractors*, International Journal of Bifurcations and Chaos, 12(1), pp. 23–41, 2002.

[35] Senani R., and Gupta S. S., *Implementation of Chua's Chaotic Circuit using Current Feedbak Op-amps*, Electronics Letters, 34(9), pp. 829–830, 1998.

[36] Elwakil A. S., and Kennedy M. P., *Chaotic Oscillators Derived from Sinusoidal Oscillators Based on the Current Feedback OpAmp*, Analog Integrated Circuits and Signal Processing, 24(3), pp. 239–251, 2000, DOI: 10.1023/A:1008369810214

[37] Tlelo-Cuautle E., Gaona-Hernández A., and García-Delgado J., *Implementation of a chaotic oscillator by designing Chua's diode with CMOS CFOAs*, Analog Integrated Circuits and Signal Processing 48(2), pp. 159–162, 2006.

[38] Lorenz E. N., *Deterministic Nonperiodic Flow*, Journal of the Atmospheric Sciences, 20, pp. 130–141, 1963.

[39] Chua L. O., Wu C. W., Huang A., and Zhong G. Q., *A Universal Circuit for Studying and Generating Chaos Part I: Routes to Chaos*, IEEE Transactions on Circuits & Systems I, 40(10), pp. 732–744, 1984.

[40] Chua L. O., Wu C. W., Huang A., and Zhong G. Q., *A Universal Circuit for Studying and Generating Chaos Part II: Strange Attractors*, IEEE Transactions on Circuits & Systems I, 40(10), pp. 745–761, 1984.

[41] Lü J., Chen G., Yu X., and Leung H., *Design and Analysis of Multiscroll Chaotic Attractors From Saturated Function Series*, IEEE Transactions on Circuits and Systems, 51(12), pp. 2476–2490, 2004.

[42] Yazdi, M. K., Khan Y., Madani M., Askari H., Saadatnia Z., and Yildirim A., *Analytical Solutions for Autonomous Conservative Nonlinear Oscillator*, International Journal of Nonlinear Sciences and Numerical Simulation, 11(11), pp. 979-984, 2010, DOI: 10.1515/IJNSNS.2010.11.11.979.

[43] Suykens J. A. K., and Vandewalle J., *Generation of n-Double Scrolls (n=1,2,3,4,...)*, IEEE Transactions on Circuits and Systems, 40(11), pp. 861–867, 1993.

[44] Zhong G., Man K. F., and Chen G., *A Systematic Approach to Generating n-Scroll Attractors*, International Journal of Bifurcation and Chaos, 12(12), pp. 2907–2915, 2002.

[45] Yu S., Tang W. K. S., and Chen G. *Generation of nxm-Scroll Attractors under a Chua-Circuit Framework*, International Journal of Bifurcation and Chaos, 17(11), pp. 3951-3964, 2007.

[46] Yu S., Qiu S., and Lin Q., *New results of Study on Generating Multiple-Scroll Chaotic Attractors Science*, China Series F, 46(2), pp. 104–115, 2003.

[47] Elwakil A. S., Salama K. N., and Kennedy M. P., *A System for Chaos Generation and its Implementation in Monolithic Form*, Proc. IEEE International Symposium on Circuits and Systems (ISCAS 2000), pp. 217–220.

[48] Delgado-Restituto M., and Rodríguez-Vázquez A., *Design considerations for integrated continuous-time chaotic oscillators*, IEEE Trans. Circuits Syst. I, 45(4), pp. 481-495, 1998.

[49] Rodríguez-Vázquez A., and Delgado-Restituto M., *CMOS Design of Chaotic Oscillators Using State Variables: A Monolithic Chua's Circuit*, IEEE Trans. Circuits Syst. II, 40(10), pp. 596–613, 1993.

[50] Yalçin M. E., Suykens J. A. K. and Vandewalle J., *Experimental Confirmation of 3- and 5-Scroll Attractors from a Generalized Chua's Circuit*, IEEE Transactions on Circuits and Systems, 47(3), pp. 425–429, 2000.

[51] González O. A., Han G., J. Pineda de Gyvez, and Sánchez Sinencio E., *Lorenz-Based Chaotic Cryptosystem: A Monolithic Implementation*, IEEE Transactions on Circuits & Systems I, 47(8), pp. 1243–1247, 2000.

[52] Yu S., Lü J., Tang W. K. S., and Chen G., *A General Multiscroll Lorenz System and its Realization via Digital Signal Processors*, Chaos 16, 2006.

[53] Lü J., Yu S., Leung H., and Chen G., *Experimental Verification of Multidirectional Multiscroll Chaotic Attractors*, IEEE Transactions on Circuits & Systems I, 53(1), pp. 149–165, 2006.

[54] Hong Li, Zhong Li, Bo Zhang, Qionglin Zheng and Wolfgang Halang. *The Stability of a Chaotic PWM Boost Converter*. Int. J. Circ. Theor. Appl. 39(5), pp. 451–460, 2011.

[55] Poddar, G., Chakrabarty, K., Banerjee, S, *Experimental Control of Chaotic Behavior of Buck Converter*, IEEE Transactions on Circuits & Systems I, 42(8), pp. 502–504, 1995.

[56] Wei-Guo L., Luo-Wei Z., Quan-Ming L., and Jun-Ke W., *Non-Invasive Chaos Control of DC–DC Converter and its Optimization*, Int. J. Circ. Theor. Appl. 39(2), pp. 159–174, 2011.

[57] Chen Y., Tse C. K., Qiu S. S., Lindenmuller L., Schwarz W. *Coexisting Fast-Scale and Slow-Scale Instability in Current-Mode Controlled DC/DC Converters: Analysis, Simulation and Experimental Results*, IEEE Transactions on Circuits and Systems I, 55(10), pp. 3335–3348, 2008.

[58] Hossein A., Markazi D., and Sohanian-Haghighi H., Chaos Analysis and Control in AFM and MEMS Resonators, *Chaotic Systems*, Esteban Tlelo-Cuautle (Ed.), ISBN: 978-953-307-564-8, InTech 2011, Available from: http://www.intechopen.com/articles/show/title/chaos-analysisand- control-in-afm-and-mems-resonators

[59] Zheng Wang, Chau, K.T. *Design, Analysis, and Experimentation of Chaotic Permanent Magnet DC Motor Drives for Electric Compaction*, IEEE Transactions on Circuits and Systems II, 56(3) 245–249, 2009.

[60] Arena P., De Fiore S., Fortuna L., Frasca M., Patané L., Vagliasindi G., *Reactive Navigation through Multiscroll Systems: from Theory to Real-Time Implementation*, Auton Robot 2008; 25: pp. 123-146.

[61] Yu S., Lü J., and Chen G., *Experimental Confirmation of n-scroll Hyperchaotic Attractors*, Proc. IEEE International Symposium on Circuits and Systems (ISCAS 2006), pp. 221–224.

[62] Radwan A., Soliman A. M., Elwakil A. S., *1-D Digitally-Controlled Multiscroll Chaos Generator*, International Journal of Bifurcations and Chaos, 17(1),pp. 227–242, 2007.

[63] Gandhi G., and Roska T. *MOS-Integrable Circuitry for Multi-Scroll Chaotic Grid Realization: A SPICE-Assisted Proof*, International Journal of Circuit Theory and Applications, 37, pp. 473-483, 2009.

[64] Gaurav Gandhi, *An improved Chua's Circuit and Its Use in Hyperchaotic Circuit*, Analog Intagrated Circuits and Signal Processing, 46, pp. 173–178, 2006.

[65] Trejo-Guerra R., Tlelo-Cuautle E., Cruz-Hernández C., Sánchez-López C., and Fakhfakh M., *Current Conveyor Realization of Synchronized Chua's Circuits for Binary Communications*, IEEE DTIS, ISBN 978-1-4244-1577-9, Tozeur, Tunisia, March 25–28, 2008.

[66] Sánchez-López C., Trejo-Guerra R., Muñoz-Pacheco J. M., and Tlelo-Cuautle E., *N-scroll chaotic attractors from saturated functions employing CCII+s*, Nonlinear Dynamics, 61(1–2), pp. 331–341, 2009.

[67] Trejo-Guerra R., Tlelo-Cuautle E., Jimenez-Fuentes M., Sánchez-López C., Muñoz-Pacheco J. M., *Multiscroll Floating Gate Based Integrated Chaotic Oscillator*, International Journal of Circuit Theory and Applications, (accepted) 2011.

[68] Trejo-Guerra R., Tlelo-Cuautle E., Muñoz-Pacheco J. M., Sánchez-López C., and Cruz-Hernández C. *On the relation between the number of scrolls and the Lyapunov exponents in PWL-functions-based n-scroll chaotic oscillators*, International Journal of Nonlinear Sciences & Numerical Simulation 11(11), pp. 903–910, 2010.

[69] Yalcin M. E., *Increasing the Entropy of a Random Number Generator Using n-Scroll Chaotic Attractors*, Int. J. Bifurcat. Chaos, 17(12), pp. 4471-4479, 2007.

[70] Trejo-Guerra R., Tlelo-Cuautle E., Jiménez-Fuentes M., Sánchez-López C., *Multiscroll Oscillator based on Floating Gate CMOS Inverter*, IEEE International Conference on Electrical Engineering, Computing Science and Automatic Control (CCE), pp. 541–545, 2010.

[71] Strogatz S. H., *Nonlinear Dynamics And Chaos: With Applications To Physics, Biology, Chemistry, And Engineering (Studies in Nonlinearity)*, Westview Press, 1994.

[72] Martynyuk A. A., Borne P., and Cruz-Hernández, Eds. Advances in Chaotic Dynamics and Applications, serie: *Stability, Oscillations and Optimization of Systems*, 4, Cambridge Scientific Publishers Editorial, 2010.

[73] Hirisch M H., Smale S., Devaney R. L., *Differential Equations, Dynamical Systems, and an Introduction to Chaos*, Academic Press, Second Edition, 2003.

[74] Hoppensteadt F. C., *Analysis and Simulation of Chaotic Systems*, Springer, 2000.

[75] T. S. Parker, and L.O. Chua, *Practical Numerical Algorithms for Chaotic Systems*, Springer-Verlag, NY, 1989.

[76] Ross C., and Sorensen J., *Will the Real Bifurcation Diagram Please Stand up!*, The College of Mathematics Journal, 31(1), pp. 2–14, 2000.

[77] Silva C. P., *Shil'nikov's Theorem – A Tutorial*, IEEE Transactions on Circuits & Systems I, 40(10), pp. 675–682, 1993.

[78] Rubinger R. M., Nascimento A.W. M., Mello L. F., Rubinger C. P. L., Manzanares Filho N., and Albuquerque H. A., *Inductorless Chua's Circuit: Experimental Time Series Analysis*, Mathematical Problems in Engineering, 2007, id. 83893, 2007. doi:10.1155/2007/83893

[79] Fraser, A. M. *Information and entropy in strange attractors*, IEEE Trans. Inform. Th. 35, pp. 245-262, 1989.

[80] Eckhardt B., and Yao D., *Local Lyapunov Exponents in Chaotic Systems*, Physica D 65, pp. 100–108, 1993.

[81] Abarbanel H. D. L., Brown R., and Kennel M. B., *Variation of Lyapunov Exponents on a Strange Attractor*, J. Nonlinear Sci, 1 pp. 175–199, 1991.

[82] Fa-Quiang W., and Chong-Xin L., *Generation of Multi-scroll Chaotic Attractors via the Saw-Tooth Function*, International Journal of Modern Physiscs B, 22(5), pp. 2399–2405, 2008.

[83] R. Trejo-Guerra, E. Tlelo-Cuautle, J. M. Muñoz-Pacheco, C. Cruz-Hernández, C. Sánchez-López; Operating Characteristics of Mosfets in Chaotic Oscillators in *Transistors: Types, Materials and Applications*, Ed. Benjamin M. Fitzgerald: Nova Publishers, pp. 97–118, 2010.

[84] Trejo-Guerra R., Tlelo-Cuautle E., Sánchez-L'opez C., Muñoz-Pacheco J. M., and Cruz-Hernández C., *Realization of Multiscroll Chaotic Attractors by using Current-Feedback Operational Amplifiers*, Revista Mexicana de Física, 56(4), pp. 268–274, 2010.

[85] C. Sánchez-López, J. M. Muñoz-Pacheco, V. H. Carbajal-Gómez, R. Trejo-Guerra, and E. Tlelo-Cuautle, *Automatic synthesis of chaotic attractors using surrogate functions* Joint 3rd Int'l Workshop on Nonlinear Dynamics and Synchronization (INDS) & 16th Int'l Symposium on Theoretical Electrical Engineering (ISTET), 2011.

[86] C. Sánchez-López, J. M. Muñoz-Pacheco, E. Tlelo-Cuautle, V. H. Carbajal-Gómez, and R. Trejo-Guerra, *On the Trade-Off Between the Number of Scrolls and the Operating Frequency of the Chaotic Attractors*, Proc. IEEE International Symposium on Circuits and Systems (ISCAS 2011), pp. 2950–2953.

[87] Wojtyna R., *High-Precision Low-Power Voltage Follower for Hardware Signal Processing*, Int. Conf. Mixed Design, pp. 304–309, MIXDES 2006.

[88] Wongfoo S., and Naklo W., Suadet A., and Kasemsuwan V., *A Simple Rail-to-Rail CMOS Voltage Follower*, IEEE Regional Conference TENCON 2006.

[89] Kimmo Koli, "*CMOS Current Amplifiers: Speed versus Nonlinearity*", Doctoral thesis, Helsinki, 2000.

[90] Torres-Papaqui L., Torres-Muñoz D., and Tlelo-Cuautle E., *Synthesis of VFs and CFs by Manipulation of Generic Cells*, Analog Integrated Circuits and Signal Processing, 46, pp. 99–102, 2006.

[91] Tlelo-Cuautle E., Duarte-Villaseñor M. A., and Guerra-Gómez I., *Automatic Synthesis of VFs and VMs by Applying Genetic Algorithms*, Circuits, Systems and Signal Processing, 27(3), June 2008.

[92] Toker A., and Zeki A., *Tunable Active Network Synthesis using ICCIIs*, International Journal of Electronics, 94(4), pp. 335-351, 2007.

[93] Azhari S. J., and Safari L., *A High CMRR Low Power fully Differential Current Buffer*, IEICE Electronics Express, 7(11), pp. 765–771, 2010.

[94] Hassan Faraji Baghtash, and Seyed Javad Azhari, *Very Low Input Impedance Low Power Current Mirror*, Analog Integr Circ Sig Process, 66(1), pp. 9–18, 2011.

[95] Hastings A., *The Art of Analog Layout*, Prentice Hall, NJ, 2001.

[96] Shibata T., and Ohmi T., *A Functional MOS Transistor Featuring Gate-Level Weighted Sum and Threshold Operations*, IEEE Transactions on Electron Devices vol. 39(6), pp. 1444–1455, 1992.

[97] Rodriguez-Villegas E., Jimenez M., and Carvajal R. G., *On Dealing With the Charge Trapped in Floating-Gate MOS (FGMOS) Transistors* IEEE Trans. Circ. Sys. II, 54(2), pp. 156–160, 2007.

[98] Rodriguez-Villegas E., Jimenez M., Carvajal R. G. *Reliable Techniques for the Design of Floating Gate Transistors Based Circuits*. XX Conference on Design of Circuits and Integrated Systems (DCIS), 2005. Lisbon, Portugal.

[99] Rabaey J. M., *Digital Integrated Circuits a Design Perspective*. New Jersey: Prentice Hall Electronics and VLSI Series, 1996.

[100] Tavazoei M., Haeri M., Bolouki S., and Siami M., *Using Fractionalorder Integrator to Control Chaos in Single-Input Chaotic Systems* Nonlinear Dyn., 55, pp. 179-190, 2009.

[101] Cafagna D., and Grassi G., *Hyperchaos in the Fractional-Order Rössler System with Lowest Order* Int. J. Bifurcation Chaos, 19(1), pp. 339-347, 2009.